Modeling cell response heterogeneity to pro-apoptotic ligands

Luis Carlos Gomes Pereira

UNIVERSITÉ CÔTE D'AZUR

ÉCOLE DOCTORALE
SCIENCES ET TECHNOLOGIES DE L'INFORMATION ET DE LA COMMUNICATION

THÈSE DE DOCTORAT

Modélisation de l'hétérogénéité de la réponse cellulaire aux ligands pro-apoptotiques

Luis Carlos GOMES PEREIRA

INRIA Sophia Antipolis / IRCAN CNRS

Présentée en vue de l'obtention du grade de docteur en Informatique **d'**Université Côte d'Azur

Dirigée par : Madalena CHAVES,
Jérémie ROUX

Soutenue le : 26 Novembre 2019

Devant le jury, composé de :

Elisabeth PÉCOU, Université de Nice Sophia-Antipolis, France

Laurence CALZONE, Institut Curie, France

Laurent TOURNIER, INRA Jouy-en-Josas, France

Rui DILÃO, Instituto Superior Técnico, Portugal

cnrs IRCAN Inria Sophia Antipolis Méditerranée

Modélisation de l'hétérogénéité de la réponse cellulaire aux ligands pro-apoptotiques

/

Modeling cell response heterogeneity to pro-apoptotic ligands

Jury:

Rapporteurs

Laurence CALZONE, Ingénieur de Recherche Institut Curie, France

Rui DILÃO, Professeur Instituto Superior Técnico, Portugal

Examinateurs

Elisabeth PÉCOU, Professeur Université de Nice Sophia-Antipolis, France

Laurent TOURNIER, Chargé de Recherche INRA, France

Directeur

Madalena CHAVES, Directrice de Recherche INRIA, France

Co-Directeur

Jérémie ROUX, Chargé de Recherche CNRS, France

Abstract

Apoptosis is an essential physiological process through which organisms are able to equilibrate their cell numbers and maintain tissues in healthy and functional conditions. Despite the recent advances in the field, little is known on the molecular mechanisms controlling individual cell decisions to either engage or avoid the activation of this pathway upon cancer treatment, which inevitably impacts on therapeutics development.

To obtain a global view of the intervening proteins and their role on cell response dynamics to anti-cancer drugs, a new and detailed description of the apoptosis pathway at the receptor level was translated into a system of ordinary differential equations. The model was calibrated to single-cell data, from recent experiments on a population of HeLa cells exhibiting a highly heterogeneous response when exposed to the death-inducing ligand TRAIL. The sensitivities of the apoptotic reactions in our model were evaluated using the diversity of experimental behaviors observed in vitro. A series of computational tests and analyses were performed with our model to identify the origins of cell response heterogeneity. New features of the apoptotic pathway emerged from a comparison of different heterogeneity modeling approaches, detecting a set of key reactions to be further expanded.

These analyses yield new biological insights and highlights the importance of refining regulation of death receptor complex activity, possibly through Caspase-10 as suggested from new experimental discoveries. This thesis offers a novel framework that can be used to uncover important biological insights using single-cell data of heterogeneous dynamical pathways.

Keywords: Extrinsic apoptosis; Mass-action differential equations; Cell fate decision; Heterogeneity; Parameter distribution; Caspase-8 regulation; Predictive models.

Résumé

L'apoptose est un processus physiologique essentiel permettant aux organismes de maintenir leurs tissus dans des conditions fonctionnelles. Lors du traitement du cancer, les mécanismes moléculaires qui contrôlent la décision cellulaire d'engager ou d'éviter l'activation de cette voie sont mal connus, ce qui a un impact important sur le développement thérapeutique.

Pour obtenir une vue globale du rôle des protéines impliquées dans la dynamique de la réponse cellulaire aux anticancéreux, une nouvelle description détaillée de la voie de l'apoptose au niveau du récepteur a été implémentée en un système d'équations différentielles ordinaires. Le modèle a été calibré sur des données expérimentales en cellule unique, de populations de cellules HeLa présentant une réponse hautement hétérogène au ligand, TRAIL. Les sensibilités des réactions apoptotiques dans notre modèle ont été évaluées en utilisant la diversité des comportements expérimentaux observés in vitro. Une série de tests et d'analyses informatiques ont été effectués avec notre modèle pour identifier les origines de l'hétérogénéité de la réponse cellulaire, faisant émerger de nouvelles caractéristiques de la voie apoptotique.

Ces analyses apportent de nouvelles connaissances biologiques et soulignent l'importance de la régulation du complexe des récepteurs de la mort, éventuellement par la Caspase-10, comme le suggèrent de nouvelles découvertes expérimentales. Cette thèse offre une nouvelle approche pour découvrir des informations biologiques importantes en utilisant des données en cellule unique, de voies de signalisation à dynamiques hétérogènes.

Mots-clés : Apoptose extrinsèque ; Equation différentielles d'action de masse ; Décision de la mort cellulaire ; Hétérogénéité ; Distribution de paramètres ; Régulation de la Caspase-8 ; Modèles prédictifs.

Acknowledgments

I would like to start to express my sincerest gratitude to all the jury members for their precious time and attention reading this manuscript. All their observations were extremely valuable and essential for the accomplishment and accurateness of the text. I absolutely appreciate all your efforts.

To my supervisors, Madalena Chaves and Jérémie Roux, a “vrai remerciement” for their kindness and comprehension during these last three years. Despite the difficulties during the different steps of the project they were always caring and positive, supporting me through the innumerous challenges I had to face. I hope you keep doing superb research at the level you both deserve and that one day we can work together again. Also, of course, thank you for giving me a position and a scholarship that allowed me to have a PhD on such an extraordinary and motivating field and to have the chance to progress in my personal career.

A big kiss to all my dear friends in Nice for their exclusive comfort and joy. The feedback I received from you helped me to stay motivated and appreciate the wonders of France. I will always remind the dinners and the never-ending talks in our nights-out in Nice. An enormous hug to my fantastic “Italian group”: Serena, Melania, Sofia and Alberto, your kindness and presence is unforgivable. We will be friends to the end.

To a dear close colleague in my office, Mickael Meyer, I am grateful for having meeting you and to have spent three years of my PhD with you in my team. You are an extraordinary person, always with a great smile and ready to hear everyone’s problems. Wish you all the best, you really deserve it.

To Baharia Mograbi, my second and borrowed mother, I am grateful to have shared so many lunches in your company and to have listen to your constants “Courage! Dans la joie et la bonne humeur”. You are a precious and rare human being, I will never forget you.

Last but not least, an enormous gratefulness to my mother and father. Thank you for being the best parents in the world. Your continuous skype calls refilled my motivation and cheered me up in those days where I thought nothing could comfort me and I felt the urge to go back to Portugal. You always gave me reasons to keep going and never give up. I love you both unconditionally.

Contents

List of figures

List of Tables

Glossary

Apaf-1: *protease activating factor-1*

ARROM: *Apoptosis receptor reaction ODE model*

Bax: *Bcl-2-associated X protein*

Bak: *Bcl-2 homologous antagonist killer*

Bcl-XL: *B-cell lymphoma-extra-large*

Bid: *Bcl-2 family member Bcl-2 homology domain 3 (BH3) interacting domain*

C3/C6/C7/C9: *caspase 3/6/7/9*

C8/C10: *Caspase 8/10*

CyC: *cytochrome c*

DcR-1/2: *Decoy receptor*

DED: *Death effector domain*

DISC: *Death-inducing signaling complex*

DR 4/5: *Death receptor 4/5*

EARM: *Extrinsic apoptosis reaction model*

FADD: *FAS-associated death domain*

FLIP: *FADD-like IL-1-converting enzyme (FLICE)-inhibitory protein*

IAP: *inhibitor of apoptosis protein*

IMS: *intermembrane mitochondrial space*

k: *Rate of C8 activity*

MCL-1: *myeloid leukemia cell differentiation proteins*

MOM: *mitochondria outer membrane*

MOMP: *mitochondria outer membrane* permeabilization

ODE: *Ordinary differential equation*

pC8/10: *pro-caspase 8/10*

R: *Receptor*

SMAC: *second mitochondrial activator of caspases*

tBid: *truncated Bid*

TNF: *Tumor necrosis factor*

TRAIL: *Tumor necrosis factor-related apoptosis inducing ligand*

TRAIL-R 1/2/3/4: *Trail receptor 1/2/3/4*

XIAP: *X-linked inhibitor of apoptosis protein*

***τ* (tau) :** *time of maximum C8 activity*

“It is not knowledge, but the act of learning, not possession but the act of getting there, which grants the greatest enjoyment. “

Carl Friedrich Gauss

Chapter 1

Introduction

"The unexamined life is not worth living"

- Socrates

1.1 Motivations

Apoptosis: an important pathway in systems biology and medicine

Apoptosis comprises a set of chemical reactions through which cells can be eliminated when exposed to intracellular or extracellular stress signaling events (Renault and Chipuk, 2014; Tait and Green, 2010). When cell damage becomes relevant and endangers the rightful genotypic transmission to the incoming cell generations the cell generally chooses to commit apoptosis in order to protect the tissue from alarming and malignant mutations that can propagate to a tissue-level. The proper control of apoptosis is thus essential for the correct development of biological tissues and maintenance of homeostasis and its deregulation is commonly associated to disease conditions (Jacobson et al., 1997; Kerr et al., 1972). Inhibition of apoptosis often correlates with immune disorders and cancer formation and its excessive activation is an underlying feature of Parkinson, Alzheimer and Huntington's disease. (Brown and Attardi, 2005; Qi and Shuai, 2016).

Apoptosis is defined as either intrinsic or extrinsic depending on the origin of the death-signaling stimulus (Dewson and Kluck, 2009; Rehm et al., 2002). In the intrinsic apoptosis pathway the signal source is due to an intracellular event caused e.g. by a viral infection, excessive exposure to an oxidative stress or high levels of a DNA-damaging agent, such as UV radiation, that lead to the activation of a mitochondrial dependent pathway and the production of effector caspases. The proteins belonging to the effector caspase family are capable for cleaving a subset of intracellular targets, ultimately causing nuclear condensation, DNA fragmentation and consequent cell death (Brenner and Mak, 2009; Brune and Andoniou, 2017). The extrinsic apoptosis pathway is triggered instead by a death-ligand that interacts with the death-receptors on the cell membrane, activating an intra-cellular cascade that results in the production of initiator caspases. These are capable of directly activating effector caspases in the so-called type I cells. However, in some cell-lineages known as type II cells, effector caspases are inhibited by a pool of existing anti-apoptotic proteins and the initiator caspases must follow an indirect pathway and cause first the release of molecular substances from the mitochondria to inhibit the anti-apoptotic proteins present in the cell. In fact, both intrinsic and extrinsic pathways intersect at the level of the mitochondria, differing solely in their signal provenience. In the two pathways the same order is followed: initiator caspases are activated first and only afterwards there's a rise on the effector caspases concentration inside the cell.

Although massively studied, it is still unclear which step by step conditions or molecular proportions of pro- and anti-apoptotic proteins should be achieved along the several stages of the pathway for the cell to irreversibly commit to death. This has direct implications in clinical applications, for instance in cancer. Cancer cells typically possess innate resistances to both chemotherapy and death-inducing drug agents rendering them almost unaffected to these approaches (Almendro et al., 2013; Fulda and Vucic, 2012; Juin et al., 2013; Lopes et al., 2007). In some cases, resistance arises from specific mutations at the genomic level (Holohan et al., 2013). However, in general, non-genetic factors seem to be the key mechanisms behind resistance to drug and chemotherapy treatments (Cohen et al., 2008; Kreso et al., 2013; Roesch et al., 2010; Roux et al., 2015; Sharma et al., 2010; Spencer et al., 2009). In worse case scenarios these factors can accumulate and eventually persist at the cell population level (Brock et al., 2009; Wakamoto et al., 2013).

The link between the miss-regulation of apoptosis and the resulting phenotypic impairments make it a very challenging topic in both biology and medicine. One of the major drawbacks is

to understand why the phenotypic responses of clonal or sister cells are so highly heterogeneous when exposed to identical death signals (Balázsi et al., 2011). This effect, described as "fractional-response", is a hallmark of apoptosis and is a topic that has been under intense investigation in the past decades.

Multiple modeling efforts have tried to bring to light levels of interactions and mechanisms of control that can make cells to choose between life (apoptosis escape) and death (apoptosis commitment). Along the next lines of the manuscript, the role of the most important proteins of the apoptotic system and a proposed mathematical model will be discussed in parallel as an attempt to tackle this question. In chapter 1, a deep inspection of the literature gathered a theoretical scheme of the extrinsic apoptotic reactions and a general explanation on the most relevant biological events is provided. A quick overview of previous models is also given, with a focus on five models that show how the modeling questions in apoptosis evolved in the past two decades. Chapter 1 ends with a simple description of noise in biology, its different sources and the existing strategies to model each noise source. In Chapter 2, the ARROM1 mathematical model is built from the biological information explained in Chapter 1. The signal of the available data set is briefly explained along with some methods to match the model output with the experimental signal information. Arguments are then presented on the hypothesis that the reactions defined in the literature might be incomplete and an extra set of proteins might exist so that model fittings become more coherent with respect to previous parameter values available in the literature. Chapter 3 provides some examples of how the new model version, with two new proteins, reproduces known biological results, validating the model approach. In Chapter 4, the noise sources introduced in chapter 1 are simulated into the model equations and an inspection is performed to verify which of them can reproduce the heterogeneity observed in the data set. Chapter 5 continues with the fits of the entire cell population and the analysis of which resulting distributions in parameter values and initial conditions contain the largest differences between the population of resistant and sensitive cells. Hypothesis are presented for the dependencies that might exist between the new proposed proteins in Chapter 2 and their connection to FLIP or Caspase-8, the two major apoptotic intervenients at the receptor level. Finally, Chapter 6 summarizes the results of this thesis and proposes new directions in the modeling field of apoptosis.

1.2 Apoptosis signaling network

1.2.1 TRAIL, a death-inducing molecular agent initiating apoptosis

Tumor necrosis factor (TNF)-*related apoptosis inducing ligand* (TRAIL) is a cysteine polypeptide belonging to the class of death-inducing ligand molecules termed TNF-superfamily, capable of selectively triggering apoptosis in cancer cells in vitro and in vivo (Ashkenazi et al., 1999; Walczak et al., 1999). Its application in the cancer-therapy field has been especially encouraging due to its singular mode of action, not only because of its exclusive impact on cancer cells, but also because of its capability of triggering an intracellular death response independent of the p53 signaling cascade that is commonly mutated in a variety of cancer entities (Kozłowska and Puszynski, 2016; Muller and Vousden, 2013; Olivier et al., 2010).

Like the majority of the TNF-family members, TRAIL's induction of an apoptotic response depends on its ability to recruit complementary death-receptors to the cell membrane in order to form relatively stable homodimers or heterodimers at the cell surface. In particular, two classes of death-receptors, the class *TRAIL-receptor 1* (TRAIL-R1/DR4) and/or the class *TRAIL-receptor 2* (TRAIL-R2/DR5) aggregate with TRAIL to form active structures capable of propagating the death signal to the interior of the cell (Hymowitz et al., 1999; Jones et al., 1999). Although a natural component of the human bloodstream, TRAIL baseline concentration is insufficient to induce an apoptotic response in natural tissues and its biological role in normal conditions is therefore unknown. (Gibellini et al., 2007; Mariani et al., 1997).

As part of an anti-cancer drug therapy TRAIL shows ulterior advantages as it doesn't promote the usual toxicity signals derived from cross-activation of pro-survival inflammatory pathways observed in other TNF members (Ashkenazi et al., 1999; Roberts et al., 2011; Walczak et al., 1999). However, it is also long known that besides the desired apoptotic response TRAIL also unleashes the activation of the NF-KB pathway (Chaudhary et al., 1997; Degli-Esposti et al., 1997; Schneider et al., 1997; Trauzold et al., 2001) , MAPK pathway (Tran et al., 2001), and PI3K pathways (Azijli et al., 2012; Xu et al., 2010), all of these pro-survival and undesired secondary signalling pathways. The result is an overall decrease of efficiency of the treatment as at the same time it induces pro-apoptotic signals, TRAIL also unleashes parallel pro-survival signalling responses.

Up to these days TRAIL tests in clinical trials have proven rather disappointing as it was shown in a recent metastatic pancreatic cancer study where phase II-trial patients revealed no overall improvement neither in 12-month survival rate nor on overall survival rate in comparison with a gemcitabine monotherapy [gemcitabine is a common chemotherapeutic agent] (Kretz et al., 2018). Other DR agonistic antibodies including mapatumumab, drozitumab, conatumumab , lexatumumab and LBY135 , all triggering extrinsic apoptosis in a manner similar to TRAIL, have all been discontinued after revealing also unfruitful results in clinical applications (Herbst et al., 2010; Merchant et al., 2012; Rocha Lima et al., 2012; Sharma et al., 2014; Younes et al., 2010). The reasons explaining their unsuccess are still to be properly characterized. In future applications, the optimal direction strategy will pass by the development of more potent and stable drugs that can successfully stimulate the extrinsic apoptosis pathway in a selective manner, avoiding the activation of undesired pro-survival responses. For that matter it is necessary to unveil the dynamics of these interlinked pathways and to understand the different thresholds that allows the cell to activate a so called "fractional survival", where some cells avoid the apoptotic death-fate and resist the therapy (Shlyakhtina et al., 2017).

Recent findings suggest that the interaction between the death-ligand TRAIL and the complementary death receptors is already a decisive factor that distinguishes the downstream activated pathways. Incomplete trimeric interactions with just two binding sites attached in a TRAIL-R1-TRAIL complex are sufficient for activation of a NF-kB signaling response (Morton et al 2015) and a specific oligomerization between trimeric complexes may be required for the proper activation of the apoptotic signal (Wajant, 2019). A detail understanding of these interactions is thus essential.

The time of application has also shown to be important. A pulse-like TRAIL dosage instead of a continuous treatment has demonstrated to be associated with therapy efficacy. In a study from 2016 it was shown that a 1-min pulse of TNF was more efficient in inducing a cell apoptotic response than a 30-min or 60-min pulse and it was as efficient as a continuous treatment with a 10-hours dosage. The conclusion was that the timing of cell exposure impacts cell fate decision and long applications may stimulate the death receptors in such a way that they can be more prone to activate secondary pro-survival responses. Short-pulse scenarios are then related with weaker NF-kB signaling and stronger pro-apoptotic outcomes (Lee et al., 2016).

The application of the drug, and specifically the time of successive dosages, has also shown interesting dynamics. As a consequence of the augmented levels of pro-survival proteins during the hours that follow a first TRAIL dosage, the subsequent rounds may end up ineffective if a "drug-holiday" is not considered. In this sense, and similar to other chemotherapy drug scenarios, it can be beneficial to establish neutral periods of non-administration until the pro-survival protein levels return to their basal levels (Becker et al., 2011; Das Thakur et al., 2013).

The adequate treatment may pass by the right usage and combination of multiple drugs while also considering the timing of TRAIL application so that in the end the cell system can be sensitized into a correct cell death direction.

1.2.2 DR4 and DR5, decoy death receptors, and clustering modes with TRAIL

TRAIL can bind to a variety of death-receptors (DR) in the cell membrane. The receptor isoforms propagating the apoptotic signal are the DR4 and DR5 that exist in a stable equilibrium of monomer and dimeric versions, being the monomeric the most common based on molecular studies of CD95 (Liesche et al., 2018). The binding affinity between monomeric receptors is low, justifying the existence of a higher proportion of monomeric receptors (Chan, 2000; Clancy et al., 2005; Neumann et al., 2014). Despite less common, not all the receptors in the cell membrane are functional and another class, termed decoy receptors (DcR), is able to interfere with the death-ligand signal and disrupt the interaction with the adequate receptors DR4/DR5. These are the *TRAIL-R3* (DcR1) and the *TRAIL-R4* (DcR2) receptors which not only compete for direct contact with the ligand but are also capable of sequestering free DR4/DR5 receptors and bind to them, forming non-functional complexes (LeBlanc and Ashkenazi, 2003).

1.2.3 DISC complex, the basic unit structure for activation of Caspase-8, and the role of FLIP as an inhibitor of apoptosis

TRAIL sequentially adds receptor molecules DR4/DR5 until a trimeric complex is formed. After the trimerization, other molecules join with the death receptors to form a functional *death-inducing signalling complex* (DISC), capable of propagating the signal to the remaining steps of the network. These are the *FAS-associated death domain* (FADD) molecule and the initiator *pro-caspase 8* (pC8), added in the same order and in a sequential manner (Dickens et al., 2012). While the receptor multimerization and association with the ligand is a quick

process, the addition of FADD is a limiting and delayed step, essential for the binding of pC8 to the DISC platform (Pennarun et al., 2010). FADD binds to one assembled trimeric receptor complex and acts as an adaptor molecule for the recruitment of several pro-caspases, allowing a first pC8 to be fixed and directly bind to its *death effector domain* (DED). From there, a second pro-caspase can bind to the free DED of the first pro-caspase and a chain of interlinked molecules is sequentially formed (Schleich et al., 2016). Once a dimerization occurs, by proximity-induced catalytic activation, a functional form of the pro-caspases is released from the receptors, in the form of *caspase 8* (C8), sending the apoptotic signal from the receptors to downstream reactions occurring in the cytoplasm of the cell (de Miguel et al., 2016; Dickens et al., 2012) .

A controlling step in this process depends on a homolog molecule with a very similar structure to that of the pro-caspases, the *FADD-like IL-1-converting enzyme* (FLICE)-inhibitory protein (c-FLIP), that competes for a binding position with FADD suppressing the elongation chain of linked pro-caspases and obstructing their activation (Hughes et al., 2016). Its major role is to hinder the apoptotic signal setting a threshold between quantities of pro-apoptotic caspases vs. the quantity of pro-survival FLIP molecules in the DISC unit.

1.2.4 Caspase-8, a threshold for cell-fate decision

The requirements for the activation of C8 is the presence of a DISC assembled structure with at least two attached pC8 chains, interlinked through their DED domains. In this configuration, the two pC8 proteins inter-activate themselves and form a single structure with catalytic activity that is next released from the DISC unit and navigates into the cytoplasm to participate in the cleavage of downstream molecules. The amount of C8 released from the receptor in this way is essential as a first step towards an apoptotic cell response but yet little is known about the actual mechanisms that control C8 numbers inside the cell.

Recently, with the scope of understanding and quantifying the C8 activity level in apoptotic committed cells, Roux and colleagues analyzed hundreds of HeLa-cells treated with TRAIL at multiple concentrations and concluded that the dynamics of the C8 protein plays a central role in cell-fate decision, unveiling a necessary relationship between the rate of C8 activity (**k**) and the time of maximum C8 activity ($\boldsymbol{\tau}$) for cells to properly engage into apoptosis (Roux et al., 2015). Each cell was fitted to the parametric model $\boldsymbol{k} * (\boldsymbol{t} - \boldsymbol{t_0})^{\boldsymbol{2}}$ and the optimal maximum derivative value, $\boldsymbol{max}(\boldsymbol{2k} * [\boldsymbol{t} - \boldsymbol{t_0}])$, that best separated the group of sensitive cells from the

group of resistant cells was defined as $\boldsymbol{\theta}$. The maximum derivative value assigned to $\boldsymbol{\theta}$ can then be interpreted as a biological threshold**,** able to distinguish surviving cells from dying cells in the **(k, $\boldsymbol{\tau}$)** space (red line in figure 1-C).

The work was pioneer in the field by presenting for the first time a metric to predict apoptosis propensity on a given cell. Although simplified by the usage of the lumped parameters **k** and $\boldsymbol{\tau}$, the approach was accurate enough to correctly forecast the cell fate of more than 80% of the cell population in several cell lines. This number, as a result of a model approximation that considered uniquely DISC-related events, agreed with the result of Gaudet and colleagues that mentions that the non-DISC related proteins contribute to the overall heterogeneity of the apoptotic signal in a range of 20% (Gaudet et al., 2012).

An interesting conclusion of this study was that cells can be sensitized to cross $\boldsymbol{\theta}$ in multiple ways such as by increasing the ligand (TRAIL) concentration (by stabilizing the DISC and consequently augmenting the C8 rate of activation (**k**)) or by adding drugs that stabilize the C8 molecule (e.g. bortezomib, an inhibitor of protein degradation triggered in a proteasome dependent way) [increasing the time of C8 activation ($\boldsymbol{\tau}$)]. In the opposite direction, cells can also turn more resistant to apoptosis by overexpressing anti-apoptotic proteins as the FLIP isoforms (specially the FLIP-s (FLIP short) configuration). All these scenarios are DISC-related events and do not change $\boldsymbol{\theta} = 2.61\text{x}10^{-3}\ \text{s}^{-1}$. However, when adding a drug acting downstream of C8 activation, the value of the threshold changes in a concomitant way. This was verified by the addition of the pro-apoptotic BCL-2 inhibitor, ABT-263, that by decreasing the *mitochondrial outer membrane permeabilization* (MOMP) "sensitivity", it was able to lower $\boldsymbol{\theta}$ in those cell populations, making them more prone to die. In the end, the framework was especially relevant as it compiled information from C8 trajectories that varied importantly in signal and had **(k, $\boldsymbol{\tau}$)** pair values changing tenfold and threefold, respectively, across the cell populations (Roux et al., 2015).

Although simple in the description of the underlying apoptotic pathway, the work still has the potential to be further explored and extended so as to include the role of other molecules also activated under an apoptotic stimulus but known to be C8-independent (Scott et al., 2017). A more complete version would be most useful to understand in better detail how to make a cell irreversibly enter in the death-region space (figure 1-C, D). The framework suggests several ways in which cells can be sensitized to cross the theta-threshold line but cells still remain close to the theta vicinity, calling for more effective co-drugging treatments.

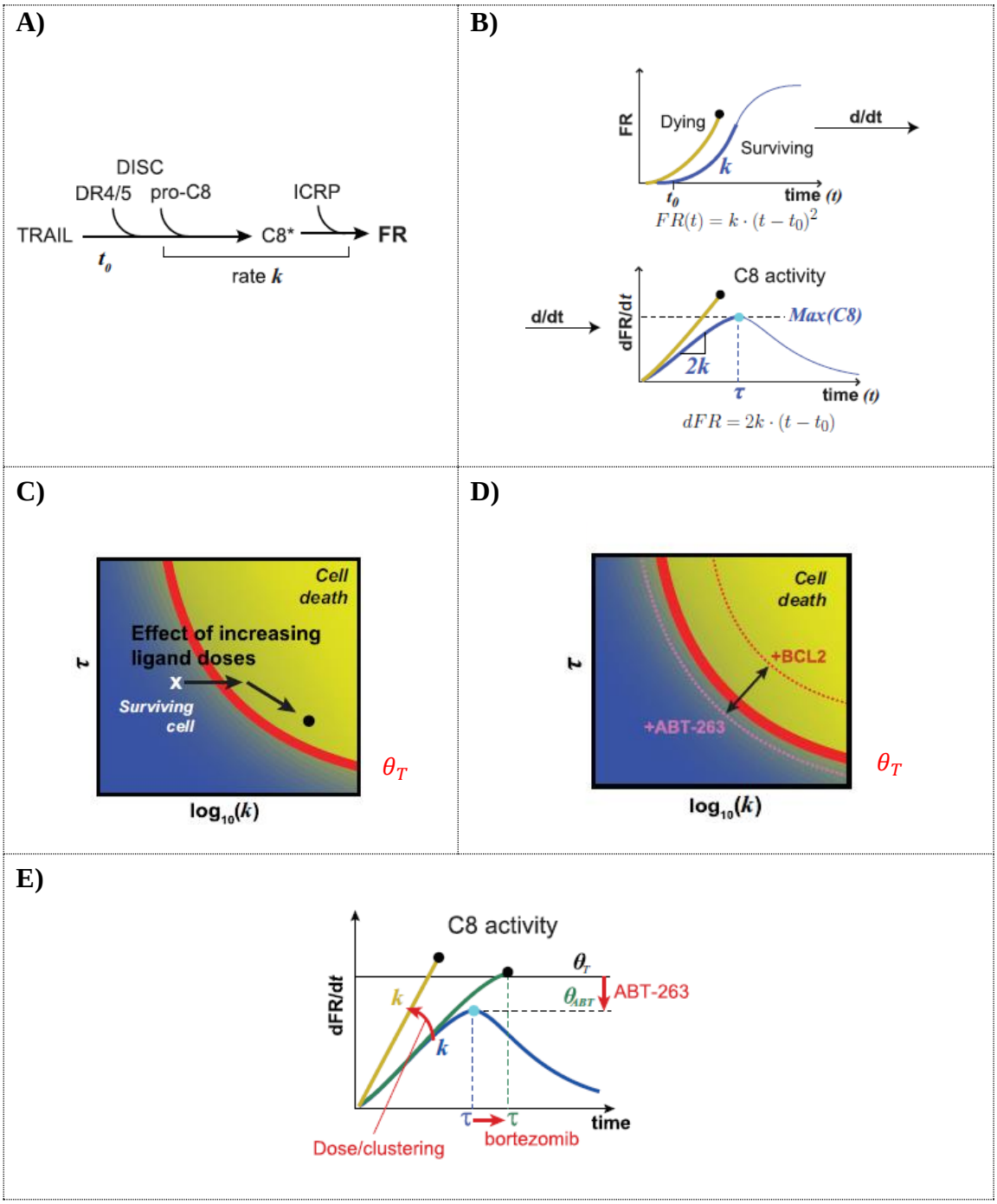

Figure 1. A cell fate prediction arising from contribution of both rate and duration of C8 activity.
A) A simplified scheme for the activation of C8 from the DISC and consequent cleavage of its substrate ICRP (a reporter fluorescent protein), returning the output signal of the cleaved fluorescence reporter (FR). The lumped parameter **k** represents the rate of C8 activation and **t0** the time required to start receiving the signal from the first cleaved ICRP molecule. **B)** The shape of an output signal produced by an averaged surviving and dying cell. Dying cells have a more pronounced parabolic trajectory curve, a sign of higher C8 activities. The model $\boldsymbol{FR(t) = k(t - t_0)^2}$ describes the period after ligand stimulation, when C8 activity increases and follows a quadratic polynomial curve and is valid until the maximum value of **dFR/dt**, corresponding to the maximum C8 activity value at time $\mathbf{t = \tau}$. **C)** Dosage increase of the ligand causes an overall increase in C8 activity (**k**) and a small decrease on the time interval required to reach the associated maximum activity ($\boldsymbol{\tau}$). The $\boldsymbol{\theta}$-value of the population remained unchanged **D), E)** Co-treatments cause a deviation on the (**k, $\boldsymbol{\tau}$**) values of a mean-cell of the population and on the landscape of the $\boldsymbol{\theta}$ curve. Figure adapted from (Roux et al., 2015).

1.2.5 Bcl-2 like proteins, pro- and anti-apoptotic roles

Once the DISC complexes are activated and functional C8 is generated, a group of proteins of the BCL-2 family group intervenes into the apoptosis cascade and holds the next decision to block the incoming signal or propagate it to the *mitochondria outer membrane* (MOM). This decision point, specific of type II cells, starts with the C8 cleavage of the *Bcl-2 family member Bcl-2 homology domain 3* (BH3) *interacting domain* (Bid) into a truncated form tBid that, in this form, is translocated from the cytosol to the MOM where it can interact with other elements of the Bcl-2 family. This step is of major importance and should be a result of sustained C8 activation in order to reach an important pool of tBid molecules and surpass an irreversible pro-apoptotic threshold.

The molecular targets of tBid are the *Bcl-2-associated X protein* (Bax) and *Bcl-2 homologous antagonist killer* (Bak), both responsible for MOMP and propagation of the apoptotic signal (Green, 2004; Huang et al., 2016). The agent tBid allows the oligomerization of Bax and Bak to occur, changing them into an active form that is capable of perforating the MOM and transform it into an all-or-none MOMP signal.

A tight level of control is also set by a group of pro-survival proteins, unbalancing the signal from Bax and Bak and allowing the cell to control spurious apoptotic stimulus. Under these conflicting forces a minimum limit is then set for Bax and Bak pro-apoptotic intensity. Among the pro-survival proteins there is the *B-cell lymphoma-extra-large* (Bcl-XL) and the *myeloid leukemia cell differentiation proteins* (Mcl-1) which bind to Bax and Bak and convert them into their inactive and non-oligomerized form not capable of triggering MOMP (Llambi et al., 2011; Willis, 2005).

As a synthesis, the Bcl-2 family members can be divided into three groups: pore-forming effector proteins, Bax and Bak; BH3-like proteins such as tBid; and the pro-survival proteins such as Bcl-2, Bcl-xL and Mcl-1. The effector proteins are capable of forming mitochondrial pores but only after a conformational change induced by the BH3-like proteins (Chipuk et al., 2010). On the other hand the pro-survival proteins sequester the pro-apoptotic ones, rendering them inactive until a sufficiently high stoichiometric proportion of BH3-like proteins participates and sets the effector proteins free from the inhibitory effect of the pro-survival proteins (Sarosiek et al., 2013). This occurs by direct competition where the BH3-like proteins interact with the pro-survival Bcl-2 members and release them from the effector proteins, making them accumulate at the MOM. Lower intensity apoptotic signals are not able to

summon sufficient BH3-like proteins and in these conditions effector proteins are constantly translocated by the pro-survival proteins from the MOM back to the cytosol (Edlich et al., 2011; Schellenberg et al., 2013; Todt et al., 2015).

A positive feedback loop has been proposed for the BCL-2 effector family member Bax, where already activated Bax could reinforce the apoptotic signal by contributing to the activation of still inactive Bax molecules (Cui et al., 2008; Tan et al., 2006). In this way the cell could decrease the necessary levels of tBid required to trigger MOMP or reinforce the response into an all-or-none switch. This complicated network of interactions is not completely understood and may hide other still unknown dynamics.

1.2.6 MOMP, an irreversible commitment to cell-death

Upon a sufficient amount of tBid accumulation and Bax / Bak oligomerization at the MOM, the MOMP event ensues and molecular agents such as *cytochrome c* (CyC) and the *second mitochondrial activator of caspases* (Smac) are released from the *mitochondrial intermembrane space* (IMS) into the cytoplasm (Tait and Green, 2010). Both of these agents are implicated in effector caspases activation (Galluzzi et al., 2009). CyC accumulation together with the apoptotic *protease activating factor-1* (Apaf-1) create the apoptosome, a stimulation platform for *caspase-9* (C9) activation. C9 positively contributes for the activation of the effector caspases -3 (C3), -6 (C6) and -7 (C7) and from this point apoptosis is irreversibly unleashed (Riedl and Salvesen, 2007). Smac contributes to effector caspases onset by causing direct binding and inhibition of *X-linked inhibitor of apoptosis protein* (XIAP), ensuring a fast activation of C3, C7 and C9 and a stronger pro-apoptotic response (Deng, 2002).

While the onset of MOMP is highly variable and can last up for several hours after an extrinsic or intrinsic apoptotic stimulus exposure, the time frame of a MOMP response after tBid translocation to the membrane is in the order of minutes and suggests a switch type like-response (Albeck et al., 2008; Goldstein et al., 2000; Rehm et al., 2009). The speed of MOMP event depends on the accumulation of Bax/Bak at the MOM. Since only 10% of the Bax cytosolic pool is already sufficient to cause MOM depolarization and consequent MOMP, the speed of these ending processes is fast and tightly regulated among all the molecular intervenients (Hantusch et al., 2018).

After MOMP signaling, all the above identified processes are reinforced by a positive feedback look of the form C3 → C6 → C8 that strengthens the apoptotic response inside the cell (Cowling and Downward, 2002; Sohn et al., 2005) and convert it into a "point of no return" towards cell death (Bhola and Letai, 2016).

1.2.7 Global overview on the extrinsic apoptosis pathway

To summarize the contents explained in sections 1.2.1 - 1.2.6 a scheme is presented in figure 2, with a global overview on the most representative reactions of the extrinsic apoptosis pathway. On a general outlook, two types of signaling events counteract the correct progression of the apoptotic signal: native anti-apoptotic proteins and active degradation of the existing pro-apoptotic proteins. The former includes the negative effect of decoy receptors on TRAIL, the action of FLIP on the inhibition of the DISC, the impact of the Bcl-2 pro-survival proteins on sequestration of the Bcl-2 effectors and also the binding and inactivation of C3 by XIAP. The second line of defense against apoptosis relies on the ubiquitin-mediated degradation of pro-apoptotic proteins by the proteasome complex. That is achieved for instance by XIAP that induces not only direct contact inhibition over the effector caspase C3 but also degrades it through this mechanism (Suzuki et al., 2001). The presence of multiple layers of control is an opportunity and a challenge for scientists in the field of biology and mathematical modelling in the incoming years, not only for the local dynamics that mediate every step decision but also on the global aspects that inter-regulate the pathway.

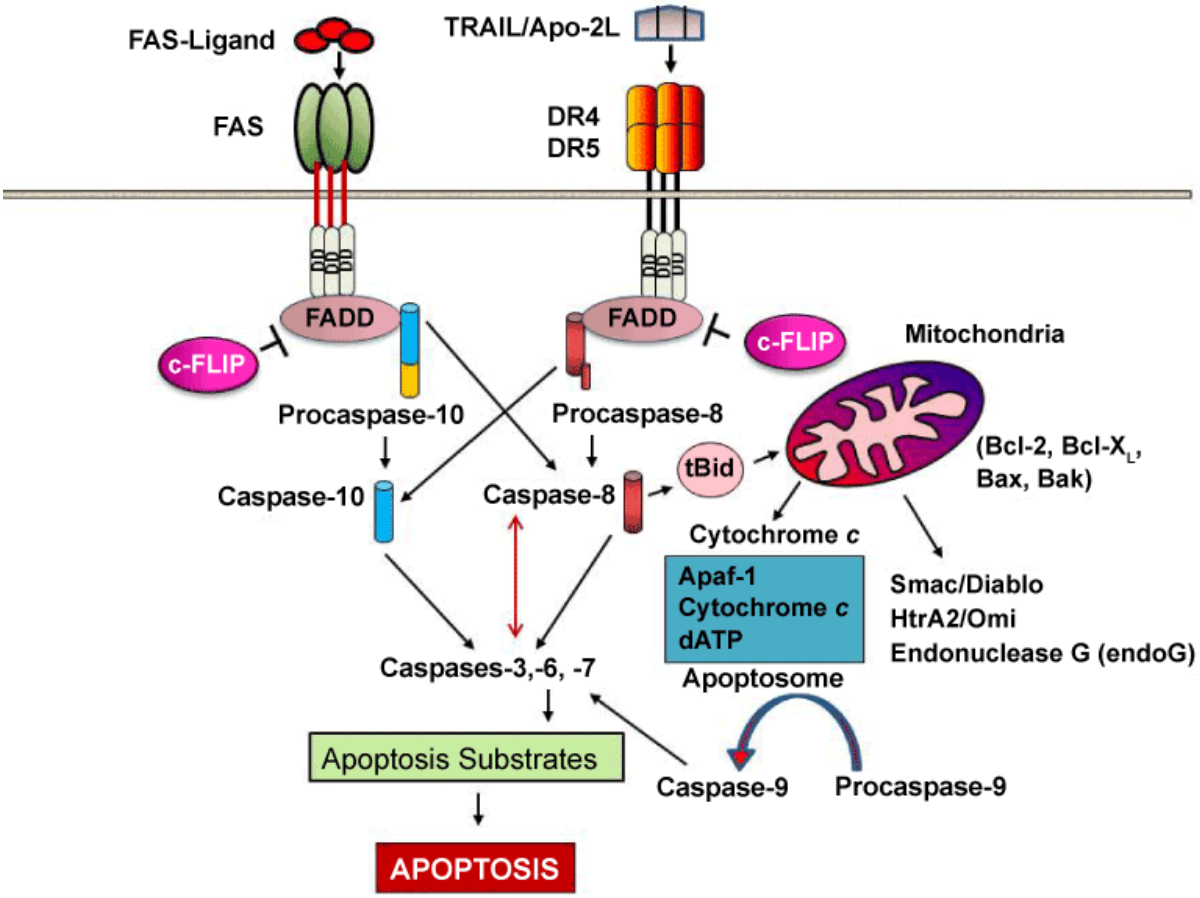

Figure 2. Summary network of the extrinsic apoptosis signaling pathway.

TRAIL interacts with the death-receptors DR4/DR5 forming a trimeric structure that attaches FADD in the cell membrane. Pro-caspase-8/10 and FLIP compete for FADD-binding, assembling one active caspase-8/10 molecule when two procaspase-8/10 interact without the interference of FLIP. Bid is then cleaved to tBid by the active caspases and migrates into the mitochondrial outer membrane wall where it oligomerizes Bax and Bak. These two effector proteins have to increase in number until surpassing the level of the anti-apoptotic Bcl-2 members Bcl-2 and Bcl-XL. When MOMP is triggered cytochrome C and Smac lead to the activation of C3,C6 and C7 that further reinforce the apoptotic signal by increasing the level of active C8 through a positive feedback loop. Figure extracted from (R Safa, 2013).

1.3 Modelling in Apoptosis

1.3.1 Fussenegger's model, 2000

Models of Apoptosis date as far back as the beginning of the century when Fussenegger and colleagues proposed a model for apoptosis with both extrinsic and intrinsic associated pathways (Fussenegger et al., 2000). The model included some of the knowledge of the time such as the receptor role in the activation of functional C8 and the importance of mitochondria in intersecting and transducing both exterior and stress-induced signals. Assembling those facts, the authors were capable of describing known phenomena like the ability to inhibit the apoptotic cascade by overexpressing *inhibitors of the apoptotic proteins* (IAPs) and to define quantitative proportions of anti-apoptotic BCL-2 molecules necessary to reduce the amount of produced effector caspases in the system. Also, supported by cancer-like scenarios with an overexpression of BCL2-anti-apoptotic proteins, the model permitted the calculation of compensation ratios of pro-apoptotic proteins that could reverse the resistant phenotype and a relevant role was given to the reactions happening at the receptor level in what concerns their impact on the overall response of the system (figure 3-C)).

Although not entirely innovative in its conclusions it was a pioneer work that launched the usage of ODE's in the mathematical field of apoptosis in a manner that agreed with the biological description of the known chemical reactions. In what concerns the underlying mathematical approach, the model did not follow standard mass-action description and the expression for the rates laws are somehow unclear. Same examples are provided in table 1.

Table 1. Sample of some of the rate laws used in Fussenegger's publication

Rate of death domain clustering	**Rate of FADD addition**
$r_b = \frac{k_t([R]_T - [RL])[L]}{K_S^{-1} + [L]}$	$r_F = \frac{k_a[F][RL]_T}{(1 + K_A[F] + K_A K_B[F]^2)} - \frac{[RL.F_2]}{K_A K_B[F]}$
Rate of formation of the Apaf-1	**Rate of effector Caspases activation**
$r_{A1} = \frac{k_h[C_c][A1]_T}{(1 + K_H[C_c] + K_I[b_x])} - k_{-h}[A1.C_c]$	$r_{k3a} = \frac{k_q[c_{Ez}][c_{ka}]_T}{(K_p^{-1} + [c_{Ez}] + K_R K_p^{-1}[I_{Ea}])}$

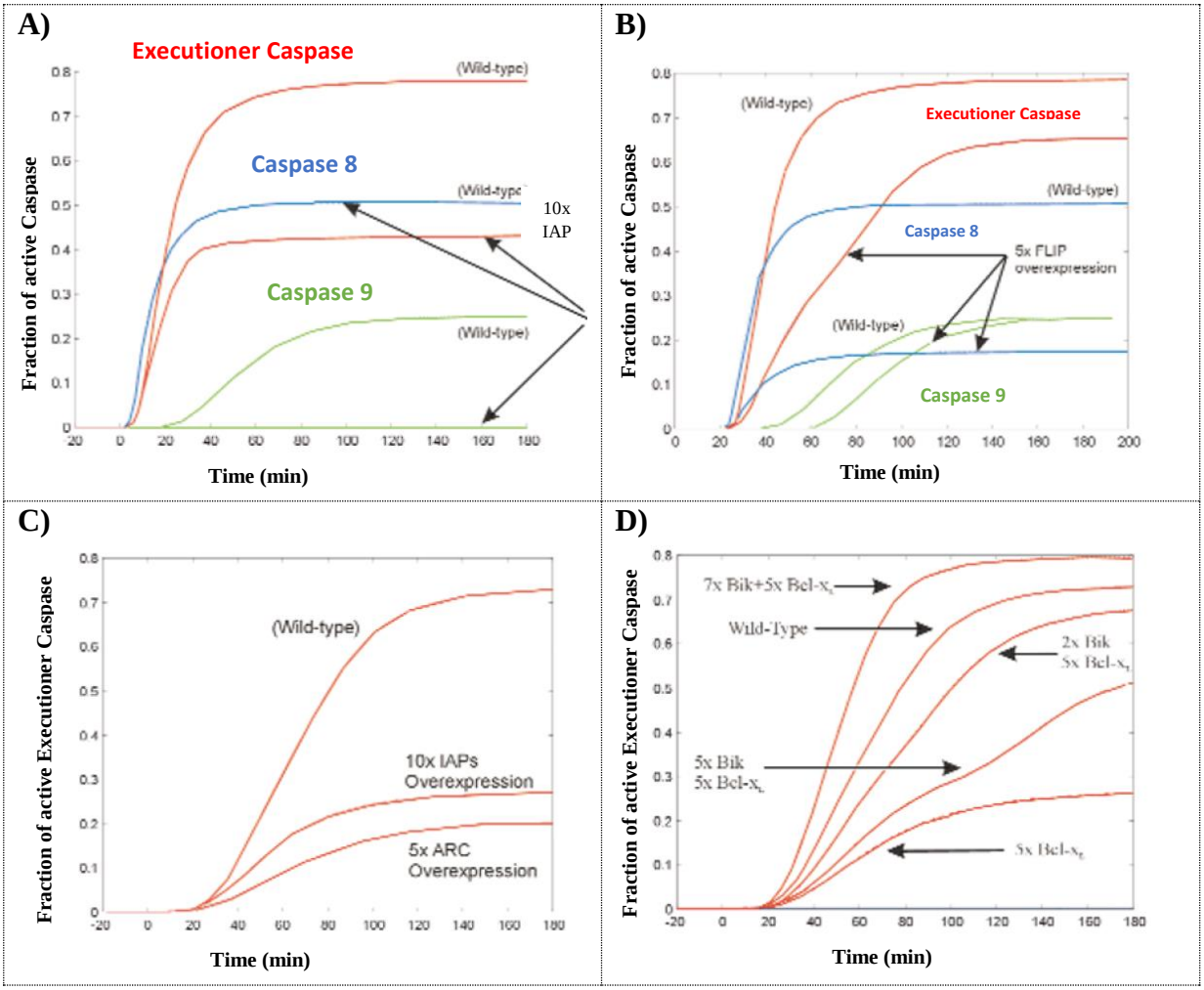

Figure 3. Fussenegger's apoptosis-related model results.

A), B), C) The authors have shown that different anti-apoptotic proteins cause dissimilar effects on the level of initiator caspases (C8) and executioner caspases (C3/C6/C7). **A)** Overexpressing *inhibitor of apoptosis protein* (IAP) diminishes the final steady state values of C9 and that of the executioner caspases. C8 evolution is unchanged after IAP overexpression (middle blue-line). **B)** FLIP overexpression impacts the levels of all three represented caspases. **C)** Increasing five times the amount of decoy-receptor proteins causes a larger decrease in the fraction of executioner caspases than overexpression of IAP ten times the standard levels. The remark is that receptor events have a larger impact on the output of the simulated signaling cascade. **D)** A cancerous cell, defined by high levels of anti-apoptotic proteins such as Bcl-XL, regains executioner caspases basal levels when submitted to elevating levels of pro-apoptotic proteins like the Bcl-2-interacting killer (Bik). Figure extracted from (Fussenegger et al., 2000).

Summary

- ✓ Global description of the underlying biological processes
- ✓ Therapeutic strategies point to the apoptotic receptor reactions as an important target that should be up- or down- regulated in the case of cancer and Alzheimer's disease, respectively
- ✓ Role of the receptor compartment as an important layer of the network

---

- × Mathematical rate laws are not clear
- × Incomplete and oversimplified representation of the receptor valency
- × Caspase-8 dynamics, as explained in section 1.2.4 of this manuscript, was not known back at the time of the publication

1.3.2 Albeck's EARM1 model, 2008

An upgrade on the Fussenegger's model was given by Albeck and colleagues on a global vision of the extrinsic apoptosis signaling pathway (Albeck et al., 2008). The authors increased the previous description to a four-compartment model named EARM1 (*extrinsic apoptosis reaction model 1*) containing a receptor compartment (figure 4, gray box), a mitochondrial compartment (figure 4, yellow box), a C3-associated positive feedback loop compartment (figure 4, green box) and a posT-MOMP compartment (figure 4, blue box).

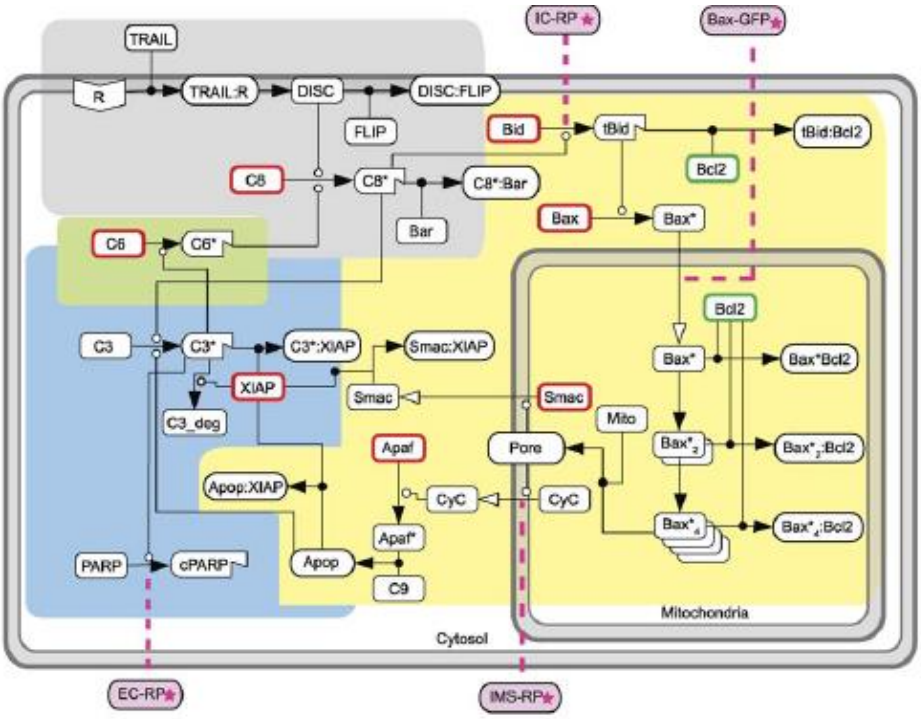

Figure 4. Albeck's EARM1 network of reactions.

A four-compartment model was proposed by Albeck and colleagues for the extrinsic apoptosis pathway. In the receptor compartment (gray area) the formation of the DISC is simplified by the attachment of a single ligand, after which C8 is directly activated into C8*. The production of C8 is simplified with a lumped representation that does not correspond to the dynamics explained in section 1.2.4 of this manuscript. The mitochondrial compartment (yellow area) includes a vast number of reactions from the cleavage of Bid into tBid promoted by C8, down to the formation of the apoptosome after MOMP. A simplified illustration of the positive feedback loop reinforcing C8 activation is included (green area). The feedback loop was shortened and C6 was activated by C3* without any intermediate steps. Finally, in blue, active C3* cleaves PARP into cPARP and irreversible apoptosis is reached. All the boxes highlighted in pink refer to nodes were available experimental data existed in the form of a signal emitted by a reporter protein (RP). Figure extracted from (Albeck et al., 2008).

The authors were able to explain two-time separated events: a pre-MOMP variable time delay period followed by a posT-MOMP spontaneous event "snap-action" signal corresponding to effector caspases activation in cells treated with cycloheximide (a potent inhibitor of protein synthesis). The high heterogeneity on the delay period was associated to the level of activity of the initiator caspase C8, which was confirmed experimentally (Albeck et al., 2008). This activity depended on the dose of the ligand but the influence dissipated at the mitochondria level with the MOMP, formation of pores, SMAC release and effector caspases activation being dose independent through an irreversible cell fast switch-type activation signal. In fact, in order to agree with the dynamics of the experimental data, the snap-action signal topology depended critically on the reactions happening in the mitochondrial compartment, setting a local control that is independent from the upstream parts of the network such as the receptor layer. The snap-action signal was also shown to be independent of the downstream feedback loop C3 → C6 → C8, not requiring the reinforcement of a positive feedback interaction to establish the all-or-none behavior of MOMP.

At the time, no quantifications were established on the topic of "fractional killing". This was a direct consequence of treating cells with cycloheximide, which creates a biological context that inevitably leads to cell death, independently of activation of apoptosis. In this setting, the authors were unable to study different contributions of the network for the underlying cell-fate death or survival decision.

The EARM1 was further on extended up to EARM1.4 version. Spencer and colleagues used EARM1.1 to show that variability in protein initial conditions could reproduced the experimental distributions in time-of-death (Spencer et al., 2009). Variability in time-of-death was found to be caused by specific proteins of the apoptosis pathway, which were defined as sensitive nodes of the network, and were obtained with simulations on the EARM1.3 version (Gaudet et al., 2012). Finally, an EARM1.4 model proposal allowed a study to establish the ratio of XIAP/C3 as a distinguishing factor in cells executing a type I (mitochondrial-independent) or type II (mitochondrial-dependent) apoptosis. Type I occurs when this ratio is small and type II is preferable when the same ratio attains higher values (Aldridge et al., 2011).

Summary

- ✓ First steps in the positioning of C8 dynamics as a central node of the network controlling the variability in time-of-death
- ✓ Description of the MOMP event as a switch type response that depends on the movement of proteins through different compartments where the scales of the reaction rates change
- ✓ A small number of pore molecules is enough to release a wave of SMAC and CyC to the cytosol, resulting in a snap action signal independent of upstream or downstream events

---

- × Units of [molecules per cytosolic compartment] are not clear and difficult to reproduce
- × Incomplete representation of the receptor valency
- × Caspase-8 dynamics, as explained in section 1.2.4 of this manuscript, was not known back at the time of the publication

1.3.3 Schlatter's & Calzone's model, two Boolean modeling approaches

The transduction and processing of intracellular signals often results from the contribution of multiple chemical agents and signaling pathways whose exact dynamics are frequently unknown. This lack of information greatly compromises the usage of continuous-time modelling approaches, which depend on precise model parameters, and can eventually bias model predictions. In this sense a simpler but useful alternative to study the interactions in a reaction network is to consider a Boolean or logical modeling framework to qualitatively assess the interactions and dependencies between the considered molecular species. The concentration of every element is replaced by a binary variable {0, 1}, in either an "on" or "off" state, and the collection of interactions is embed in an oriented graph that can integrate several types of dependencies, including activation and inhibition effects and positive and negative feedback loops.

In the field of apoptosis two studies based on Boolean formalisms stand out by the complexity and relevance of their conclusions, the work of (Schlatter et al., 2009) and (Calzone et al., 2010). In the former, a large network of reactions describing the intrinsic and extrinsic apoptosis and a myriad of associated pathways was proposed to analyze the effect of an input of Fas ligand, TNF-a, UV-B irradiation, interleukin-1b and insulin into the phenotype outcome of the system. The complexity of the reported interactions made the authors choose for a multi-value node representation where each variable could assume multiple states, instead of the common "1" or "0" and all-or-none definition, to account for "low-active amount" and "high-active amount" and establish higher-valued states where one variable could surpass the inhibitory role of another or instead reinforce the inhibition of a given substrate. The inclusion of more detailed timescale dynamics, with subsets of reactions being active only at certain time points, proved also essential to reproduce threshold dependencies and reaction delays that are known to be apoptotic signatures. The phenotypic outcome of the system was found to depend considerably on the feedback loops and highly connected nodes which included crosstalks with the survival and insulin pathways. A non-reported negative feedback loop from Smac to RIP (a central molecule in the necroptosis pathway inhibiting DISC and C8 activation) was suggested as a mechanism to enhance the stability of the DISC structures and lead to more effective apoptotic responses (Schlatter et al., 2009). Although hypothetical, the possibility of uncovering a new level of regulation in an already complex network is definitely one of the potential benefits of using modeling approaches and overall strengthen the results of this model.

The model of (Calzone et al., 2010) tried to establish a functional relationship between the NF-kB survival pathway and the cellular decision for either apoptosis or RIP1-dependent necrosis, after activation of the death-receptors on the cell membrane. By assembling a large network of reactions with the most representative elements of these three signaling pathways, the C3 activation, a significant drop in ATP levels and emergence of NF-kB were set as representative hallmarks of apoptosis, necrosis and survival decisions, respectively. A Boolean variable was assigned to each node and rules were imposed to define multiple events, such as the activation of a protein. For instance, C8 was considered to effectively change into an active state after direct stimulation by either DISC-TNF or DISC-FAS but only in the absence of FLIP. In this case, the associated logical rule was defined as (DISC-TNF OR DISC-FAS) AND NOT FLIP. By analyzing the multiple steady-states of their system, the authors could

propose novel insights about cellular decisions towards different cell-death modalities. Even in the presence of C8-mediated cleavage of RIP1 the system was shown to contain attractors eventually converging into a necrotic phenotype, suggesting that the presence of C8 per se does not imply a cellular apoptotic response. For cells in which important apoptotic elements were mutated (APAF1, BAX, C8, FADD deletions and z-VAD treatment), simulations uncovered the existence of an optimal TNF treatment coincident with maximum proportions of obtained necrotic cells. The authors also found the role of the positive feedback loop from C3 to C8 to be non-essential when TNF or FAS levels were constant in the cell medium. Oppositely, when the same ligands are to be administrated in pulses the feedback loop ensures the persistence of the apoptotic signal (Calzone et al., 2010). This result reassures the importance of positive feedback loops in natural tissues where the cell receives non-sustained death-signals from its surrounding environment. The work still has the potential to uncover, with the availability of more data, the paradigms of cell decision towards necrosis, necroptosis or apoptosis and enlighten how we can force the cell into a specific type of death.

In what concerns the modeling framework, many formulations are available (among Boolean, ODE's or PDE's) and the modeler can choose for a more qualitative or quantitative approach according to the data at hand and the desired analysis or conclusions to extract. Some authors chose to build hybrid models combining both Boolean and ODE components and some are available in the field of apoptosis, such as the model for the NF-kB module proposed by (Chaves et al., 2009).

1.3.4 Bertaux's model, a stochastic protein-turnover approach 2014

It is long known that identical sister cells often respond in different ways when exposed to equivalent stimulus. In apoptosis these differences have been attributed to inequalities in protein numbers that, when summed up for the plethora of intra-signaling reactions of a network, can influence the phenotype decision. In an effort to study these effects, Bertaux and colleagues used the EARM1 model, previously proposed by Albeck, and added a second contribution in the form of a gene stochastic layer (Bertaux et al., 2014). Each protein of the network interacted with other proteins of the system and also received an extra-input signal resulting from the fluctuations of the corresponding gene expression (figure 5). The goal was to follow the impact of random fluctuations in time in the absolute protein quantities, instead of the traditional sampling of variable initial conditions at the beginning of the simulation that is a common tool used to reproduce the behavior of non-identical cells. This analysis allowed for the simulation of a population of sister cells whose proteome decorrelate in time due to the inherent fluctuations of the underlying gene expression, as observed experimentally (Spencer et al., 2009).

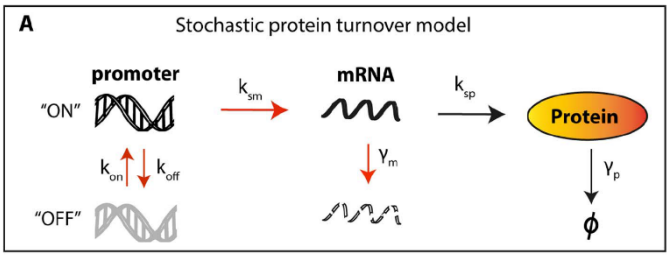

Figure 5. Bertaux's stochastic protein turnover model.
All the network of proteins of the EARM1 model was equipped with a stochastic layer using a random telegraph approach: mRNA production and degradation rates were modeled as stochastic processes with protein production and degradation rates treated as deterministic processes. Simulations for the stochastic elements were executed with the Gillespie algorithm. Figure extracted from (Bertaux et al., 2014).

The approach allowed the authors to evaluate the contribution of intrinsic noise, produced at the gene layer, and conclude that it was enough to justify the temporal and reversal resistance to TRAIL observed in HeLa cells after an initial TRAIL exposure (Flusberg et al., 2013). Their congruence with the experimental results required the fluctuations of the short-lived protein Mcl1 to be large and rare, imposing low value ranges for the ON-OFF promoter switching rates of this protein. In this case modelling was able to explain the acquired resistance of cells already

treated with TRAIL as a complex interplay of three distinct effects: selection acting on the cells with the highest anti-apoptotic protein amounts; transcriptional noise making protein production to switch between on and off states and protein degradation as a force that tends to decay protein numbers back to their original values (making resistance only temporary). The co-participation of these environmental pressures could not be deduced without a modelling approach and reinforced the need of mathematical laws to determine and quantify individual system-level contributions.

By assembling Mcl1 dynamics with rare and large fluctuations, FLIP with promoter fast turnover rates and a default model of protein turnover for the remaining proteins of the system, the authors could also reproduce the MOMP time distributions registered by Spencer and colleagues (Spencer et al., 2009). The work was important as it defined a strategy to introduce fluctuations in a principled manner and study the contribution of gene expression variability in networks of interacting proteins.

Summary

- ✓ A methodology was proposed to analyze the effect of gene expression fluctuations on a given network of interacting proteins
- ✓ A justification was presented for the temporal and reversal resistance acquired by HeLa cells after a TRAIL exposure
- ✓ After cell division, the loss of synchrony of sister cells with time was reproduced, in line with the findings of Spencer and colleagues

- × Model parameters were fitted from a data set concerning cells treated with TRAIL and cycloheximide. Cycloheximide blocks protein production and changes the universe of interactions at the protein level. This may cause the model predictions to be unrealistic in HeLa cells treated exclusively with TRAIL
- × Incomplete representation of the receptor valency
- × Caspase-8 dynamics followed the same representation as in Albeck's EARM1 model
- × Under-estimation of the role of FLIP, which is known to be a potent inhibitor of apoptosis

1.3.5 A summary list of models of apoptosis

Author / Year	***Focus of the model***
(Fussenegger et al., 2000)	*Intrinsic + Extrinsic apoptosis*
(Bentele et al., 2004)	*Extrinsic apoptosis*
(Eissing et al., 2004)	*Positive feedback loop of C3 on C8*
(Hua et al., 2005)	*Extrinsic apoptosis*
(Stucki and Simon, 2005)	*Mitochondria + IAP + C3*
(Bagci et al., 2006)	*C8 + Mitochondrial reactions*
(Legewie et al., 2006)	*Intrinsic + Extrinsic Apoptosis*
(Rehm et al., 2006)	*Effector caspases dynamics*
(Chen et al., 2007b)	*Bcl-2 apoptotic switch*
(Chen et al., 2007a)	*Bax + Bcl-2 interaction*
(Albeck et al., 2008)	*Extrinsic apoptosis*
(Cui et al., 2008)	*Bcl-2 dynamics*
(Chaves et al., 2009)	*Apoptosis + NF-kB dynamics*
(Schlatter et al., 2009)	*Intrinsic + Extrinsic apoptosis*
(Zhang et al., 2009)	*Intrinsic + Extrinsic apoptosis*
(Calzone et al., 2010)	*Apoptosis + NF-kB + Necrosis pathways*
(Howells et al., 2011)	*Bcl-2 dynamics*
(Aldridge et al., 2011)	*Extrinsic apoptosis: Type I vs Type II cells*
(Huber et al., 2011)	*Bcl-2 family members dynamics*
(Gaudet et al., 2012)	*Extrinsic apoptosis*
(Stoma et al., 2013)	*Extrinsic apoptosis Type I vs Type II cells*
(Bertaux et al., 2014)	*Extrinsic apoptosis*
(Kallenberger et al., 2014)	*C8 dynamics*
(Würstle et al., 2014)	*Intrinsic apoptosis*
(Воропаева and Voropaeva, 2017)	*P53 dynamics*

(Roux et al., 2015)	*C8 dynamics*
(Paek et al., 2016)	*Intrinsic apoptosis: p53 dynamics*
(Ballweg et al., 2017)	*P53 dynamics + Bax dynamics*
(Yin et al., 2017)	*Bcl-2 dynamics*
(Bouhaddou et al., 2018)	*Pan-cancer pathways, including apoptosis*
(Buchbinder et al., 2018)	*Extrinsic apoptosis*
(Márquez-Jurado et al., 2018)	*Extrinsic apoptosis: Role of mitochondria*
(Lederman et al., 2018)	*Extrinsic apoptosis: Role of TRAIL*
(Miura et al., 2018)	*Intrinsic apoptosis: JNK dynamics*
(Chong et al., 2019)	*Intrinsic apoptosis: p53 dynamics*

1.4 Heterogeneity in biology, intrinsic and extrinsic noise

Signals in biology are noisy. Even when an adequate degree of confidence lies in the technique used for signal acquisition and the experimentally-associated errors are minimized, cells have nonetheless their own inherent stochastic fluctuations. These fluctuations are caused by inter-cellular differences in genetic and non-genetic expression levels that contribute for unique cell signatures in time (Chabot et al., 2007; Elowitz, 2002; Newman et al., 2006; Ozbudak et al., 2002; Raj et al., 2006; Raser, 2004; Stewart-Ornstein et al., 2012). The exact role and nature of signal fluctuations in biology is not entirely understood but some defend that cell diversification might be essential for the evolution of life. The presence of non-homogenous cells among a cell population allows both adaptation and robustness of the organism to different stresses and a high-level tissue response might depend on the inclusion of heterogeneous single-cell outputs as a whole (Bódi et al., 2017; Dueck et al., 2016; Lehner and Kaneko, 2011; Pujadas and Feinberg, 2012). Although positive and advantageous in the sense of evolution it can also be extremely deleterious when it promotes drug-resistant phenotypes, such as is often the case in cancer cells.

The current literature summarizes heterogeneity in biology as the result of intrinsic and extrinsic noise contributions. Intrinsic noise is derived directly from the reaction kinetics, a natural consequence of the thermodynamics of every chemical process that causes the reaction times to be stochastic (Gillespie, 1976). This impacts the absolute number of reaction products at a given time point, such as the total quantity of expressed RNA and proteins, causing even isogenic cells to decorrelate importantly in a matter of few hours (Spencer et al., 2009) . This phenomenon is highly dependent on the quantity of the intervening molecules and is increasingly relevant for systems with low number of particles. It is usually introduced in studies of gene expression and RNA dynamics where the reactants are not abundant but its influence on large scale signaling networks, where protein quantities are commonly high, has been confirmed to be minimal (Iwamoto et al., 2016; Labavić et al., 2019). The inclusion of intrinsic noise in model simulations usually follows the Gillespie algorithm, which returns an exact solution for the associated master equation (Gillespie, 1977). For gene expression models, where intrinsic noise is more notable, ON-OFF " telegraph-models" are well established and are able to explain gene noise levels and its impact in RNA and protein amounts (Blake et al., 2006, 2003; Golding et al., 2005; Harper et al., 2011; Lionnet and Singer, 2012; Raj et al., 2006; Raj and van Oudenaarden, 2008; Raser, 2004; Suter et al., 2011).

Different from the intrinsic noise, the extrinsic noise relates instead to differences in protein numbers that are naturally diverse in distinct cells, up- or down-regulating the associated signaling pathways in which they participate. It is not certain if intrinsic and extrinsic noise are related and if extrinsic noise is not more than a direct consequence of fluctuations in gene expression that cause consequent variability in protein numbers (Eling et al., 2019). From the point of view of mathematical approaches it can be modelled as a deterministic event by setting different protein initial conditions on each simulated cell (Gaudet et al., 2012). The simulation of extrinsic noise is usually considered by sampling initial conditions with a coefficient of variation (CV) =30% around the initial mean values, a typical value for protein variability in biological systems (Sigal et al., 2006; Spencer et al., 2009).

In summary, intrinsic noise refers to the natural randomness of a reaction event, either to produce or not produce a biochemical product. Distinctly, extrinsic noise points to the system at a beginning of the simulation, with the differences in protein quantities in the cell population being sampled and transferred to the model as a set of different initial conditions. Depending on the signaling pathway at study, the magnitude of each noise source may vary and it is unclear which contribution is more relevant for total signal variability in every scenario. Usually when the object of study is the interaction between proteins, commonly expressed in abundant amounts, extrinsic noise is expected to have a more preponderant effect. By contrast, in gene layouts and mRNA interactions, with molecular numbers in much lower scales, intrinsic noise starts having a non-negligent contribution.

The inclusion of both types of noise has been introduced and compared in recent studies. One example was the switch-like activation of nuclear ERK under EGF stimulation. To understand these dynamics and the impact of noise on the all-or-none decision of activating nuclear ERK, an ODE model was built and both noise contributions were simulated. In this study the authors concluded that the observed experimental heterogeneity could be reproduced by imposing a CV=25% in protein initial quantities, a range compatible with experimentally determined protein variability in apoptosis. This result gave evidence for the role of extrinsic noise as the main source of variability in this system. Intrinsic noise input was found to be negligibly small for the abundance of the simulated proteins (Iwamoto et al., 2016). One important result of the same work was the finding that proteins participating in enzymatic reactions act as “sensitive nodes” of the network, contributing more pronouncedly to the generated output heterogeneity than the remaining proteins involved in simpler binding-

unbinding reactions. This evidence set for the first time the hypothesis that cells can use certain types of chemical interactions to control or amplify their underlying extrinsic noise.

Efforts to understand the allowed window of variability in intervening proteins and consequences for signal transmission are becoming a new trend in systems biology. In the context of the cell cycle, Bouhaddou and colleagues were able to correlate entry into S-phase in actively dividing cells with the initial levels of C-RAF and B-RAF proteins, therefore creating a metric for cell cycle progression. These two RAF isoforms are produced in relatively low amounts and are consequently subject to substantial intrinsic noise when expressed. Their noise level is amplified downstream by a positive feedback loop that results in an all-or-none activation switch of cJun, thereby forming a decision point for entry into S-phase. To simulate the natural variability in protein and mRNA numbers the authors performed simulations with intrinsic noise on an initial standard cell and let the molecular numbers fluctuate over a period of 24h simulation time. This technique is an approach to obtain a population of distinct cells, each with their own proteomic signature that can then be used as the model new set of initial conditions. In this way the authors could use the obtained distributions of protein levels to also infer the impact of extrinsic noise on the model output and observe threshold effects of the two RAF proteins isoforms on cell cycle progression (Bouhaddou et al., 2018).

In the field of apoptosis, the idea of obtaining a separating metric that can accurately predict the commitment into effective death is also receiving strong attention. It has been addressed that required levels of C8 activity for TRAIL-treated cells are necessary to properly engage cells into an apoptotic phenotype (Roux et al., 2015). Others suggested the mitochondria to be the central player of apoptosis, capable of modulating each cell individual time-of-death and the overall content of the cell apoptotic proteins (Márquez-Jurado et al., 2018). In this last result, the authors could observe that resistant and sensitive cells had clear differences in their mitochondrial numbers and a direct correlation was established between higher cellular mitochondrial content and an augmented probability of entry into apoptosis and reduced time-of-death. This defined a novel threshold for mitochondrial content, responsible for a range of variability in apoptotic protein numbers in the order of 50%, and established mitochondrial density as a new metric for prediction of resistance/sensitivity to apoptotic death (Márquez-Jurado et al., 2018).

Heterogeneity in the apoptosis signaling pathway

Apoptosis is a fascinating pathway to study due to its singular dynamics and long list of contributing agents. One of its underlying and most curious aspects is related to the heterogeneity of every cell decision to either engage, properly fulfill the pathway and commit to death, or to avoid the stimulus, consider the signal as spurious and remain alive. This property receives the name of "fractional-response" and describes the capacity of closely related cells (such as sister cells) to present distinct phenotypic outputs when exposed to the same stimulus.

The reason to explain "fractional-response" in the apoptosis signaling pathway arises from both extrinsic and intrinsic noise contributions causing every cell to be unique in terms of its biomolecular content. This behavior is observed even for saturating drug doses, showing that it is due to an intrinsic property of the system (Roux et al., 2015). When focusing exclusively on the population of sensitive cells (dead cells), a high degree of heterogeneity is nonetheless observed in every cell's time-of-death (Rehm et al., 2009; Spencer et al., 2009). Attention has been given to this phenomenon and nowadays the most accepted hypothesis is that variability in apoptotic protein levels is the main cause of dispersion in individual cell-fate response and in the distribution of time-of-death (Spencer et al., 2009).One argument supporting this idea resides on the fact that cells co-treated with cycloheximide and actinomycin D present an equivalent extent of variability on maximum C8 activity levels, excluding genetic contributions as the main cause for heterogeneity in the apoptotic response (figure 6).

Another evidence was presented by Spencer and colleagues that showed that sister cells who underwent a recent division cycle have similar times-of-death during a short initial period but synchrony is lost as the time post-division increases (Bhola and Simon, 2009; Rehm et al., 2009; Spencer et al., 2009). This supports the hypothesis that cell-to-cell differences in protein levels justify their time-of-death: recently divided cells who obtained similar protein content from the mother cell die synchronously. As time post-division increases, intrinsic noise acts on the cell and causes fluctuations in sister cells proteomic content, decorrelating their associated time-of-death (Sigal et al., 2006). The result was also confirmed through modeling. When changing protein initial conditions in the EARM1 model equations, the resulting distributions in time-of-death reproduced the experimental variability, setting extrinsic noise as the major contributor for cell's variability in the apoptotic response (Gaudet et al., 2012; Spencer et al., 2009). Furthermore, heterogeneity was found to derive mostly from the intervening proteins

upstream of the MOMP event, namely the quantity of expressed receptors, pC8 and the BCL-2 family agents setting a complex interplay between several molecular contributors (Albeck et al., 2008).

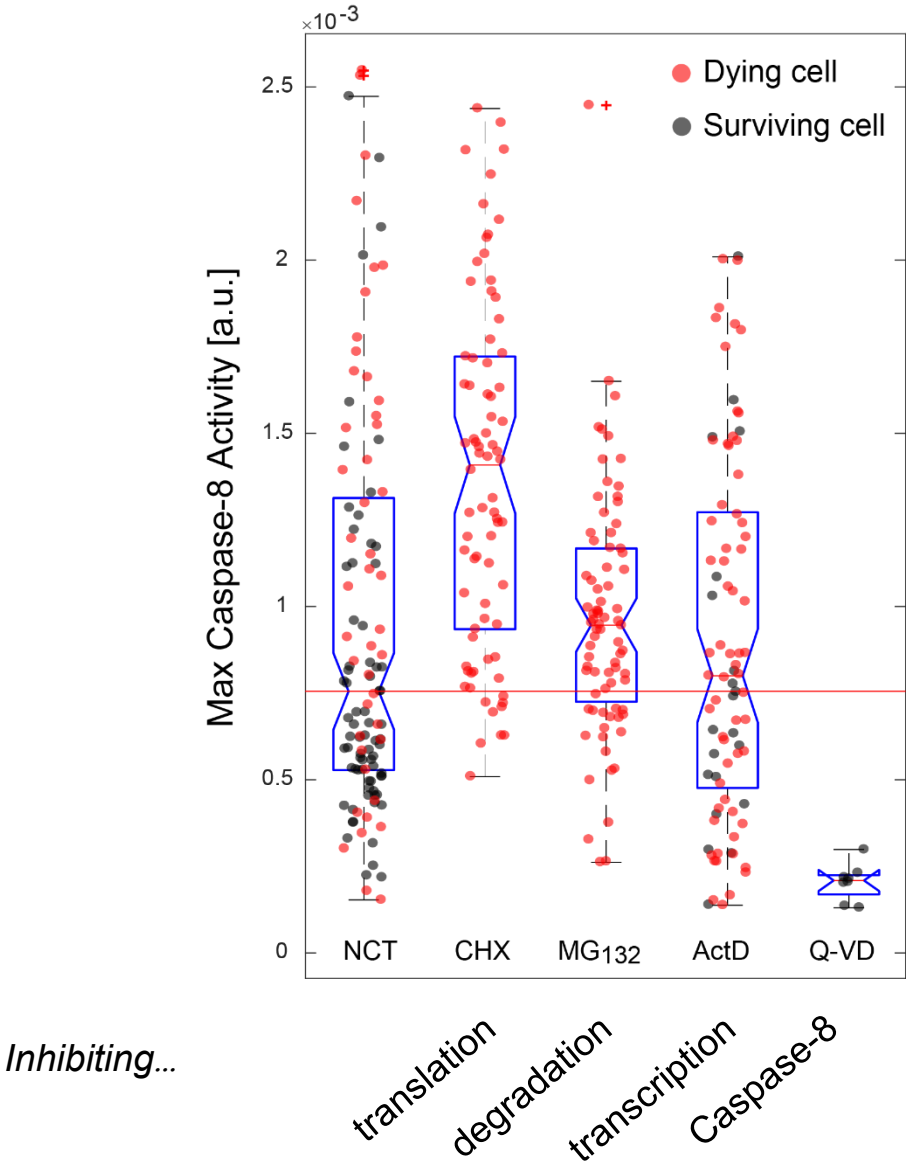

Figure 6. Variability on maximum C8 activity values for a population of HeLa Cells under different co-treatment scenarios.

Five different scenarios are represented. NCT refers to "normal condition treatment" and illustrates cells treated exclusively with the death-ligand TRAIL at 50 ng/ml. CHX indicates a co-treatment with cycloheximide, an inhibitor of protein synthesis. MG-132 is a non-specific inhibitor of protein degradation, ActD an inhibitor of RNA transcription and Q-VD a strong inhibitor of C8 activation. The first, third and fourth columns have similar distributions on the registered maximum C8 activity values, an argument that the contribution provided by the gene layer does not justify by itself the observed heterogeneity.

Heterogeneity on the reaction rates, a rational for non-reliability on the signaling reactions

When the network of proteins in a signaling pathway is not fully known or there are external events that may affect the cell volume, such as cell size increase along the cell cycle, one may consider variability on the reaction rates to justify scaling effects on the parameter values. This approach was used to study global noise effects on a gene expression model in bacteria and in cellular growth (Labhsetwar et al., 2013; Mori et al., 2016; Sherman et al., 2015) and in the analysis of p53 dynamics in intrinsic apoptosis (Ballweg et al., 2017). On one of these studies, Sherman and colleagues used a standard "telegraph-model" and included an extra non-intrinsic variability on mRNA and proteins, on both production and degradation rates, obtaining Gumbel-like distributions for the production of proteins. While varying the reaction rates, the resulting protein distributions acquired ranges that intrinsic noise alone could not provide. This approach was useful to discriminate unexplained noise sources but it required the solving of rather complicated mathematical expressions and the usage of simplifications that were very particular to that study, making it difficult to extrapolate to general scenarios (Sherman et al., 2015).

With this quick review on the different approaches used to simulate generic noise in biology, an emerging idea is that there is currently room for improvement and a concrete and unifying concept on how to simulate noise is still unavailable. Efforts on this field would be an undeniable contribution to both biology and medicine, providing more in-deep explanation for the always present heterogeneity in the cell universe. That would impact a considerable number of therapeutic approaches, namely in cancer, which demands more studies to understand the origins of cell-to-cell heterogeneity and to edify strategies to model its sources and the consequent emerging resistant phenotypes.

Chapter 2

Modeling receptor-ligand interactions for the extrinsic apoptosis pathway

"We built too many walls and not enough bridges"

- Isaac Newton

Many unanswered questions remain in apoptosis. Some of them relate to the regulatory mechanisms that control the passage or the inhibition of the signaling pathway in its several steps. This decision is made at innumerous points, starting by the number of activated receptors contributing to total DISC-created structures, followed by the rate and quantity of C8 activated molecules, competing quantities of Bcl-2 pro-survival and pro-apoptotic proteins, and many others. Determining the basis of the different and sequential threshold events requires a combination of adequate experimental data with explanatory system biology approaches.

Models of apoptosis are common and a summary list was provided in section 1.3.4. Some concern a whole-system approach (Albeck et al., 2008; Bertaux et al., 2014; Fussenegger et al., 2000) while others were more synthetic and oriented to a specific subset of the network (Chen et al., 2007a; Cui et al., 2008; Roux et al., 2015; Yin et al., 2017). The mathematical methods employed for the system analysis are also quite diverse. Some authors interpret threshold

events as a “first-passage time” problem (Ghusinga and Singh, 2019; Paek et al., 2016) associated to when a protein reaches a critical level for the first time. This methodology has been commonly supported by stochastic models of gene expression to account for noise contributions in threshold-crossing events. With these techniques, protein levels become variable and a distribution for “first passage time” is obtained, allowing the modelers to infer the type of feedback interactions that can decrease noise effect on the mean-value of these distributions. In particular, Ghusinga et Singh determined “buffering” strategies to filter noise depending if the relevant protein is stable or unstable. For stable long-lived proteins the inexistence of any feedback regulation seems to be the best scenario for the cell to control its molecular heterogeneity. When otherwise the protein is unstable, the presence of a positive feedback loop turns out to be the optimal strategy to increase the threshold-time accuracy (Ghusinga and Singh, 2019).

Big models assembling a multitude of interacting signaling pathways have also been emerging. With the goal of understanding the impact of a series of pathways in cancer and how they participate in the cell stochastic decision to proliferate or die, Bouhaddou and colleagues designed a model with a substantial network of proteins to unveil the origins of cell fate decision in cancer cells (Bouhaddou et al., 2018). Each of the model subnetworks was simplified and no conclusions were extracted about the agents controlling cell-fate decision. Nonetheless the work was an evidence that efforts to build robust and “complete” networks are rising despite the associated simulation challenges. The tendency for the incoming years is to increase network information and avoid over-simplified assumptions so that single-cell interpretations can be made.

Some of the most famous works in the apoptosis modelling field have focused their results in the BCL-2 family interactions and how a switch-like activation can be achieved during MOMP (Albeck et al., 2008). This switch-like activation is frequently considered a bistable result from which the cell can bifurcate between the branch of life or death (Bagci et al., 2006; Cui et al., 2008; Kolch et al., 2015; Legewie et al., 2006) but little attention has been given to the upstream reactions and their potential impact on cell-fate decision (Eissing et al., 2004).

In this project, a new model is proposed for the receptor-associated reactions of the extrinsic apoptosis pathway. The model gathers the set of reactions that start with TRAIL interaction with the complementary death-receptors, includes the formation of active DISC structures and finishes with the production of active C8 and subsequent cleavage of its substrate Bid. While

modeling this set of reactions the work tries to elucidate possible factors explaining the heterogeneity observed on C8 activity values in a previous work (Roux et al., 2015) and pinpoint differences on the receptor layer reactions that can distinguish resistant cells from sensitive cells. The mathematical formalism was chosen to be simple and reproducible by others and results from direct application of mass-action rate laws to the associated chemical events. This approach was chosen so that the contribution of all the considered molecular agents could be analyzed without simplified lumped parameters and "ad-hoc" mathematical expressions. In this way and using parameter rates in line with already published values, the dynamics of C8 activation, the role of FLIP as a strong anti-apoptotic protein, the increase in C8 activity for higher ligand valencies, among other known facts, were explicitly studied in a descriptive network that also permitted the inclusion of different noise sources so that a justification could be presented for the degree of heterogeneity observed in the extrinsic apoptosis signaling pathway. This and further modelling versions could take us one step closer to the elucidation of "fractional killing" and to the identification of its molecular determinants.

2.1 A network of reactions defining a model structure for the receptor layer of the extrinsic apoptosis network

Modelling TRAIL interactions

The literature concerning TRAIL, its structure and interaction modes with the death receptors is vast and not entirely clear. In this framework, TRAIL interactions with the death receptors were assumed to occur exclusively among TRAIL and monomeric receptors. Interactions between TRAIL and already formed dimeric or trimeric receptors could have been considered but recent findings suggest that dimeric and trimeric pre-established configurations do not contribute to the apoptotic signaling response (Liesche et al., 2018). Following this idea, TRAIL is presumed to react with a single receptor molecule in a reversible manner according to,

$$\mathrm{TRAIL} + \mathrm{R} \leftrightarrow \mathrm{TRAIL{:}\,R} \qquad \textit{(complex monomerization)}$$

TRAIL is also administrated in a pulse-like way so that the initial number of molecules of TRAIL are not re-introduced in the system and the initial quantity decays while reacting with the existing monomeric receptors in the cell membrane. TRAIL synthesis rate is then set to zero.

Modelling TRAIL-receptor interactions

Amid the four classes of death-receptors mentioned in section 1.2.2, just one hypothetic receptor class was considered in the model reactions. This class referred to the DR4/DR5 receptors which were grouped and modelled as a single class R, given their equivalent pro-apoptotic role. The decoy receptors were not incorporated due to their scarce proportion in the cell membrane (Zhang et al., 2000).

TRAIL ligand interacts with an increasing number of receptors according to the next rules,

$$\text{TRAIL: R} + \text{R} \leftrightarrow \text{TRAIL: 2R} \qquad \textit{(complex dimerization)}$$

$$\text{TRAIL: 2R} + \text{R} \leftrightarrow \text{TRAIL: 3R} \qquad \textit{(complex trimerization)}$$

$$\rightarrow \text{R} \qquad \textit{(R-protein synthesis)}$$

$$\text{R} \rightarrow \qquad \textit{(R-protein degradation)}$$

All reactions are reversible to account for attachment and detachment events and delays between TRAIL exposure and the formation of an active death-ligand-three-receptor complex. The R protein is a natural component of the cell membrane and it is assumed to be constitutively produced and degraded by the cell.

Modelling DISC events

A considerable number of reactions are important to study at this point. The inclusion of the pro-caspases and the FLIP molecules into the receptor complexes is essential to gather both pro-apoptotic and anti-apoptotic effects taking place at the DISC structure and evaluate their overall contributions to the propagation or filtering of the apoptotic signal. For that matter, a simplification of nomenclature is first applied and the only modelled pro-caspase was pC8. Some authors defend that pC8 and pC10 share an equivalent pro-apoptotic role while others

place the last as an anti-apoptotic agent (Horn et al., 2017). To avoid introducing unclear dynamics, pC10 was removed from the modelling approach. As for FADD, its participation in the model reactions was also discarded and instead it was assumed that each receptor can attach one pC8 or FLIP molecule per binding site, permitting a better quantification of the number of attached molecules into the DISC unit. When two pC8 molecules connect to the DISC the minimum structure is gathered to produce an active C8, independently if it contains additional FLIP molecules or not. The next set of reactions summarizes the above considerations:

$$\mathrm{TRAIL{:}\ 2R} + \mathrm{n1} * \mathrm{pC8} + \mathrm{m1} * \mathrm{FLIP} \rightarrow \mathrm{TRAIL{:}\ 2R{:}\ n1pC8{:}\ m1FLIP}$$

(Addition of pC8 and/or FLIP to a dimeric complex)

$$\mathrm{TRAIL{:}\ 3R} + \mathrm{n2} * \mathrm{pC8} + \mathrm{m2} * \mathrm{FLIP} \rightarrow \mathrm{TRAIL{:}\ 3R{:}\ n2pC8{:}\ m2FLIP}$$

(Addition of pC8 and/or FLIP to a trimeric complex)

$\rightarrow \mathrm{pC8}$ *(synthesis of pro-caspase)*

$\rightarrow \mathrm{FLIP}$ *(synthesis of FLIP)*

$\mathrm{pC8} \rightarrow$ *(degradation of pro-caspase)*

$\mathrm{FLIP} \rightarrow$ *(degradation of FLIP)*

The integers n1, m1, n2, m2 are stoichiometric constants defining the number of pC8 or FLIP molecules attaching to the respective complex. Their values can assume the quantities (n1,m1)={0,1,2} and (n2,m2)={0,1,2,3} , with (n1 + m1) = {1,2}, and (n2 + m2) = {1,2,3}. Dimeric and trimeric complexes cannot attach more than two or three molecules, respectively. Different possible combinations of n1, m1, n2 and m2 generate a vast number of complexes that do not contribute to the propagation of the apoptotic signal and are thus capable of creating non-negligible delays on the response of the system.

Modelling C8 production

The dynamics of C8 were detailly included in the model as this is one of the new points that distinguishes the current approach from previous models. C8 activation occurs when two contiguous pC8 molecules interact and inter-promote the cleavage of each other's DED domains (de Miguel et al., 2016; Dickens et al., 2012; Horn et al., 2017). While this is simple for a dimeric ligand with two attached receptors, where two pC8 molecules link directly with two receptor sites to form an active C8 molecule, in the case of a trimeric ligand its exact dynamics are not precisely known (Wajant, 2019). Here it is assumed that for a ligand with valency **n**, higher than 2, a total of ${}_{2}^{n}C$ receptor site combinations can be used to produce a functional C8 molecule.

Combining the interplay of FLIP as an inhibitor of apoptosis and the fact that two pC8 molecules should effectively bind to form an active C8, the next set of reactions define the only possible pathways culminating with C8 activation under a trimeric ligand stimulus, such as TRAIL.

$$\mathrm{TRAIL{:}\ 2R} + \mathrm{pC8} \leftrightarrow \mathrm{TRAIL{:}\ 2R{:}\ pC8}$$

$$\mathrm{TRAIL{:}\ 2R{:}\ pC8} + \mathrm{pC8} \leftrightarrow \mathrm{TRAIL{:}\ 2R{:}\ 2pC8}$$

$$\mathrm{TRAIL{:}\ 2R{:}\ 2pC8} \leftrightarrow \mathrm{TRAIL{:}\ 2R} + \mathrm{C8}$$

(C8 production in a dimeric receptor-valid conformation)

$$\mathrm{TRAIL{:}\ 3R} + \mathrm{pC8} \leftrightarrow \mathrm{TRAIL{:}\ 3R{:}\ pC8}$$

$$\mathrm{TRAIL{:}\ 3R{:}\ pC8} + \mathrm{pC8} \leftrightarrow \mathrm{TRAIL{:}\ 3R{:}\ 2pC8}$$

$$\mathrm{TRAIL{:}\ 3R{:}\ 2pC8} \leftrightarrow \mathrm{TRAIL{:}\ 3R} + \mathrm{C8}$$

(C8 production in a trimeric receptor-valid conformation)

$$\mathrm{TRAIL{:}\,3R} + \mathrm{FLIP} \leftrightarrow \mathrm{TRAIL{:}\,3R{:}\,FLIP}$$

$$\mathrm{TRAIL{:}\,3R{:}\,FLIP} + \mathrm{pC8} \leftrightarrow \mathrm{TRAIL{:}\,3R{:}\,FLIP{:}\,pC8}$$

$$\mathrm{TRAIL{:}\,3R{:}\,FLIP{:}\,pC8} + \mathrm{pC8} \leftrightarrow \mathrm{TRAIL{:}\,3R{:}\,FLIP{:}\,2pC8}$$

$$\mathrm{TRAIL{:}\,3R{:}\,FLIP{:}\,2pC8} \leftrightarrow \mathrm{TRAIL{:}\,3R{:}\,FLIP} + \mathrm{C8}$$

(C8 production in a trimeric receptor-valid conformation)

No more than one FLIP molecule can attach to the trimeric configuration, otherwise there is not enough free receptor sites to bind two pC8 molecules and generate an active C8 protein.

Modelling C8 interactions

The model proposed for this project does not include downstream reactions after the C8 cleavage of its substrate Bid and as so the dynamics of the Bcl-2 like family members were not considered. In the available experimental data set a fluorescent probe was used as a method to follow the C8 dynamics in time, which in the model reactions is represented as the molecule FP. This probe is built artificially to contain a protein structure similar to Bid, so that it can also be targeted and cleaved by C8 and return an emission signal in its cleaved form, here represented by cFP.

$$\mathrm{C8} + \mathrm{Bid} \rightarrow \mathrm{C8} + \mathrm{tBid} \qquad (\textit{C8 cleavage of Bid})$$

$$\mathrm{C8} + \mathrm{FP} \rightarrow \mathrm{C8} + \mathrm{cFP} \qquad (\textit{C8 cleavage of FP})$$

The two processes were simulated as having equal reaction rates since both Bid and FP contain equivalent protein structures and, intuitively, their interaction with C8 should occur at a similar pace.

In figure 7 a summary of the most important molecular products participating in the simulated network of reactions is represented.

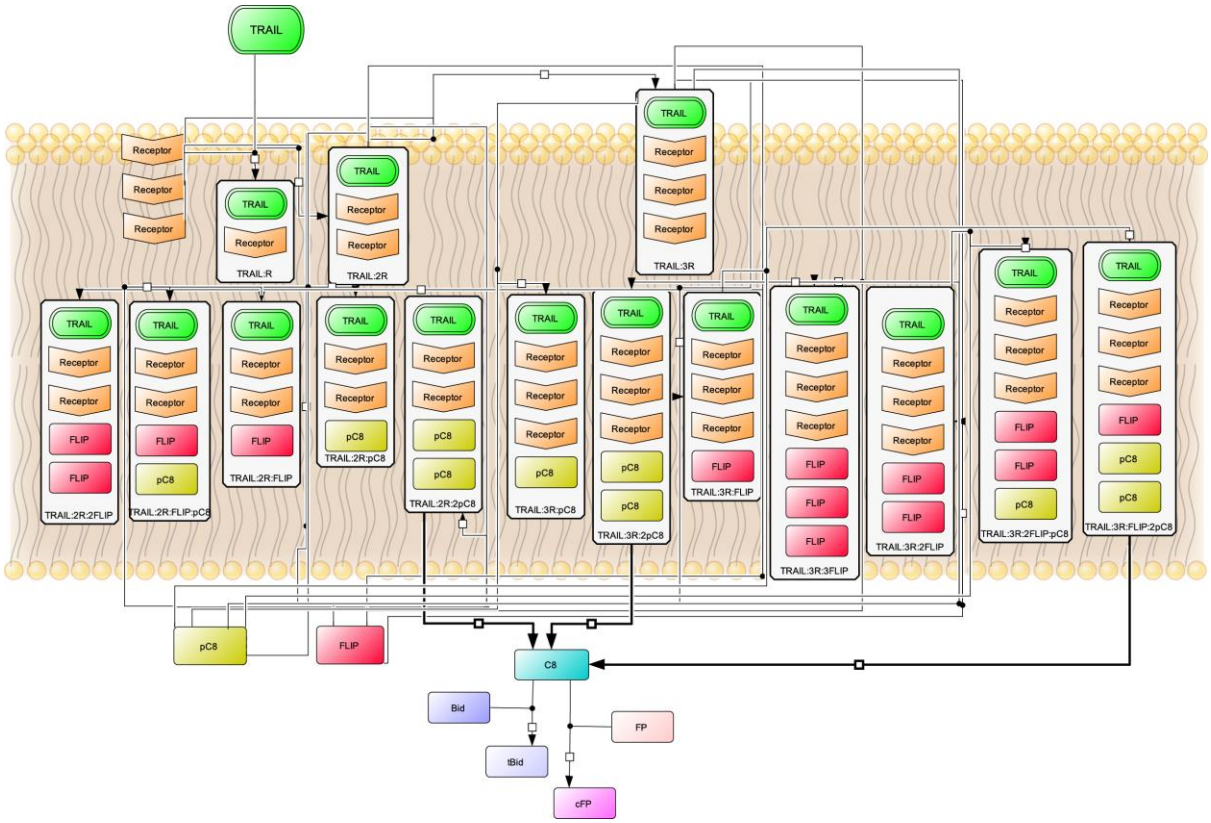

Figure 7. Network structure for the modeled receptor-reactions in the extrinsic apoptosis pathway. TRAIL interacts with death-receptors, giving rise to monomeric, dimeric and trimeric TRAIL-Receptor structures. In each form, pC8 and FLIP can attach to the available number of docking sites and produce intermediate complexes. When a structure contains two interacting pC8 molecules, an active C8 is generated that then cleaves Bid and FP to tBid and cFP, respectively. Green boxes: TRAIL; Orange boxes: Receptor; Red boxes: FLIP; Pallid Green boxes: pC8; Blue boxes: C8; Purple boxes: Bid; Pallid purple boxes: tBid; Pallid pink boxes: FP; Pink boxes: cFP.

2.2 Available Experimental data

All the results concerning this thesis were obtained by matching generated model outputs against an extensive data set of HeLa Cells available in the work of (Roux et al., 2015). The data contemplated several treatment scenarios with cells administrated with TRAIL drug doses of 2.5 ng/ml, 5 ng/ml, 10 ng/ml, 25 ng/ml , 50 ng/ml , 100 ng/ml , 250 ng/ml and 500 ng/ml. Multiple co-drugging treatments were also available in the data set. Even though the full data set was rich in its case-by-case description, the focus of this thesis was the subset of single-cell trajectories at the specific dose treatment of TRAIL at 50 ng/ml. The decision came directly from the opportunity to perform direct comparisons with other modeling approaches also conducted at this ligand concentration, such as the EARM1 model (Albeck et al., 2008). A chance then stands for future projects to later extend this analysis to other ligand concentrations and eventually include the remaining scenarios of the data-set.

The data consisted on single-cell time course trajectories displaying a fluorescence emission signal throughout a 10-hour experiment duration, each data point separated from the previous by an interval time frame of 5 min duration. The fluorescence signal, named FRET, followed a previous molecular construction approach proposed by others (Albeck et al., 2008) and returned the ratio emitted by a molecular probe in its cleaved form relative to its signal in its uncleaved form. The probe is composed of a protein sequence similar to Bid, a substrate of C8, and acts as a decoy molecule and a direct reporter of C8 activity in time. To include information about the survival fraction of the population, all the cells were also identified at the end of the experiment as either resistant or sensitive, allowing for relationships to be established between cell-fate decision and C8 activity.

The general features of every single cell signal are described in figure 8. Resistant cells remained alive for the full-time length of the treatment and are defined by a complete sigmoidal shape curve with a delay-phase, an exponential growing phase and a stationary phase. Sensitive cells do not present the stationary phase, since cells perished, and the correspondent signal finishes before the end of the treatment.

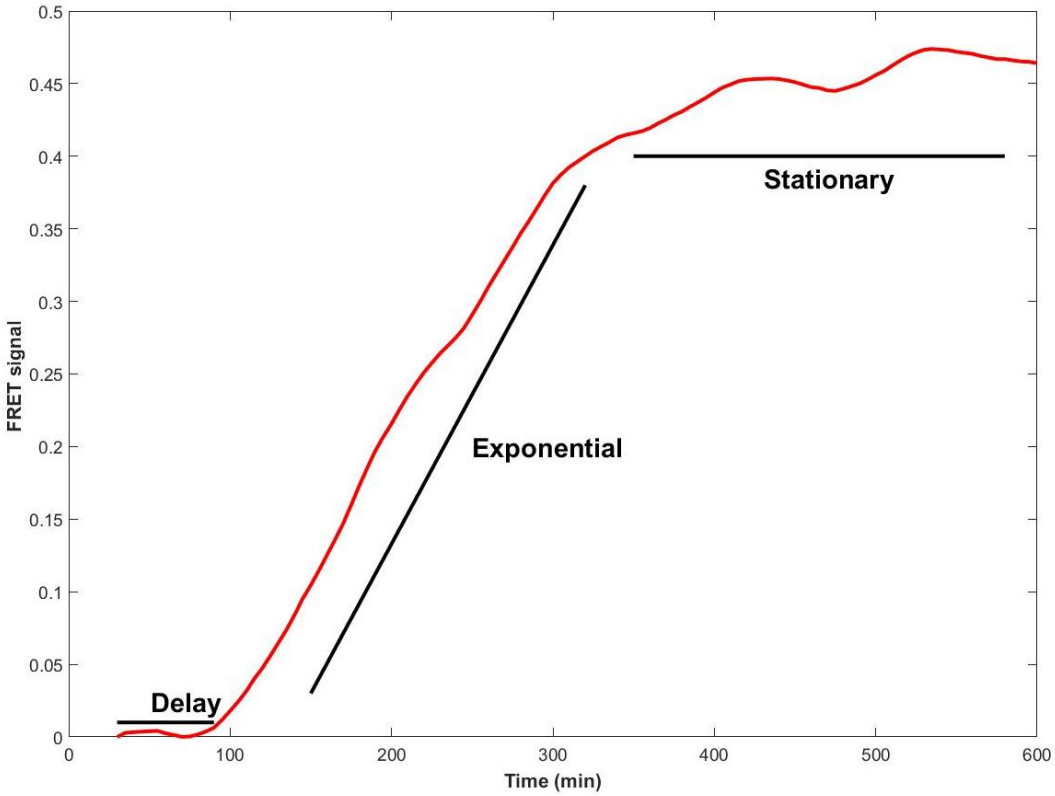

Figure 8. General features of the FRET-signal of an arbitrary cell.

Three main features can be distinguished: delay, exponential and stationary phases. The delay-phase corresponds to a residual signal where just a few fraction of the fluorescent probe molecules were cleaved by a still low number of C8 molecules. The exponential phase reflects an abrupt increase in C8 levels and a consequent pronounced increase in FRET signal. The stationary phase refers to the saturation and/or exhaustion of C8 molecules, lending the FRET signal into a stationary value.

When studying the cell population signal it is possible to confirm that, in average, the exponential phase for the sensitive population is more pronounced, consistent with section 1.2.4, where the sensitive population is expected to attain higher C8 activity values. To illustrate this effect, the signal in time for the entire cell population was assembled in sensitive and resistant populations and represented in figure 9.

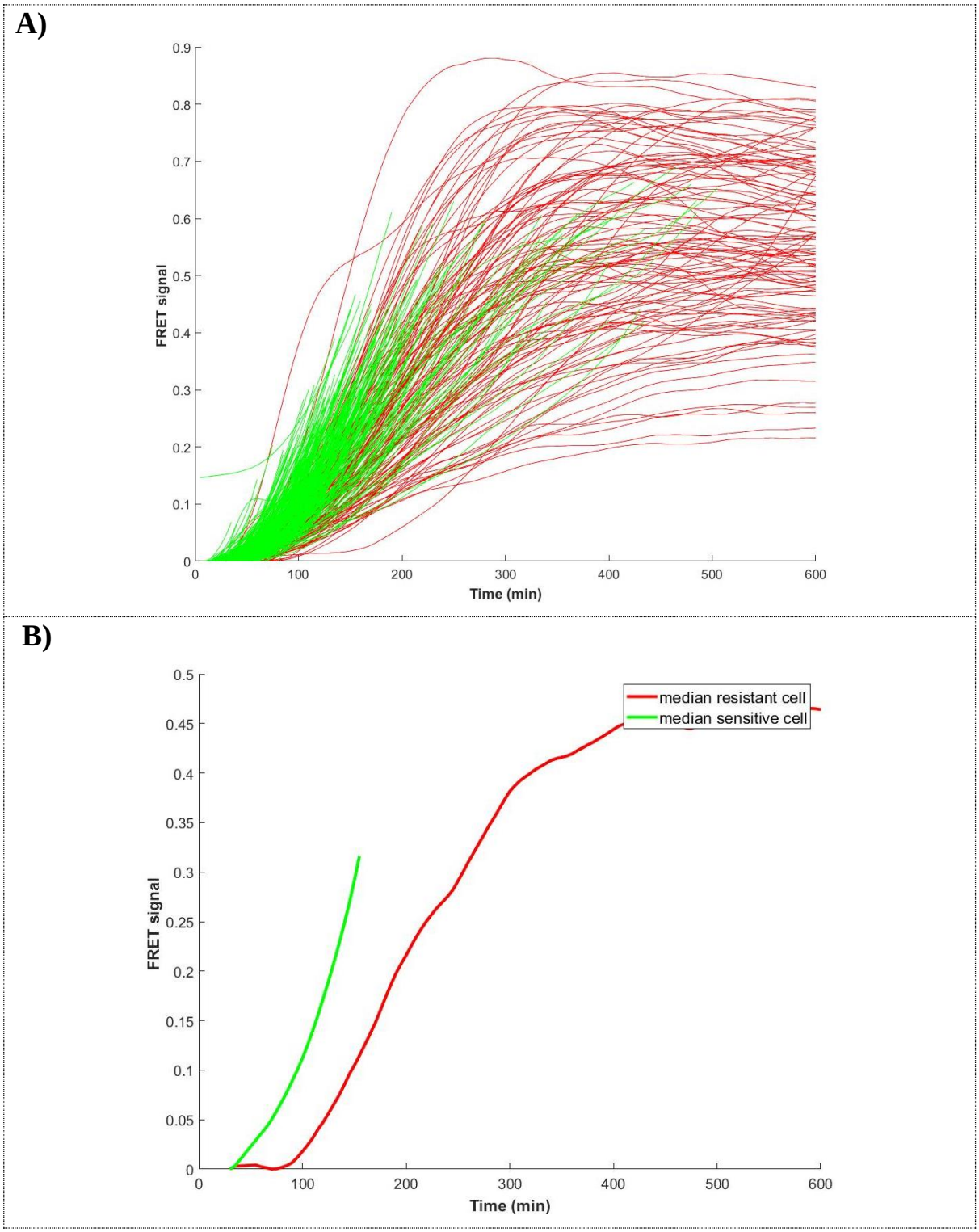

Figure 9. Signal in time of the cell population for a TRAIL treatment of 50ng/ml.

(A) The collection of cell trajectories in the data set is represented in two colors. Red trajectories refer to resistant cells, cells that remain alive ten hours after the treatment. Green trajectories represent sensitive cells, cells that respond to the treatment and died before the ten hours' time frame. **(B)** Evolution in time for the median resistant cell and for the median sensitive cell. The median sensitive cell has a more pronounced exponential phase, showing a higher mean C8 activity for this cell group.

Considering the results of figure 9 each cell was studied in terms of its maximum slope value in the exponential phase and how that value integrated or diverged from the remaining values inside the same phenotype group and in the opposing phenotype group. The first step was to assure compatibility between the model output and the experimental data units. The FRET signal in time of every single-cell was the result of a fluorescent emission signal captured by a microscope and had to be translated into the absolute number of cleaved cFP molecules. This conversion required some mathematical formalism explained in detail in section 2.3.

To keep coherence with previous models the parameter values representing reaction rates were kept as close as possible to already published values. Among the long list of models of section 1.3.4, the EARM1 model of Albeck and colleagues had the largest available list of parameters and was therefore chosen as the reference for the majority of the parameter's values. An adjustment of units was nonetheless necessary. The non-zero protein initial conditions in this work are given in absolute number of molecules, different from the units of molecules/cytosolic compartment in Albeck's model. To adjust both units the a-priori knowledge of the "*cytosolic compartment*" (CC) was essential. A cell compartment in Albeck's model relates to the proportion of the whole-cell volume occupied by the specific compartment where the protein lies inside the cell. This fraction of the whole cell volume is not explicit in EARM1's supplementary data but allows one to determinate the necessary *CC* factor. Defining molecules/cell compartment by the abbreviation *mol_per_CC* the following series of operations return the *CC* factor,

$$mol\_per\_CC = \frac{molecules}{CC} \Leftrightarrow molecules = CC * mol\_per\_CC \quad \textbf{(1)}$$

$$M = \frac{mol}{V} \quad \Leftrightarrow \quad M = \frac{molecules}{V*N_A} \quad \textbf{(2)}$$

By joining **(1)** and **(2)**,

$$M = \frac{CC * mol\_per\_CC}{V*N_A} \quad \Leftrightarrow \quad CC = \frac{M*V*N_A}{mol\_per\_CC} \quad \textbf{(3)}$$

In **(3)**, *M* defines the molar concentration, *mol* the number of moles in a volume *V* of the cell and N_A the Avogadro's number $6 * 10^{23}$ particles/mol. The *CC* factor is directly obtained

by replacing the values in table 2, extracted from Albeck's supplementary table S5 (Albeck et al., 2008), into **(3)** .

Table 2. Values extracted from EARM1's supplementary table S5 in order to calculate the Cytosolic volume factor.

State variable	Model IC (mol_per_CC)	Model IC (M)	Cell Volume (V)
[L]	$3 * 10^3$	$5.1 * 10^{-9} = 50\ ng/ml$	$10^{-12}\ l$

* IC stands for initial condition; "L" is the ligand molecule TRAIL

$$CC = \frac{5.1*10^{-9}*10^{-12}*6*10^{23}}{3*10^3} \approx 1.02 \quad \textbf{(4)}$$

Given that the value of *CC* is remarkably close to the unity the decision was to use units of molecules/CC simply as molecules without further inter-conversions.

2.3 Conversion of FRET-signal into number of ICRP-cleaved molecules

To convert the fluorescence (or Förster) resonance energy transfer (FRET) signal of each single-cell into the corresponding number of cleaved initiator caspase FRET reporter molecules (abbreviated ICRP) a method was followed from (Birtwistle et al., 2011). In their work, expressions were presented for the FRET donor and FRET acceptor channels in different microscopy emission scenarios that related fraction of emission signal from direct fluorescent protein excitation and FRET-induced emission signal. For the used data-set of (Roux et al 2015), with the general signal landscape represented in figure 8, the received signal in time *FRET-ratio (t)* results from the division of two quantities:

$$FRET - ratio(t) = FR(t) = \frac{CFP{-}signal(t)}{FRET{-}signal(t)} \quad \textbf{(5)}$$

The *CFP(t)-signal* relates to the direct emission of the excited Cyan Fluorescent Protein. The *FRET-signal (t)* is instead the emission of the FRET acceptor, here Yellow fluorescent protein (YFP), to which the FRET donor, here excited CFP, transferred its excitation energy. As long as the initiator caspase FRET reporter remained uncleaved, with CFP neighboring

YFP, the *CFP-signal(t)* was minimized and the *FRET-signal(t)* was maximized. After the onset of C8 activation the proportion of still bound CFP-YFP decreased and the *FRET-ratio(t)* rose due to the joint effects of loss in CFP quenching (*CFP-signal(t)* increase) accompanied by loss in FRET (a *FRET-signal(t)* decrease).

A technique to convert the *FRET-ratio(t)* into number of cleaved ICRP molecules is to use the equations provided by Birtwistle and colleagues under the context of how the fluorescent probes interacted in this experimental construction. Considering that the *CFP-signal(t)* was the donor channel output after direct excitation of the donor channel and the *FRET-signal(t)* the acceptor channel output due to excitation of the donor channel, **(5)** can immediately be re-written in a form that agrees with the nomenclature of Birtwistle et al, where I_D^{don} is the intensity in the donor channel after donor channel excitation and I_A^{don} the intensity in the acceptor channel after donor channel excitation (Birtwistle et al., 2011).

$$FR(t) = \frac{CFP-signal(t)}{FRET-signal(t)} = \frac{I_D^{don}}{I_A^{don}} \quad \textbf{(6)}$$

In line with the same work, **(6)** can be further extended into **(7)** using the equations 7) and 9) present in the work of (Birtwistle et al., 2011).

$$\frac{I_D^{don}}{I_A^{don}} = \frac{N_D^*(1-E\varphi_F)f_{DD}}{N_D^*E\varphi_F f_{AA} + N_D^*(1-E\varphi_F)f_{AD}} \quad \textbf{(7)}$$

Given that $N_D^*E\varphi_F$ stands for the fraction of donor molecules contributing for FRET signal, which in this case refers to the number of non-cleaved fluorescent probes FP(t), and $N_D^*(1-E\varphi_F)$ defines the number of already cleaved fluorescent probes ICRP(t), **(7)** can be adjusted into a more readable form,

$$\frac{I_D^{don}}{I_A^{don}} = \frac{ICRP(t)f_{DD}}{FP(t)f_{AA} + ICRP(t)f_{AD}} \quad \textbf{(8)}$$

It is worth mentioning that the conversion of **(7)** into **(8)** assumed the approximation $E \approx 1$, where E refers to the FRET efficiency of every donor molecule. With $E = 1$ it is hypothesized that every fluorescent probe molecule in the binding form CFP-YFP is capable of inducing FRET, which might seem restrictive and even unrealistic in some experimental scenarios. In the specific case of the data-set at hand an argument supporting this approximation

comes from the posT-treatment applied on the raw *FR(t)* signal. All the *FR(t)* trajectories were subtracted by their initial value *FR(0)* so that each cell-signal started at zero. As a consequence, the increase in *FR(t)* signal reflected the contribution of newly cleaved ICRP(t) probes corresponding to the term $N_D^*(1 - E\varphi_F)$. In this case $N_D^* E\varphi_F$ will be the not-yet cleaved fluorescent probes FP(t) and the same proportions are obtained for the cleaved and non-cleaved probes as those deduced if assuming $E = 1$.

If one excludes the degradation of the probes during the time frame of the experiments a conservation law can be written, where the initial number of bound fluorescent probes $FP(0)$ is conserved among the total of cleaved $ICRP(t)$ and uncleaved forms $FP(t)$.

$$ICRP(t) + FP(t) = FP(0) \quad \textbf{(9)}$$

By replacing **(9)** into **(8)** ,

$$FR(t) = \frac{ICRP(t) f_{DD}}{[FP(0) - ICRP(t)] f_{AA} + ICRP(t) f_{AD}} \quad \textbf{(10)}$$

and finally solving **(10)** in order to $ICRP(t)$ returns **(11)**, which can be simplified into **(12)** with the approximations $\frac{f_{DD}}{f_{AA}} \approx 1$ and $\frac{f_{AD}}{f_{AA}} \approx 0$. The parameters f_{AA} and f_{AD} represent the fractions of the acceptor and donor emissions exclusively captured by the acceptor channel, respectively, and f_{DD} stands for the fraction of the donor emission captured by the donor channel. The first ratio $\frac{f_{DD}}{f_{AA}}$ can be easily tuned by the user and as explained by Birtwistle and his colleagues in page 4 of their work, setting this ratio to the unity is a valid approximation (Birtwistle et al., 2011). The second ratio $\frac{f_{AD}}{f_{AA}}$ is expected to be very small as the crosstalk of photons between different channels should be inferior to the number of photons emitted and received inside the same channel.

$$ICRP(t) = \frac{FP(0) * FR(t)}{\frac{f_{DD}}{f_{AA}} + FR(t)\left[1 - \frac{f_{AD}}{f_{AA}}\right]} \quad \textbf{(11)}$$

$$ICRP(t) = FP(0) * \frac{FR(t)}{1 + FR(t)} \quad \textbf{(12)}$$

With **(12)** one can relate the fluorescent ratio in time *FR(t)* with the effective number of cleaved fluorescent proteins *ICRP(t)*, for a given initial quantity of uncleaved fluorescent protein *FP(0)*. *ICRP(t)* in units of molecules can then be used as input in a set of ODE's for fitting purposes, adjusting the output units between the model (density of molecules) and the experimental trajectories [FRET (FR) signal]. In the following sections the ICRP molecules are denoted as cFP, a simplified nomenclature to refer to *cleaved fluorescent protein*.

2.4 ARROM1: Initial conditions and parameter values

ODE equations resulting from mass action rate laws need both initial conditions and reaction rates to be fully-known in order to perform a model simulation. In the model hereby presented, the initial conditions referred to a vector-list including a total of twenty-eight protein species (signaling proteins in section 2.1 plus intermediate complexes). This vector, altogether with seventy-six parameters defined the model in its original form. This initial version was named "Apoptosis receptor reaction ODE model-version 1" (ARROM1) and the choice to implement it in the form of an ODE modeling approach resulted from the goal of actively simulating the time-course dynamics of all the proteins in section 2.1. The law of mass action allows for a detailed description of the binding and dissociation reactions between molecular species, taking into account the stoichiometry of the different molecules that participate in each reaction. This framework provides a more realistic way to model the steps following TRAIL - receptor binding.

Given that some of the seventy-six parameter values of ARROM1 were not available in the literature, some simplifications were made at the level of the enzymatic reactions. These were grouped according to the similarity of the interacting proteins. All forward and reverse reactions adding or removing FLIP from a complex with equal number of receptors were given the same reaction rates. The exact same principle was applied for pC8: three groups for the forward reactions and three groups for the reverse reactions, each group referring to a number of receptors from one to three. These simplifications, although small, led to a simpler model version, now with thirty-two parameters. The tables A1.1 and A1.2 in Appendix 1 contain the full list of averaged initial conditions along with the parameter values used as *initial_guess* to run the model simulations.

All the fittings to the ARROM1 model were executed by means of the MATLAB fitting algorithm *fminsearchbnd* with imposed boundaries. The algorithm searches for a combination

of parameter values that minimizes the objective function defined by the user, here the squared difference between the cFP(t) model output and the experimental trajectory. This command differs from the standard *fminsearch* command by allowing the user to set lower and upper boundaries on the landscape of possible fitted parameter vectors proposed by the algorithm and is available to download from the Mathworks file exchange webpage. The fitting changed the vector of initial conditions and reaction rates in table A1.1 and A1.2 in such a way that variations were constrained as much as possible to maintain the magnitudes similar to those of the *initial_guess*.

2.5 ARROM2: a ligand-receptor model with an extra set of proposed reactions

ARROM1 assumes a rich description of the reactions occurring in the receptor layer of the extrinsic apoptosis pathway. The first test was to check if the model was capable of fitting a *median_cell* trajectory without changing the parameter values indicated in table A1.2. Here, the *median_cell* was the cell with the median maximum slope value of the whole cell population and its trajectory can be seen as a "median" behavior of the C8-apoptotic signal in HeLa cells when treated with TRAIL at 50 ng/ml. This test validates if initial condition variation, using the protein values in table A1.1 as *initial_guess*, was sufficient to reproduce the *median_cell* FRET-signal. The resulting fit was poor and the vector of parameters in table A1.2 had to be included in the fit and allowed to vary. Different *initial_guess* vectors were tested in the surrounding 100-fold vicinity, by scaling each *initial_guess* entry by a random assigned-value in the interval [0.1: 10], and the obtained fit was equally poor proving the need to include higher parameter variability.

Since some parameter rates are unknown and no certainty exists on the magnitude of their values, the *fminsearchbnd* algorithm was allowed to perform a fit to the *median_cell* while changing the ARROM1 model parameters inside a bounded interval [1/factor; factor]**parameter_values_initial_guess*, with factor=10000 (*parameter_values_initial_guess* defines the vector of parameters in table A1.2). This approach gave a very large margin for the fitting algorithm to check for different parameter combinations that could provide a good fit. The produced fit was very proximal to the *median_cell* experimental trajectory (figure 10). The differences between the *parameter_values_initial_guess* and the parameter values obtained

after the fit were analyzed and assigned to three clusters depending on the scale of their relative deviations. These values are listed in Appendix 2, table A2.1.

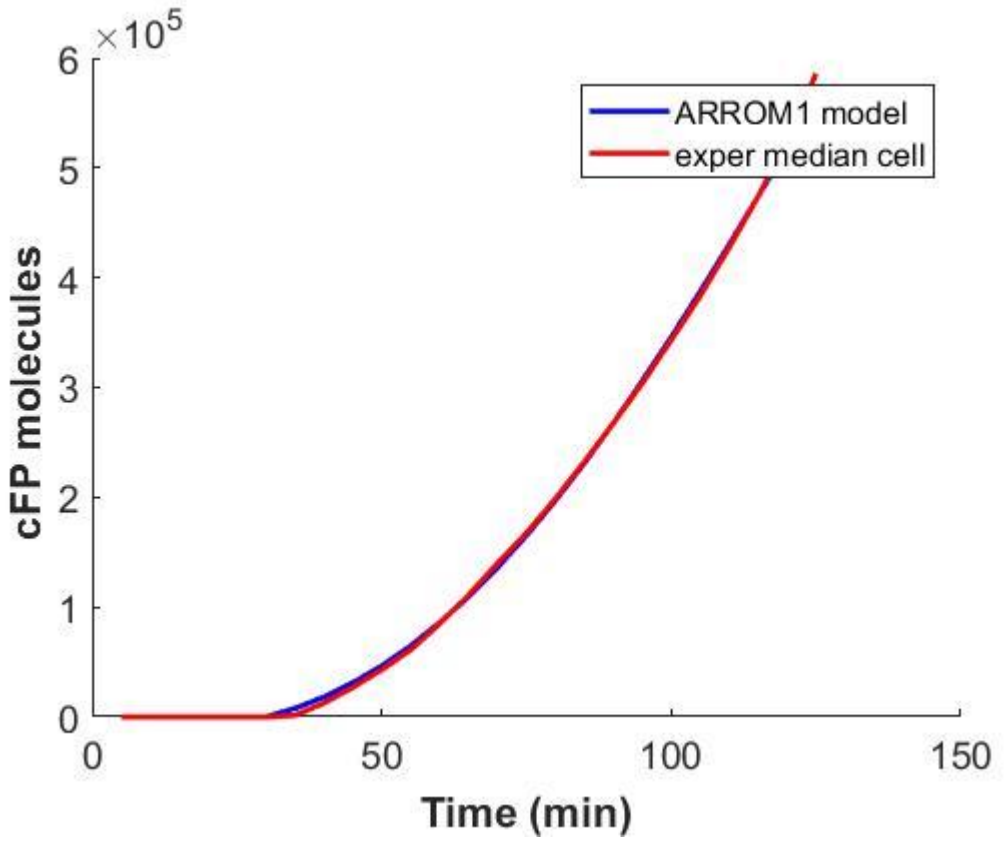

Figure 10. Fitting the median_cell of the HeLa-cell population treated with TRAIL at 50ng/ml.
In red, the *median-cell* of the experimental data set. In blue, the output of the ARROM1 model when fitting both initial conditions and parameter values to the *median_cell*. The model returned a residual value of 7.4e4 molecules, one order of magnitude lower than the maximum attained value for cFP molecules, proving the quality of the fit (Here the residual value refers to the sum of squared differences between the cFP model output and the median experimental trajectory).

The *parameter_values_initial_guess* changed substantially after fitting the ARROM1 model to the *median_cell* trajectory. Focusing on the parameters with relative deviations superior to one-hundred (table A2.1) their effective contributions to the model output can be tested by means of a recent algorithm proposed by (Casagranda et al., 2018). This method essentially weights each differential equation term and erases terms with percentage contributions lower than a chosen threshold-value. Setting a value of 10% for this threshold and consequently eliminating all the terms with lower contributions in time, only the parameters [2, 4, 6, 16] stood out with higher than threshold values. The figures 11-14 show the decision analysis for the parameter [2, 4, 6, 16] altogether with the contribution in time for

all the remaining terms in the differential equations in which they participate. All the ARROM1 model equations are available in Appendix 4 of this manuscript.

Parameter 2 = k2

A)

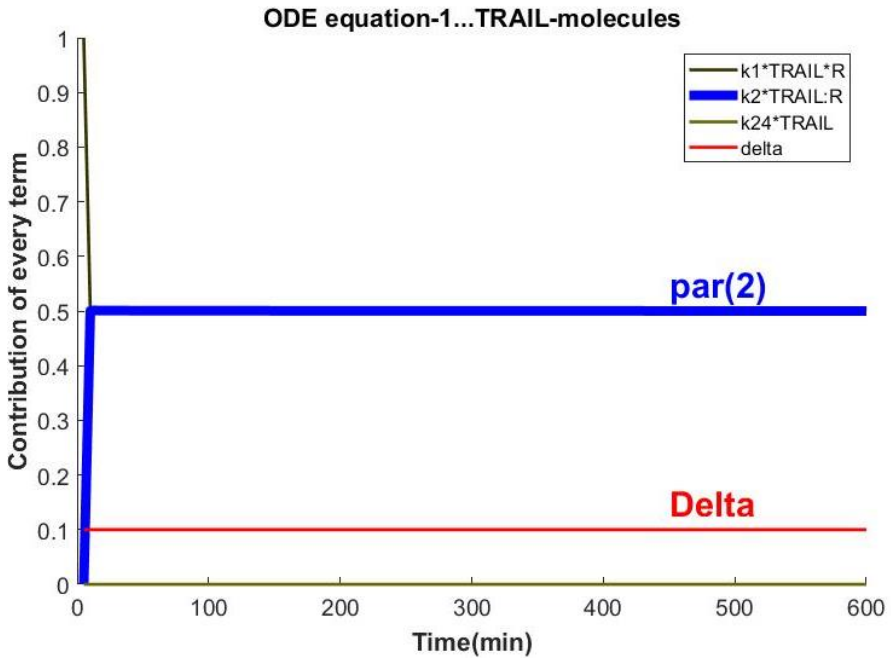

B)

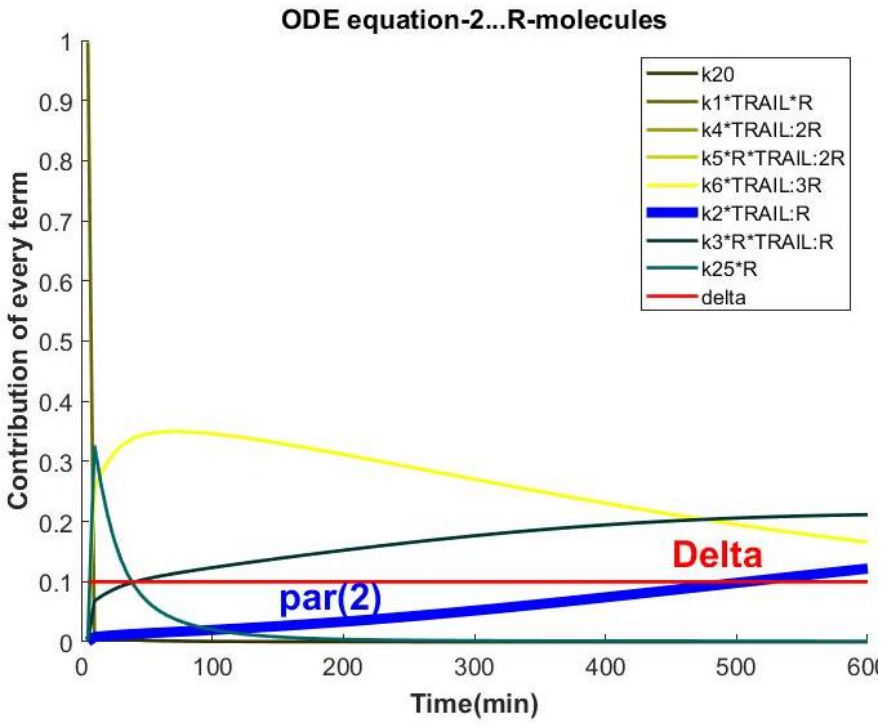

C)

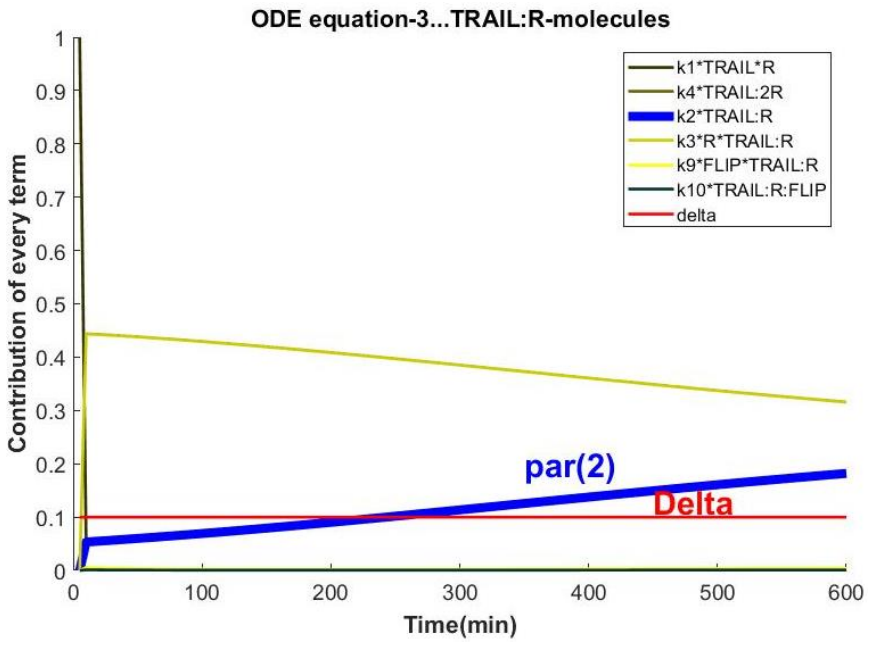

Figure 11. Most contributing terms in the ARROM1 model for the set of ODE equations where k2 intervenes. The vector of parameters used to run the simulation results from the fit of ARROM1 model to the *median_cell* trajectory.

Representation of the relative contribution in time for all the terms in the ODE equation 1, 2 and 3 of the ARROM1 model. In each figure, the value of the threshold is represented in red by delta=0.1. The contribution in time highlighted in bold blue illustrates the term with k2. In the plots **A)**, **B)** and **C)** the differential equation term with k2 has either a predominant contribution (plot-A) or an increasing contribution in time (plot-B and plot-C). The plots were generated according to the method proposed by (Casagranda et al., 2018).

Parameter 4 = k4

A)

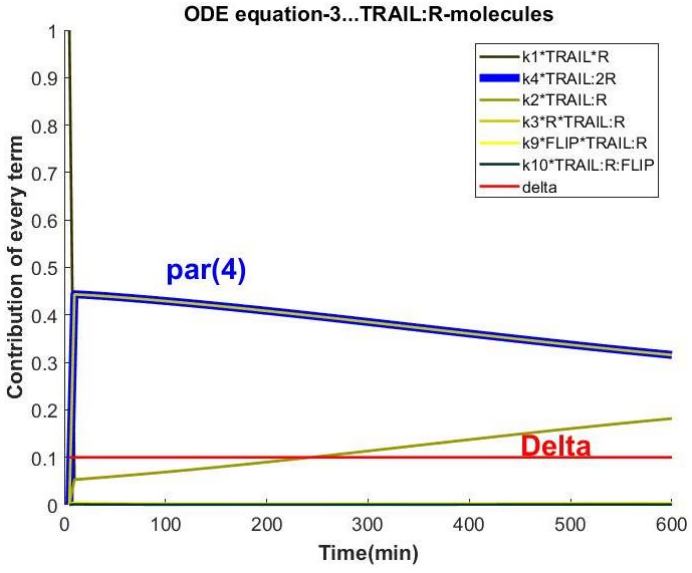

B)

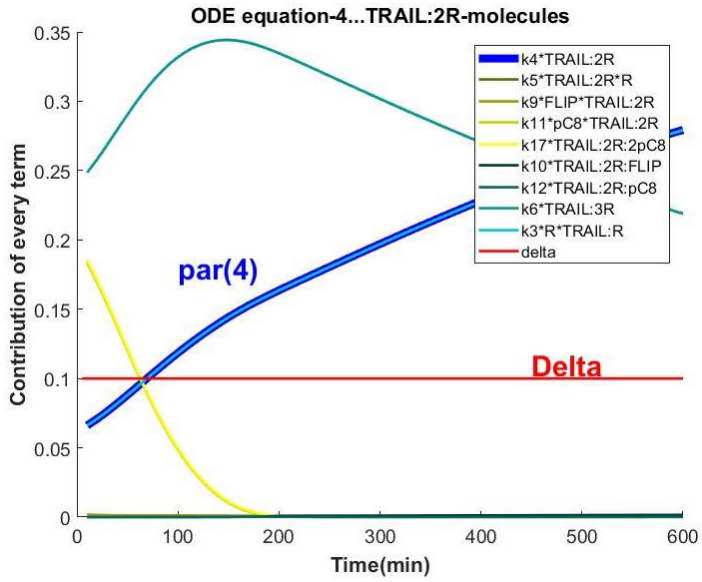

Figure 12. Most contributing terms in the ARROM1 model for the set of ODE equations where k4 intervenes. The vector of parameters used to run the simulation results from the fit of ARROM1 model to the *median_cell* trajectory.

Representation of the relative contribution in time for all the terms in the ODE equation 3 and 4 of the ARROM1 model. In each figure, the value of the threshold is represented in red by delta=0.1. The contribution in time highlighted in bold blue illustrates the term with k4. In the plots **A)** and **B)** the differential equation terms with k4 have a predominant contribution in time. The plots were generated according to the method proposed by (Casagranda et al., 2018).

Parameter 6 = k6

A)

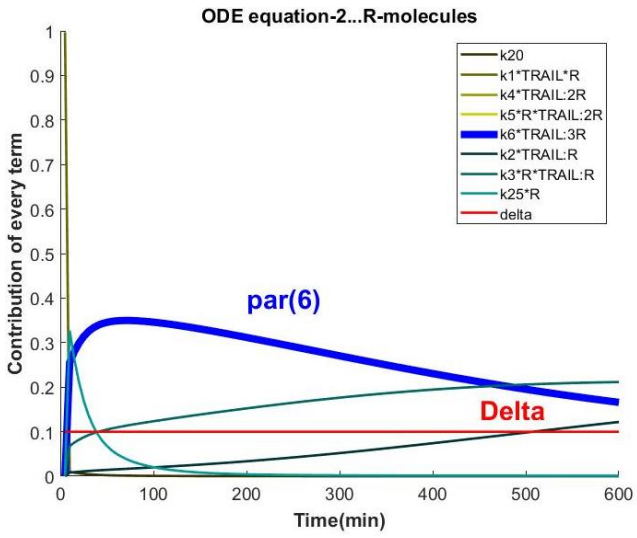

B)

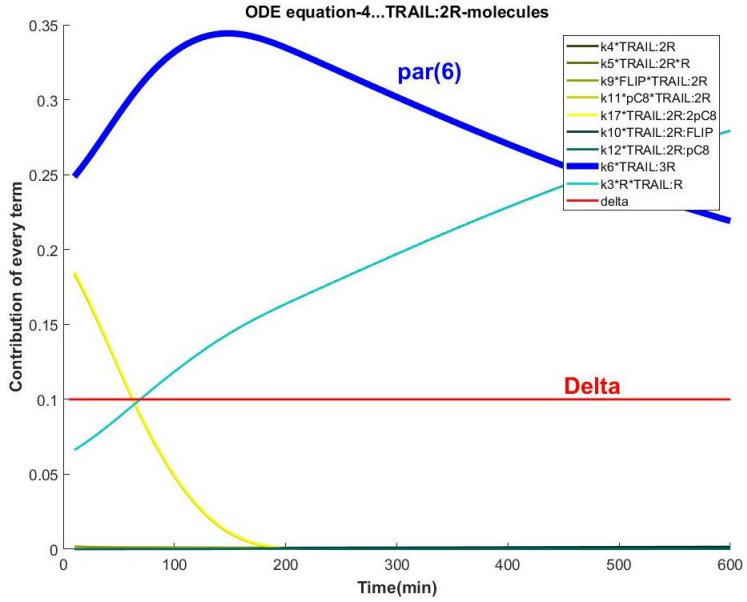

C)

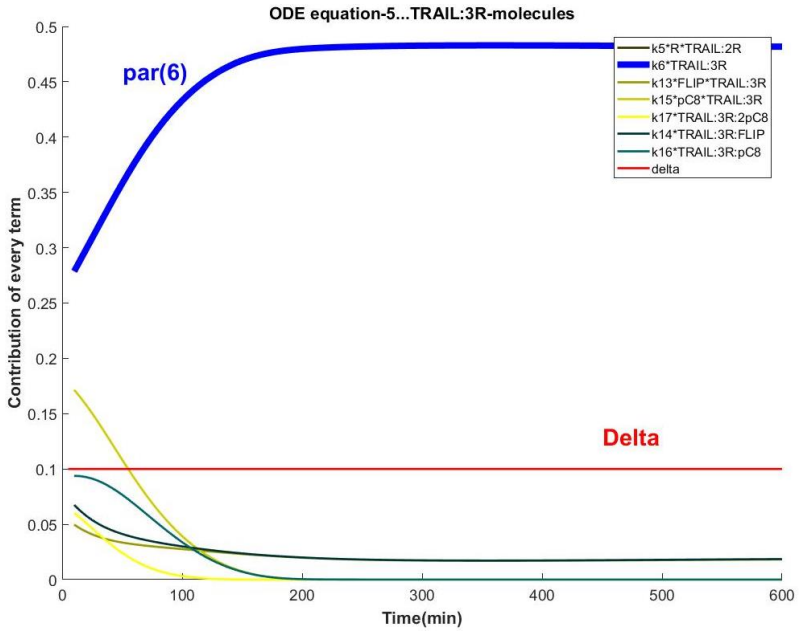

Figure 13. Most contributing terms in the ARROM1 model for the set of ODE equations where k6 intervenes. The vector of parameters used to run the simulation results from the fit of ARROM1 model to the *median_cell* trajectory.

Representation of the relative contribution in time for all the terms in the ODE equation 2, 4 and 5 of the ARROM1 model. In each figure, the value of the threshold is represented in red by delta=0.1. The contribution in time highlighted in bold blue illustrates the term with k6. In the plots **A)**, **B)** and **C)** the differential equation terms with k6 have a predominant contribution in time. The plots were generated according to the method proposed by (Casagranda et al., 2018).

Parameter 16 = k16

A)

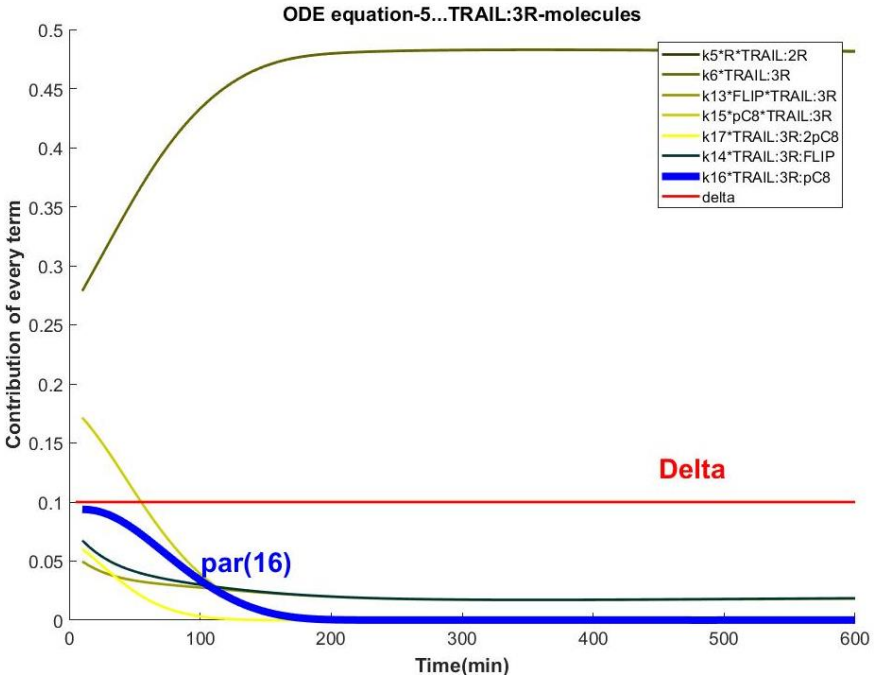

B)

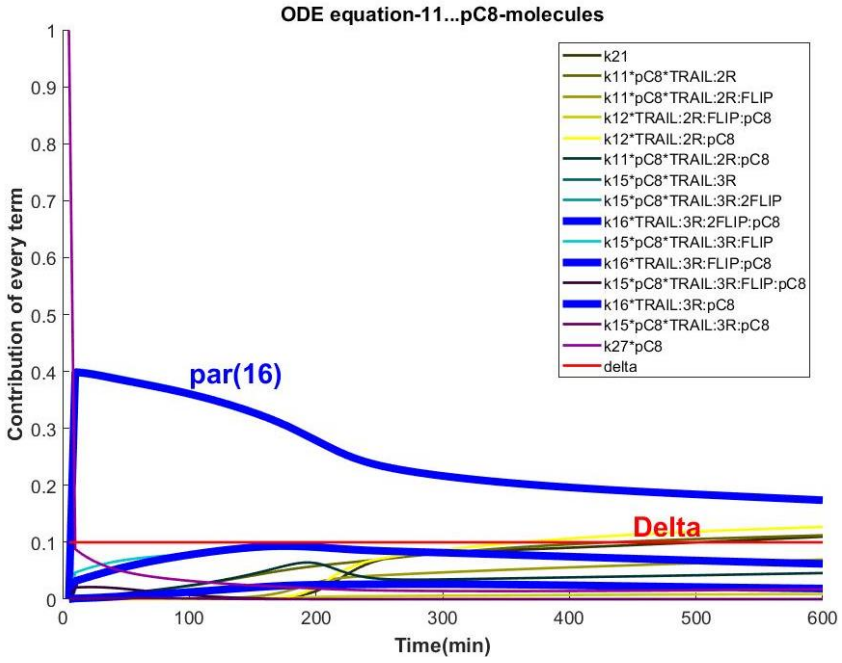

C)

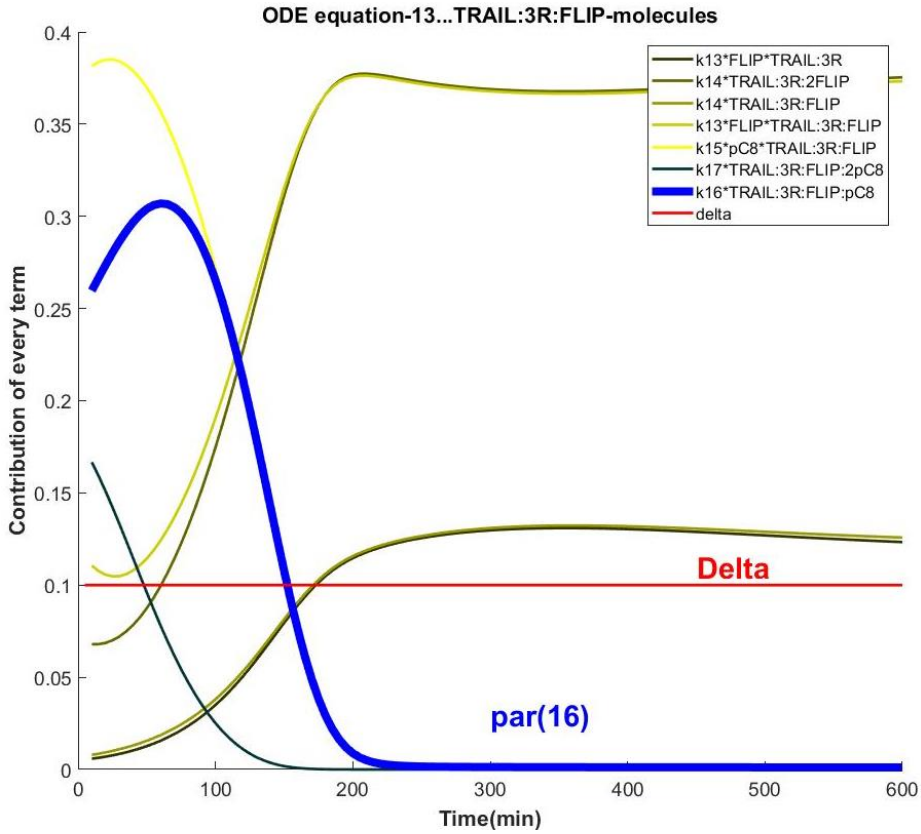
ODE equation-13...TRAIL:3R:FLIP-molecules
k13*FLIP*TRAIL:3R
k14*TRAIL:3R:2FLIP
k14*TRAIL:3R:FLIP
k13*FLIP*TRAIL:3R:FLIP
k15*pC8*TRAIL:3R:FLIP
k17*TRAIL:3R:FLIP:2pC8
k16*TRAIL:3R:FLIP:pC8
delta
Contribution of every term
Time(min)
Delta
par(16)
0
0.05
0.1
0.15
0.2
0.25
0.3
0.35
0.4
0
100
200
300
400
500
600

D)

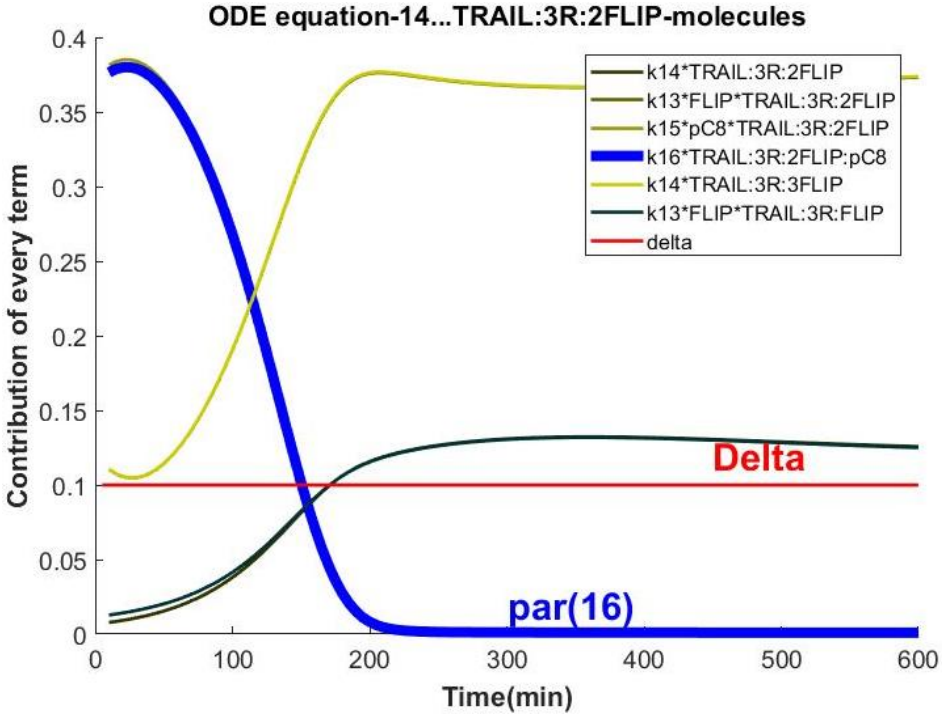
ODE equation-14...TRAIL:3R:2FLIP-molecules
k14*TRAIL:3R:2FLIP
k13*FLIP*TRAIL:3R:2FLIP
k15*pC8*TRAIL:3R:2FLIP
k16*TRAIL:3R:2FLIP:pC8
k14*TRAIL:3R:3FLIP
k13*FLIP*TRAIL:3R:FLIP
delta
Contribution of every term
Time(min)
Delta
par(16)
0
0.05
0.1
0.15
0.2
0.25
0.3
0.35
0.4
0
100
200
300
400
500
600

E)

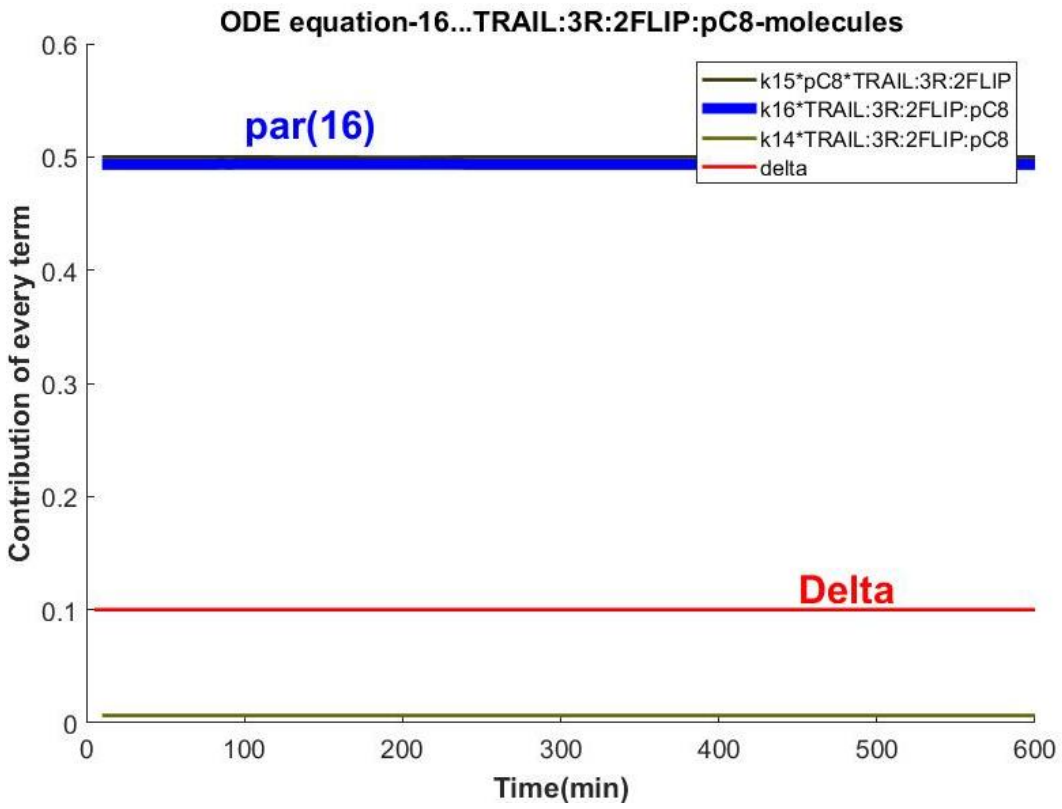
ODE equation-16...TRAIL:3R:2FLIP:pC8-molecules
k15*pC8*TRAIL:3R:2FLIP
k16*TRAIL:3R:2FLIP:pC8
k14*TRAIL:3R:2FLIP:pC8
delta
par(16)
Delta
Contribution of every term
Time(min)
0
0.1
0.2
0.3
0.4
0.5
0.6
0
100
200
300
400
500
600

F)

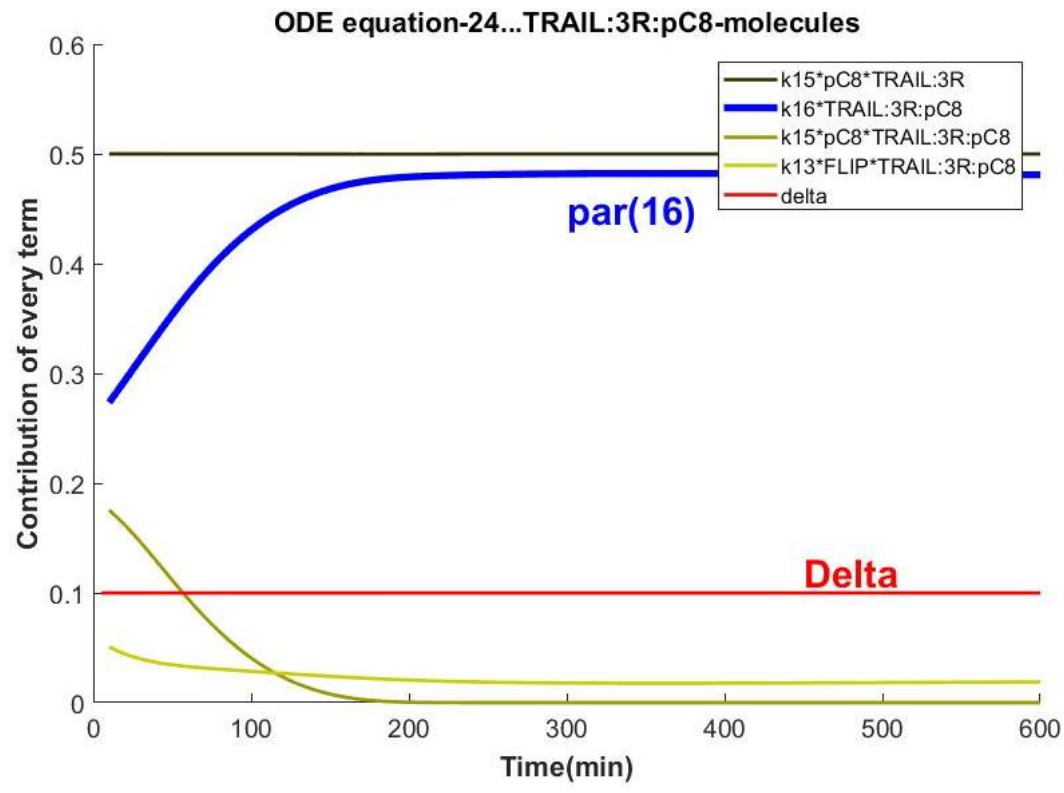
ODE equation-24...TRAIL:3R:pC8-molecules
k15*pC8*TRAIL:3R
k16*TRAIL:3R:pC8
k15*pC8*TRAIL:3R:pC8
k13*FLIP*TRAIL:3R:pC8
delta
par(16)
Delta
Contribution of every term
Time(min)
0
0.1
0.2
0.3
0.4
0.5
0.6
0
100
200
300
400
500
600

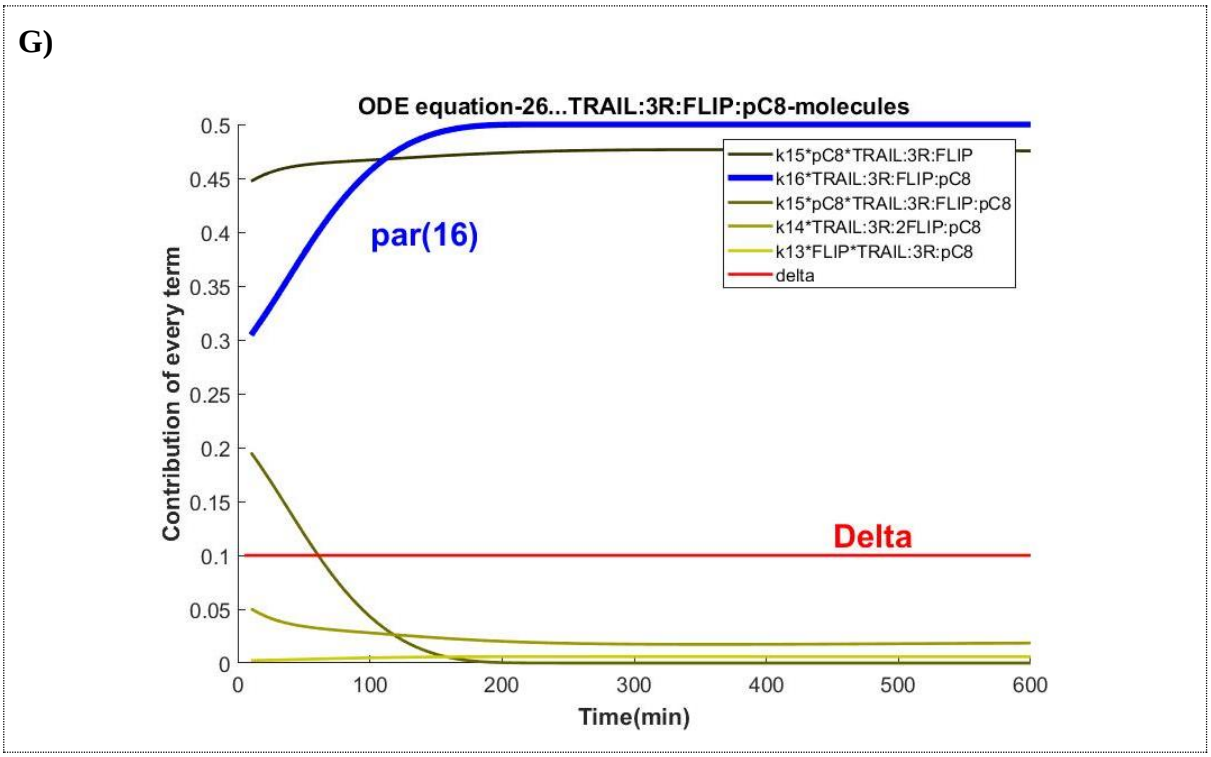

Figure 14. Most contributing terms in the ARROM1 model for the set of ODE equations where k16 intervenes. The vector of parameters used to run the simulation results from the fit of ARROM1 model to the *median_cell* trajectory.

Representation of the relative contribution in time for all the terms in the ODE equation 5, 11, 13, 14, 16, 24 and 26 of the ARROM1 model. In each figure, the value of the threshold is represented in bold red by delta=0.1. The contribution in time highlighted in bold blue illustrates the term with k16. In the plots **B)**, **E)**, **F)** and **G)** the differential equation terms with k16 have a predominant contribution in time. For the remaining plots, k16 either has a decreasing or a negligible contribution in time. The plots were generated according to the method proposed by (Casagranda et al., 2018).

When analyzing figure 14 an immediate observation is that some of the differential equations in which k16 participates show a relative contribution in time for this parameter that is not significant (figure 14-A, C, D). The parameter 16 is related to the dissociation of pC8 molecules from a given complex. In figures 14-E, F, G the represented ODE equations refer to complexes where the pC8 is still part of the molecule and the same plots show that in these cases the term with parameter 16 has a dominant relative contribution. In figure 14-A, C, D the input from parameter 16 in the respective ODE's is due to the conservation of mass between reactions and the dynamics of these three complexes depends mostly on other terms. As so, parameter 16 was accepted as an important contributor of the parameter deviation indicated in table A2.1.

To validate the importance of the parameters [2, 4, 6, 16] on the fitting quality of the ARROM1 model to the experimental *median_cell*, a second fit was performed, this time

constraining the parameters in table A1.2 into a range between [0.1; 10]**parameter_values_initial_guess*, except for parameters [2, 4, 6, 16] which were allowed to vary in an unconstraint interval. This way it was possible to access the dependence of the model output with respect to this subset of parameters. In these conditions the model fit was still very close to the experimental trajectory. Table 3 shows the *initial_guess_values* and the variation obtained for the parameters [2, 4, 6,16] after fitting the experimental *median_cell* in the described conditions.

Table 3. Comparison of parameter values before and after fitting the experimental *median_cell* while allowing the parameters [2, 4, 6, 16] to vary in an unbound interval.

All the parameter list and initial conditions in the ARROM1 model was allowed to vary in a constrained small range [0.1 ; 10]* *parameter_values_initial_guess* with the exception of parameter [2, 4, 6, 16] that were given unbound limits.

Parameter	Initial guess (s^{-1})	After fitting (s^{-1})
2	$3.8 * 10^{-3}$	1.6
4	$3.8 * 10^{-3}$	81.7
6	$3.8 * 10^{-3}$	950.4
16	10^{-3}	13.32

Table 3 shows a rescaling between three and five orders of magnitude on the four parameters [2, 4, 6, 16] after the fitting was performed. This highlights a scenario where the network of reactions considered in ARROM1 is insufficient to clearly explain the experimental FRET signal and a large variation on a small subset of parameters is necessary to compensate for the missing reactions. Given that in table 3 the variation on the parameters [2, 4 , 6, 16] was sufficient to produce a good fit to the *median_cell* the assumption is that the missing reactions might exist in these four nodes of the network.

It is not possible to exclude that another combination of parameters with unlimited bounds, other than the parameters [2 4 6 16], could also provide a good fitting to the *median_cell*. However, in quantitative terms, these four parameters were part of the group with the highest relative deviations (table A2.1) and with the highest contributions to the model output as shown in figure 11-14, standing out from other parameters.

In synthesis, the correct fitting of the *median_cell* required both initial conditions and parameters to change their *initial_guess_values* in table A1.2. Nonetheless, the variation of the parameters [2, 4, 6, 16] was already enough to return an equally good fit to the *median cell*, with the values shown in table 3. The strategy was then to propose a new reaction scheme for the nodes of the model associated to these four parameters. Since they refer to dissociation reactions occurring at the level of the receptor, one can argue that a common unknown protein might be controlling the dissociation of chemical species from the DISC complex. To test this hypothesis the protein was named a generic protein molecule X. The simplest approach is to assume that X directly interacts with an anchored substrate at the receptor level and causes the release of a molecule from this configuration. Given that the parameters [2,4,6,16] describe receptor dissociation and pC8 dissociation events, which are clearly not equivalent reactions, the molecule X was further divided into X1 and X2, each protein responsible for one of the chemical processes represented in **(13)** and **(14)**,

$$\mathrm{TRAIL{:}\,nR} + \mathrm{X_1} \rightarrow \mathrm{TRAIL{:}}\,(n-1)\mathrm{R} + \mathrm{R} + \mathrm{X_1} \qquad \textbf{(13)}$$

$$\mathrm{TRAIL{:}\,3R{:}\,mpC8} + \mathrm{X_2} \rightarrow \mathrm{TRAIL{:}\,3R{:}}\,(m-1)\mathrm{pC8} + \mathrm{pC8} + \mathrm{X_2} \qquad \textbf{(14)}$$

In the above reactions **(13)** and **(14)**, integer numbers n and m are included to represent the stoichiometry of the associated molecule. Integers n and m can assume the values {1, 2, 3} and {1}, respectively. The numbers n=1, n=2 and n=3 are associated to the parameters 2, 4 and 6, respectively. The parameter 16 is linked to the values $m \in \{1, 2\}$. The aim was to verify if the inclusion of **(13)** and **(14)** into ARROM1 would decrease the relative deviation on the parameters [2, 4, 6, 16] and ideally if the fits could be performed changing only the initial conditions of the system, while fixing the vector of parameters or at least narrowing their variation into a small range. This would be a hint that the weight given by the model on these reaction events would be distributed through the new added reactions **(13)** and **(14)**. To simplify the model, at this point it is further assumed that the concentration of both proteins X1 and X2 remain constant, avoiding the introduction of two new differential equations whose dynamics are virtually unknown.

The ensemble of ARROM1 together with the modified reactions **(13)**, **(14)** was named the new model version ARROM2. Incorporating the new reactions in the model implies that parameters [2, 4, 6] are multiplied by X1 and that parameter 16 is multiplied by X2 only in the pC8 dissociation reactions not involving FLIP. Accordingly, parameters [2, 4, 6] and the X1

value are not independent, and X1 is fixed at 1000 molecules. Parameter 16 appears in the equations with FLIP independently of X2, so both parameter 16 and X2 are fitted.

A repetition of the previous test was then conducted and, as before, ARROM2 was fitted to the *median_cell* and the new relative deviation on the model parameters [2, 4, 6, 16] was asserted after the fitting. In this case all the parameters were restricted to a local interval of [0.1; 10]**initial_guess_values* in table A1.2. The results of the test are shown in table 4. A complete list of the model parameters resulting from this fitting is available in table A3.1.

Table 4. Comparison of parameter values [2, 4, 6, 16] and protein X2, before and after fitting of the experimental *median_cell* to the ARROM2 model.

All the parameter list in ARROM2 together with its vector of initial conditions varied in a constrained small range of [0.1; 10]**initial_guess_value*.

Parameter	Initial guess	After fitting
2	$3.8 * 10^{-3}\ (s^{-1})$	$4.3 * 10^{-3}\ (s^{-1})$
4	$3.8 * 10^{-3}(s^{-1})$	$4.5 * 10^{-3}\ (s^{-1})$
6	$3.8 * 10^{-3}\ (s^{-1})$	$9.8 * 10^{-3}\ (s^{-1})$
16	$10^{-3}\ (s^{-1})$	$2 * 10^{-3}\ (s^{-1})$
X_1	10^3 molecules	10^3 molecules
X_2	10^3 molecules	$3.05 * 10^3$ molecules

The values in table 4 now show a more reasonable variation on the parameters [2, 4, 6, 16] after fitting the *median_cell* trajectory. The addition of the two new proteins X1 and X2 at realistic amounts tuned the system and made it more controlled at the parameter level no longer requiring large variations on their orders of magnitude in order to fit the experimental *median_cell*.

It is possible that other unknown X proteins might exist and interact on other points of the network but here the main conclusion is that ARROM1 seemed to be incomplete and additional agents had to be included to absorb the parameter discrepancy in table A2.1.

Chapter 3

Validation of ARROM2: a receptor-ligand model in agreement with experimental data

"He who thinks great thoughts, often makes great errors"

- Martin Heidegger

3.1 FLIP, a strong anti-apoptotic protein with irreversible binding at the DISC structure

The participation of FLIP as an inhibitor of apoptosis is a fundamental control step that limits the amount of C8 molecules activated from the DISC complex. In previous publications it was shown that the overexpression of FLIP could reduce the apoptotic stimulus down to spurious levels (R Safa, 2013; Thome et al., 1997) and a proportion of 2:3 in the ratio of FLIP-s:pC8 proteins was verified to set the C8 activity levels to nearly insignificant values and reduce the death rate to less than 5% in HeLa cell populations treated with TRAIL (Roux et al., 2015).

The balance between pro-apoptotic and anti-apoptotic stimulus at the DISC results from a complex interplay of pC8 molecules, FLIP and perhaps the involvement of still undetermined

inputs like the proteins X1 and X2 (proposed in section 2.4). As one can review from table A1.1, the mean pC8 and FLIP values in an average HeLa cell are around 150000 and 10000 molecules, respectively. This proportion greatly favors the pro-apoptotic response of pC8 given that the binding and unbinding rates for pC8 and FLIP are equal in the ARROM2 model. The justification for equal association rates is that FLIP and pC8 share the same structure, with the exception that FLIP has one less DED domain in one of its terminals (Schleich et al., 2016). Accordingly, the rate at which the two molecules attach to the receptor molecules through their DED should be identical. However, since FLIP does not chain with other pC8 or FLIP molecules, the rate at which it detaches from the receptor complex might be different from the pC8 detachment rate.

In figure 15 different scenarios are compared, with FLIP unbinding rates at different levels. The result of Roux and colleagues is recovered only by setting a much lower dissociation rate for FLIP, in the limit equal to zero, corresponding to a scenario of an irreversible reaction. This hypothesis agrees with the idea that FLIP can block the pC8 elongation chains forming non-functional heterodimers (Schleich et al., 2016).

Given the agreement between experimental results and model predictions in figure 15, all the simulations with the ARROM2 model in the next sections had the FLIP dissociation rates replaced by zero so as to include the result of this section. Tests confirmed that replacing FLIP dissociation rate by zero does not affect the fitting quality of the model to the *median_cell*, reproducing an equally good fit as the one shown in figure 10.

A)

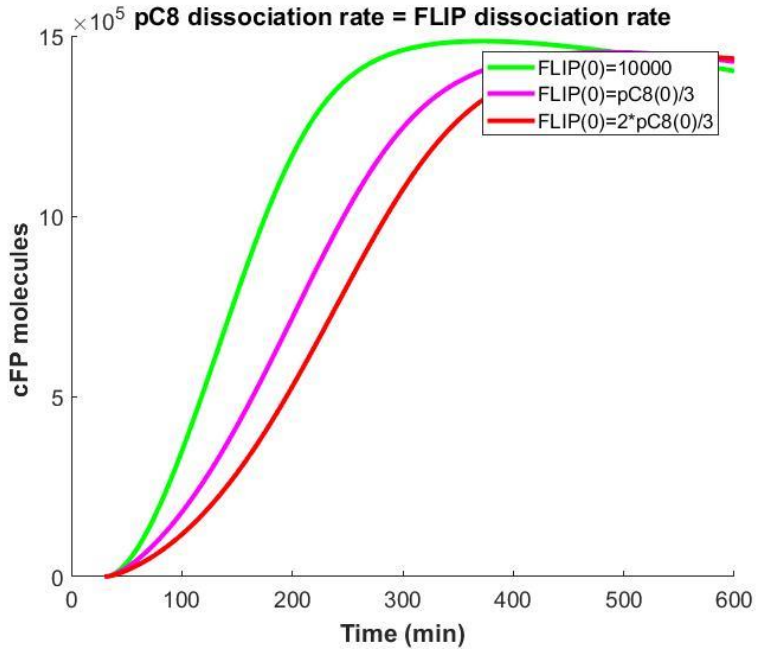

B)

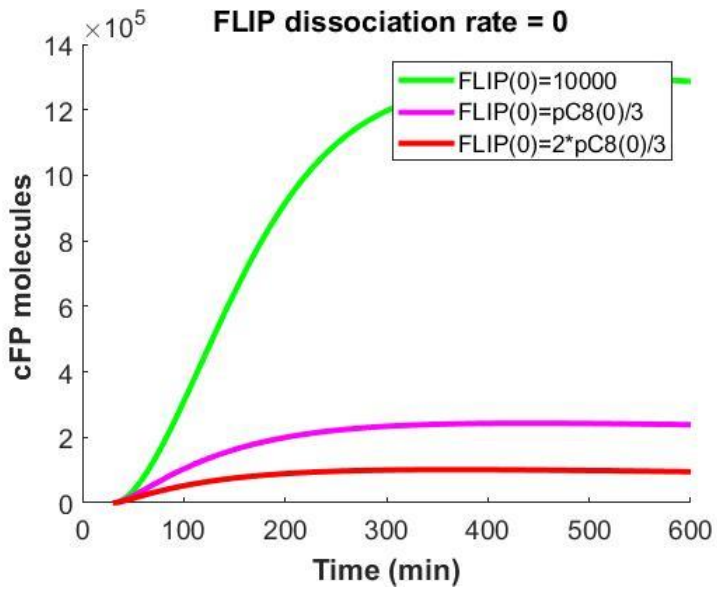

Figure 15. FLIP unbinding rates show evidence of an irreversible reaction.

A) Standard dissociation rates for both pC8 and FLIP molecules do not show the expected decrease in C8 activity (decrease in maximum slope in the exponential phase) when FLIP is overexpressed. **B)** For a null value of FLIP dissociation rate from the receptor an increase in the anti-apoptotic potency of FLIP occurs and the output signal decreases abruptly for higher FLIP initial concentrations. For an initial quantity of FLIP equal to 10^5 molecules [$\frac{2}{3}$ pC8(0) = $\frac{2}{3} * 150000$] (result of Roux and colleagues) the amount of cleaved cFP molecules decreases almost ten times (red curve) and the maximum derivative in the exponential phase also decreases importantly.

3.2 Dimeric vs. Trimeric ligand valency, an unequal receptor binding rate

Increase in C8 activity for higher order assembled receptor clusters is a known result with clinical relevance. Up to date, death-ligands have been tested for a valency order up to 8 (capable of attaching up to 8 receptors) and the overall conclusion is that ligand valency is positively correlated with an increase in the potency of the resulting death signal (Roux et al., 2015; Swers et al., 2013).

In this thesis, the death-ligand, TRAIL, is an input molecule capable of forming at maximum a trimeric interaction with the associating receptors. No experimental data was available to study the dynamics of a specific ligand with valency higher than three but ARROM2 allows one to analyze the signal of a trimeric assembled cluster and compare it with the total C8 activity signal generated by a dimeric assembled cluster. The simulation of a ligand with valency two was performed by setting the three-receptor binding rate **k5** to zero, resulting in a TRAIL-receptor cluster with a maximum of two-attached receptors. Also, the result from section 3.1 was included and FLIP detachment rates (parameters [8, 10, 14] in ARROM2 model) were set to zero.

The comparison between the full trimeric model and the simplified dimeric model returned the output in figure 16, where it's clear that the dimeric and the trimeric versions return an identical cFP signal when the binding and detachment rates of receptors in the TRAIL:2R and TRAIL:3R complexes are assumed to be equal (figure 16-A)). To correct for this unrealistic result, multiple tests were performed where it was possible to conclude that most of the C8 molecules were produced from the dimeric structure TRAIL:2R:2pC8. This was due in part from the fact that the rates of receptor binding and unbinding were equal in both dimeric and trimeric configurations (as originally proposed in table A1.2). Consequently, as the C8 production from the dimeric complex is faster, the dimeric structure TRAIL:2R:2pC8 ended up having a dominant contribution in the total generated C8. To increase the trimeric contributions on the ratio of total activated C8, from both TRAIL:3R:2pC8 and TRAIL:3R:2pC8:FLIP, a higher rate had to be set on the reaction TRAIL:2R + R → TRAIL:3R (binding receptor reaction, parameter **k5** on table A3.2) or ,alternatively, a lower rate could on the reaction TRAIL:3R → TRAIL:2R + R (unbinding receptor reaction, parameter **k6** on table A3.2). With these modifications, the TRAIL:3R/TRAIL:2R proportion raised substantially and C8 production from TRAIL:3R complexes became more pronounced.

Setting the referred binding or dissociation rate to a higher and lower value, respectively, produced the expected result, with a higher maximum slope for the simulated cFP signal (figure 16-B). Biologically, this result has implications on the binding/unbinding scheme between receptors. Once a dimeric configuration is formed, the addition of a third receptor can perhaps be eased to form a more stable structure. In this scenario, the dissociation of a receptor from this more stable structure becomes more difficult and the correspondent dissociation rate decreases. For an arbitrary number of receptors, the continuous addition of an extra receptor would lead to more stable complexes, increasing the binding rate of the next receptor to be added and decreasing its dissociation rate after formation of the correspondent complex.

The result obtained in this section could be extended to a valency of order n. If C8 activity is expected to increase relative to the valency of order n-1 then the binding affinity of the reaction TRAIL: (n-1) R + R → TRAIL:nR should be higher than the binding affinity of TRAIL: (n-2) R + R → TRAIL: (n-1)R (addition of more receptors is favored) and the dissociation rate of TRAIL:nR should be lower than the dissociation rate of TRAIL:(n-1)R (unbinding of receptors is not favored). Tests confirmed that replacing **k5** and **k6** by the simulated proportions did not affect the fitting quality of the model to the *median_cell*, reproducing an equally good fit as the one shown in figure 10.

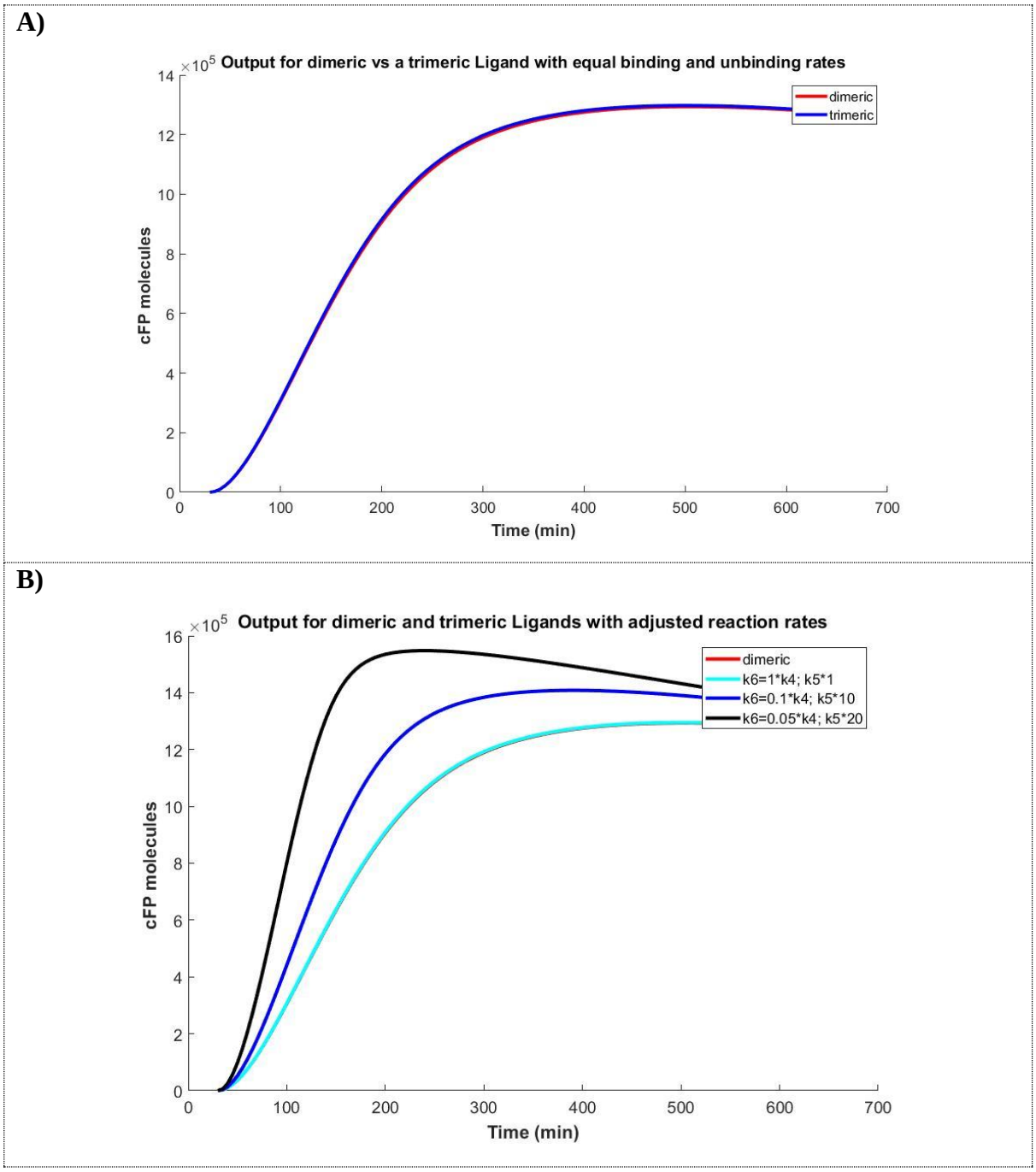

Figure 16. Ligand valency results impose higher binding rates and/or lower dissociation rates of the receptor in the trimeric complex.

A) Assuming an equal binding/unbinding rate of the receptor molecule in the dimeric and trimeric complexes results in indistinguishable C8 activity levels for both valencies. **B)** Higher C8 activities for a trimeric ligand imply the trimeric complex to be a more stable structure. Accordingly, both the rates of formation and dissociation of a trimeric complex have to be higher and lower, respectively, than the ones of a dimeric complex. The pallid blue curve represents the ARROM2 model (with both dimeric and trimeric complexes) with all the original rates of table A3.2. The C8 activity (maximum slope of the curve) increases as the parameter **k6** (rate of receptor dissociation from TRAIL:3R) diminishes and the parameter **k5** (rate of production of TRAIL:3R) increases. The parameters [8, 10, 14] were set to zero to include the result from section 3.1 in which FLIP shows evidence of low dissociation rates. Parameter **k4** refers to the dissociation rate of a receptor from the dimeric structure TRAIL:2R.

Chapter 4

Sources of heterogeneity in apoptotic cell-fate decision

"*The task is not to see what has never been seen before, but to think what has never been thought before about what you see everyday*"

- Erwin Schrödinger

As discussed in the previous section 1.4, one of the ambitions of this work was to propose an explanation for the heterogeneity of cell-response in Hela cells when treated with the death-inducing ligand TRAIL. The variability is a limiting factor that weakens the effect of clinical drugs and overall hardens the comprehension of the extrinsic apoptosis pathway. To describe the observed variability in the experimental data set, different tests with the ARROM2 model were executed to explore the contributions of different sources of variability in the signaling network. Three potential sources of heterogeneity were studied: intrinsic noise, extrinsic noise and parameter noise. The results from sections 3.1 and 3.2 were included, by replacing parameters [8, 10, 14] by zero, and also decreasing parameter **k6** by 10-fold and increasing parameter **k5** by 10-fold. These modifications were applied on the list of parameters in table A3.2.

Throughout this thesis, three properties of the model and data curves will be considered to qualify variability in cell response:

- **Starting delay**: Each single cell trace presents a time-lag between drug administration and onset of response;
- **Kick-off slope**: the derivative of cFP activation, which was identified in (Roux et al., 2015) as a distinguishing feature between phenotypes;
- **Steady-state value**: after 10 hours, resistant cells approach a steady state in the amount of cFP. Here steady state does not refer to the end value of the simulated curve but instead to its value at the end of the experimental follow-up, at t=10 hours;

4.1 Intrinsic noise: A computational approach with the Gillespie algorithm

A simplified stochastic version of the ARROM2 model was implemented following the standards of the Gillespie algorithm (Gillespie, 1977). All the main branches of the deterministic model were kept, preserving TRAIL:R, TRAIL:R:FLIP, TRAIL:R:pC8, TRAIL:2R, TRAIL:2R:FLIP, TRAIL:2R:pC8, TRAIL:2R:pC8, TRAIL:3R:FLIP, TRAIL:3R:pC8, TRAIL:3R:2pC8, the C8 production and respective substrates cleavage. All the other intermediate complexes in the deterministic version were excluded. This reduction accelerated the system so that it could produce a reasonable amount of simulations in useful time.

The first step, commonly ambiguous when performing stochastic tests with the Gillespie algorithm, was to decide for an adequate scaling parameter omega(Ω). Omega is the usual parameterization related to the system's size, allowing one to inter-convert molecular concentrations (deterministic version) into number of molecules (stochastic version). Omega dimensions are given in volume units and it acts as a tuning parameter, scaling the system into a more deterministic or stochastic configuration. Increasing values of omega denote a rise in the associated volume of the system, defining a more "deterministic-like approach" with larger molecular numbers. Oppositely, decreasing values of omega reflect lower particle quantities in a smaller simulated volume and a higher stochasticity of the associated system (Gonze and Ouattara, 2014). No "a-priori" values exist for omega and different scales were tested to inspect the generated degree of variability around a referenced curve. Figure 17 shows the output of the stochastic implementation of ARROM2, for different values of omega, altogether with the deterministic version of the selected curve.

A)

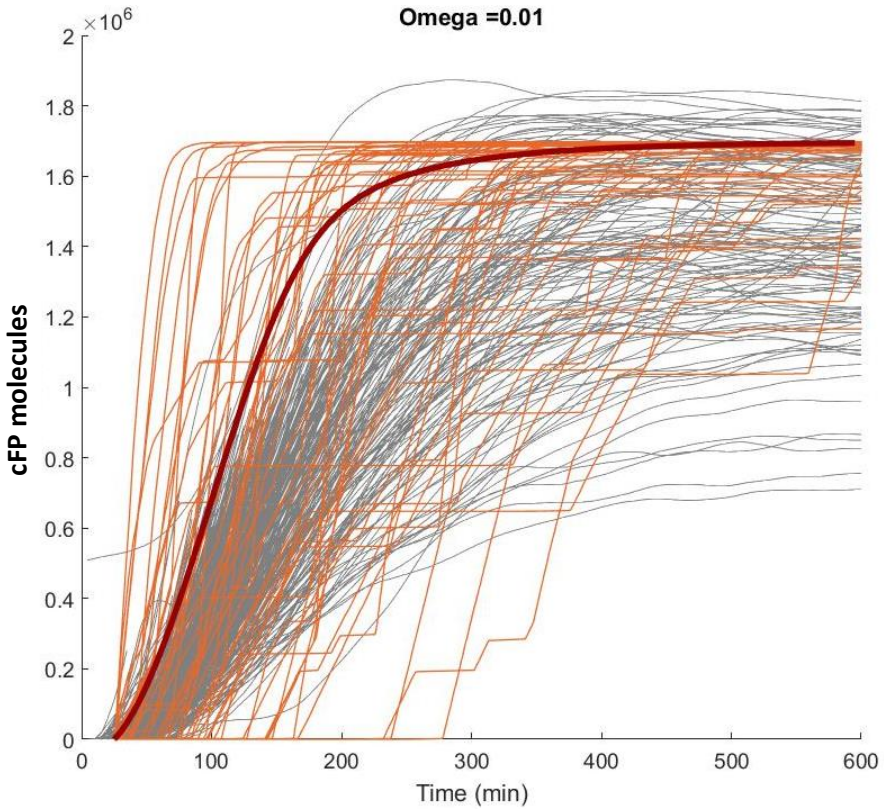
Omega =0.01
×10^6
2
1.8
1.6
1.4
1.2
1
0.8
0.6
0.4
0.2
0
cFP molecules
0
100
200
300
400
500
600
Time (min)

B)

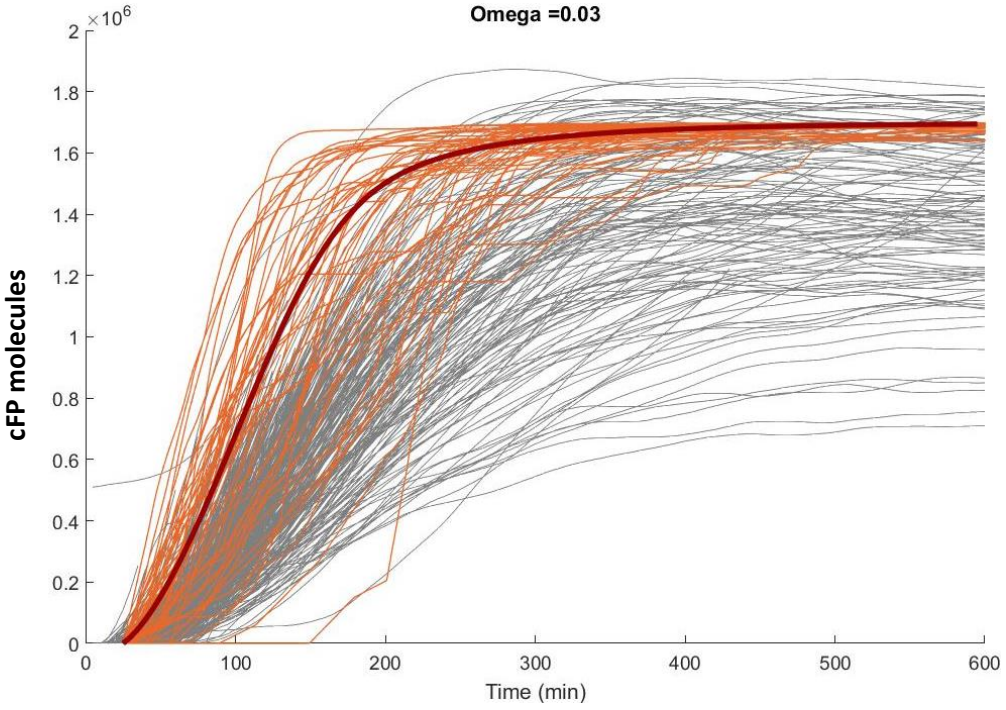
Omega =0.03
×10^6
2
1.8
1.6
1.4
1.2
1
0.8
0.6
0.4
0.2
0
cFP molecules
0
100
200
300
400
500
600
Time (min)

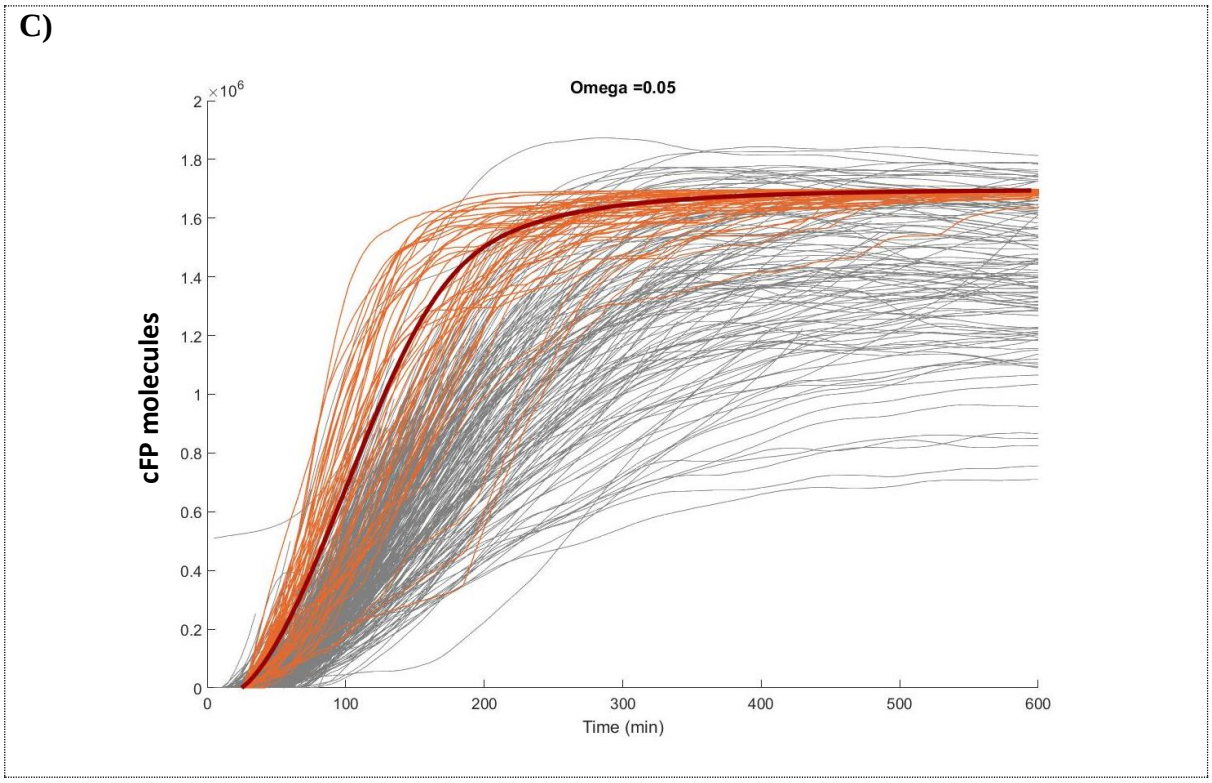

Figure 17. Stochastic simulation of the ARROM2 model using the Gillespie algorithm.

Intrinsic noise generates random perturbations in the reaction events and distorts the signal of the curves. **A)** Ω=0.01, **B)** Ω=0.03, **C)** Ω=0.05. Gray curves represent the experimental trajectories of the data set of HeLa-Cells treated with TRAIL at 50 ng/ml. The red curve is the deterministic representation of a reference curve. All the curves in orange tone define stochastic simulations of the referenced curve, obtained by implementing the stochastic algorithm originally proposed by Gillespie (Gillespie, 1977) . Fifty stochastic simulations are represented in each of the three plots **A)**, **B)** and **C)**.

From figure 17, and for the tested omega values, two extreme scenarios can be contemplated. In figure 17-A, with Ω =0.01, the system is highly stochastic and the simulated curves shows delay-phases of variable duration, whereas for simulations with omega larger or equal to 0.05 the landscape of the simulated curves is already too close to the reference curve and does not reproduce the heterogeneity profile of the data-set. For Ω=0.01 the range of slopes and delays due to intrinsic noise are much larger than those observed in experiments, while the intermediate value Ω=0.03 generates a reasonable variability, quite close to that observed in the data-set. Nevertheless, for all Ω values, the acquired window of steady state values is too narrow and does not seem to reflect the spread in the experimental trajectories. The conclusion is that intrinsic noise is not enough to explain cell heterogeneity in the extrinsic apoptosis pathway.

4.2 Extrinsic noise: a computational approach with initial condition variation.

Extrinsic noise refers to differences in initial protein quantities in different cells. Here, the impact of this noise source was done by simulating one thousand *median_cell* trajectories with a different set of initial conditions and asserting if the resulting curves could reproduce the variability of the data-set. The initial condition variation was executed by choosing a random value for each protein inside an interval of 30% around the protein *median_cell* initial content (table A3.1). The value of 30% was chosen from previous results, where protein variability in the extrinsic apoptosis pathway has already been reported to be in a range of 30% (Spencer et al., 2009). The vector of parameters in table A3.2 , after the modifications derived from section 3, remained equal across the one thousand simulations. As confirmed in figure 18, the variation in initial conditions produced curves overlapping with the entire sample of cell trajectories, and reproducing all three curve properties (starting delay, kick-off slope and steady state values), setting extrinsic noise as a good candidate to explain the heterogeneity of the system. This outcome reinforces previous results suggesting that protein numbers control the heterogeneity of response in the extrinsic apoptosis pathway (Gaudet et al., 2012; Spencer et al., 2009).

A)

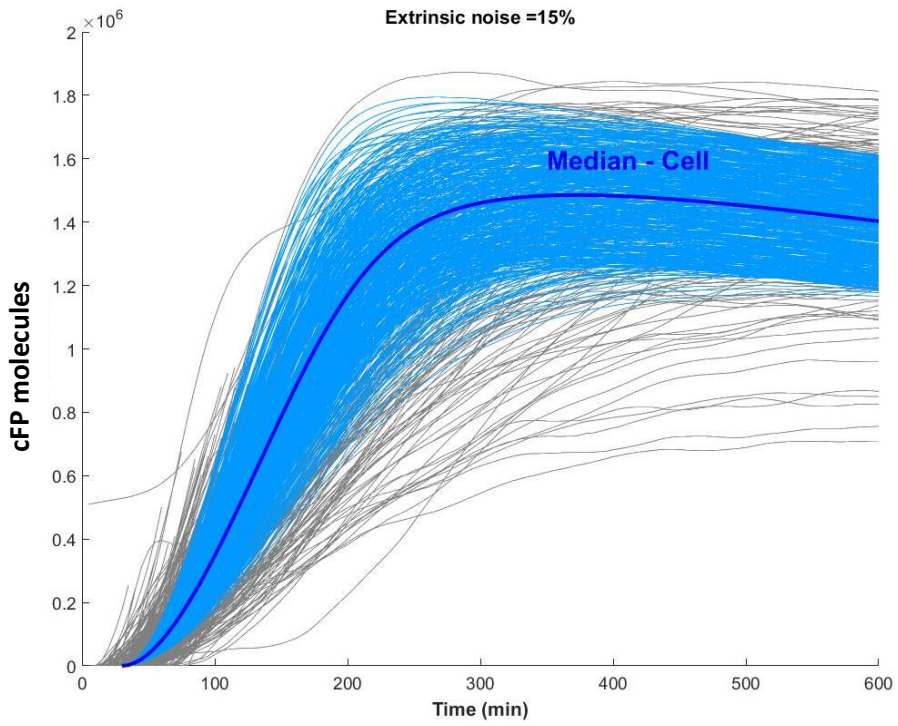

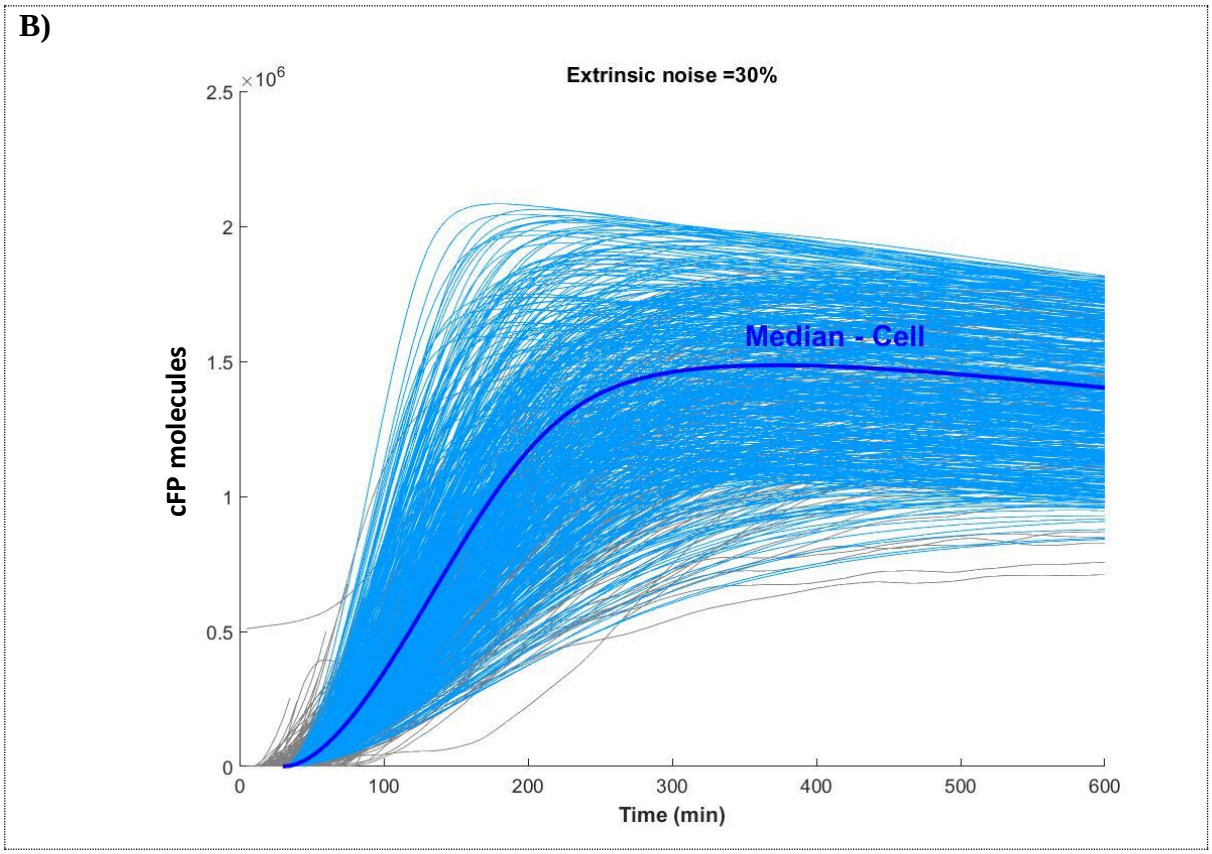

Figure 18. Extrinsic noise, simulation of *median_cell* with one thousand different initial conditions.
The *median_cell* initial conditions were sampled one thousand times in an interval of **A)** 15%, **B)** 30% around the *mean_initial_values* and the resulting curves are represented (pallid blue) altogether with the experimental trajectories (gray) and the *median_cell* trajectory with no extrinsic noise (dark blue). Two plots are represented to show a trend for extrinsic noise when set to lower or higher values.

4.3 Parameter noise: a computational approach with variation in reaction rates

Variation in the parameter rates has been addressed as a possible noise source in biological systems (Llamosi et al., 2016; Sherman et al., 2015). Here, by performing one thousand simulations with the *median_cell* parameters varied in a range of 15%, 30% and 45% around the initial values (Table A3.2 with the results from section 3 included) one can conclude that the resulting curves only match the dispersion of the data set for a parameter noise set around 45% (figure 19-B). In this case, the curves reproduce the range of maximum slopes but their geometry in the stationary phase does not correspond to the observed steady-state dispersion in the experimental trajectories. Although parameter noise can also be a justification for variability in C8 activity levels (distribution of maximum slope values), the fact that the concept of parameter variability it's not entirely realistic, the steady state distribution values are not entirely recovered and that variability in protein initial conditions already returned the correct profile for the cell population ended up in the exclusion of this noise source as a fully plausible explanation for cell decision in apoptosis.

A)

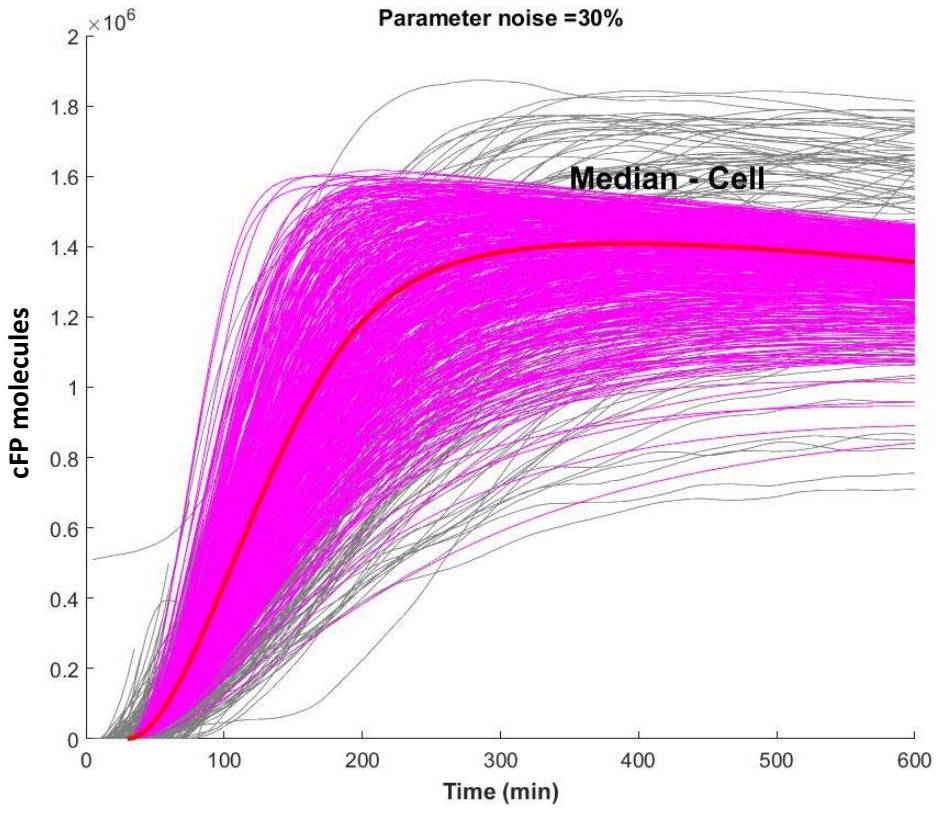

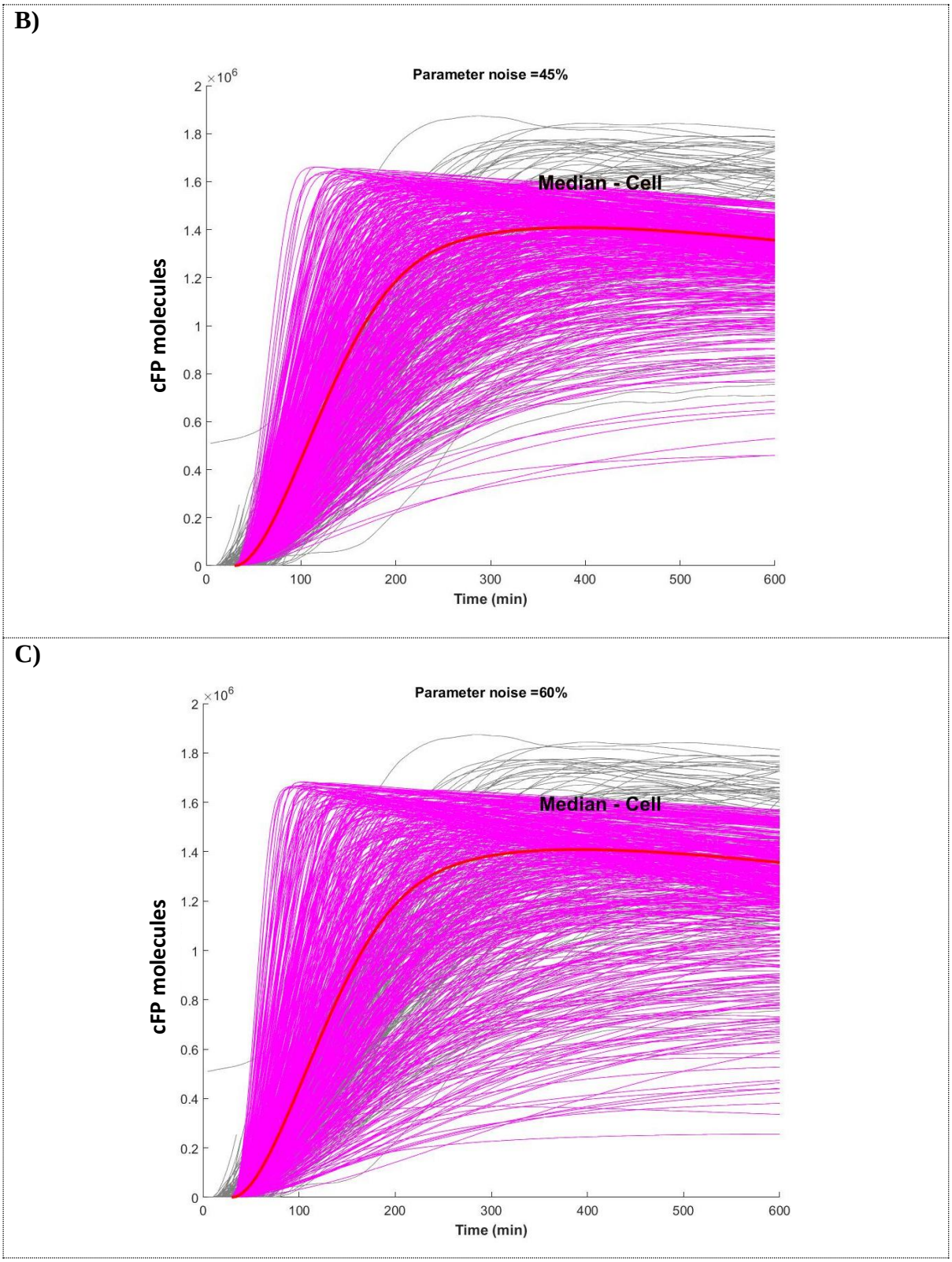

Figure 19. Parameter noise simulation on the ARROM2 model.
Heterogeneity caused by imposing variability on the parameter values of the *median_cell*. In gray, all the experimental trajectories of the data set. The *median_cell* parameter vector was sampled one thousand times in an **A)** 30% **B)** 45% **C)** 60% interval around its initial values and the resulting curves, represented in pink, cannot reproduce entirely the steady-state dispersion of the experimental trajectories. The *median_cell* initial trajectory without parameter variation is shown in red.

Chapter 5

Fitting the entire cell population and searching for signatures in sensitive and resistant populations

"Life is like riding a bicycle. To keep your balance you must keep moving"

- Albert Einstein

Understanding the determinants of cell resistance to TRAIL is a fundamental topic in recent studies (Roux et al., 2015; Spencer et al., 2009) and a goal in apoptosis modelling (Bertaux et al., 2014; Bouhaddou et al., 2018; Buchbinder et al., 2018). In this thesis, the employed strategy to decipher the origins of fractional killing followed an individual fitting of the ARROM2 model to every single cell in the data set. The fitting to a total of four hundred and fourteen cells returned a distribution of parameter values that was inspected in order to extract the most relevant divergences specifically assigned to each phenotype. The list of *parameters_initial_guess* used for the fitting of the cell trajectories is available in table A3.2, where the results of section 3 were also included: FLIP dissociation rates [**k8**, **k10**, **k14**] were set to zero, parameter **k5** multiplied by 10 and parameter **k6** divided by 10. Following the result from section 4.2 and 4.3 , where both protein initial condition variation and parameter noise

contribute for the heterogeneity of model simulations, the methodology followed a cell-by-cell fitting allowing a varying set of initial conditions and a varying vector of parameters. Given the results of chapter 4 and the lower contribution of parameter noise in total generated heterogeneity, a restrained interval of 2-fold variation was set on the *parameters_initial_guess* in table A3.2, while a more significant interval of 10-fold variation was allowed for the initial condition amounts of the proteins {R, FLIP, pC8, Bid, FP, X2}. Under this framework ARROM2 captured the variability of cell responses over the ensemble of cell trajectories (figure 20).

After fitting the entire cell population the distributions of fitted parameter values and initial conditions were examined and the most relevant differences were detected over the list of fitted initial conditions. These differences were then represented through a moving average approach, which plots the dependence of the kick-off slope on the initial conditions of the system, as represented in figure 21.

By inspection of figure 21 one can observe different distributions in the group of resistant and sensitive cells. In figure 21-A), B), C) expected trends were obtained with the sensitive group showing higher Receptor and pC8 protein levels but reduced amounts of FLIP. An unexpected result was nonetheless obtained for protein X2. This protein is an extra component of the network whose presence was deduced in section 2.4 and it was assumed to be a contributing element in anti-apoptotic reactions at the DISC. Higher concentrations of this protein should then relate to the resistant phenotype but in fact the opposite relationship was obtained (figure 21 -D). A hypothesis then rose that more complex dynamics could be linked to this protein and eventually contributing to distinguish between the sensitive and resistant phenotypes. An intuitive test was to check if X2 could be under direct control of C8 and if more pronounced C8 dynamics (sensitive group) could impact the absolute X2 numbers inside the cell. We then establish a hypothetical relationship between X2 and C8 with descriptive dynamics in the form of a Hill-positive (HP) or Hill-negative (HN) function.

$$HP(C8) = \alpha \frac{C8}{\beta + C8} \quad \textbf{(15)}$$

$$HN(C8) = \alpha \frac{\beta}{\beta + C8} \quad \textbf{(16)}$$

Cell #5	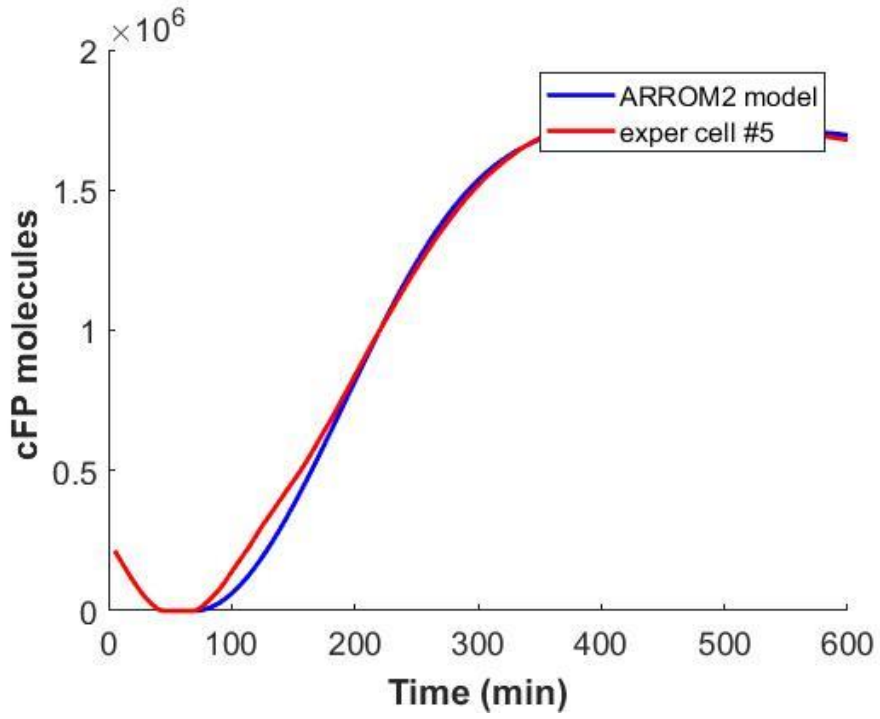 ×10^6 2 1.5 1 0.5 0 cFP molecules ARROM2 model exper cell #5 0 100 200 300 400 500 600 Time (min)
Cell #6	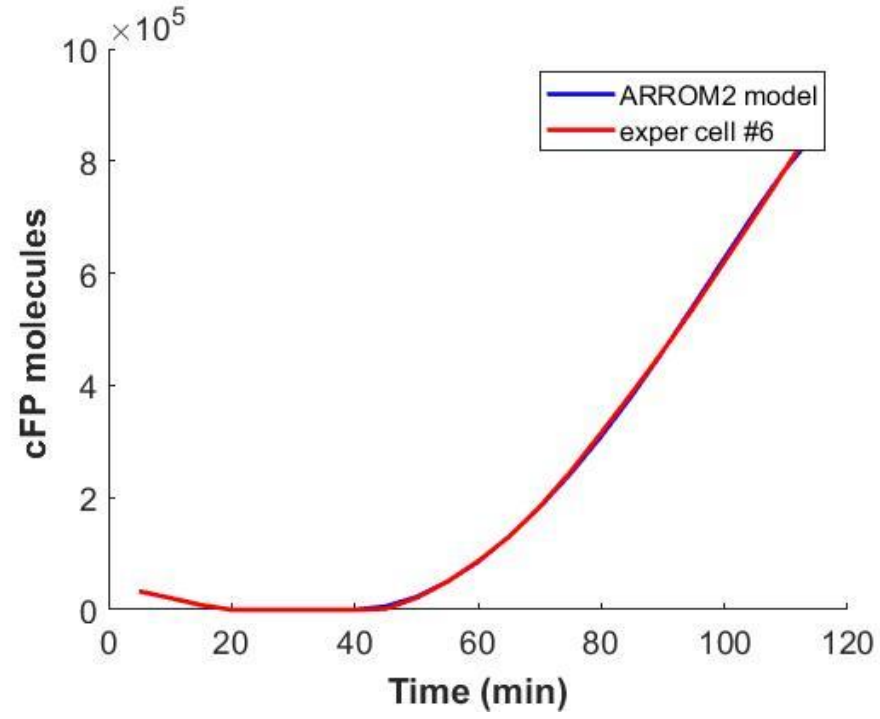 ×10^5 10 8 6 4 2 0 cFP molecules ARROM2 model exper cell #6 0 20 40 60 80 100 120 Time (min)

Cell #7	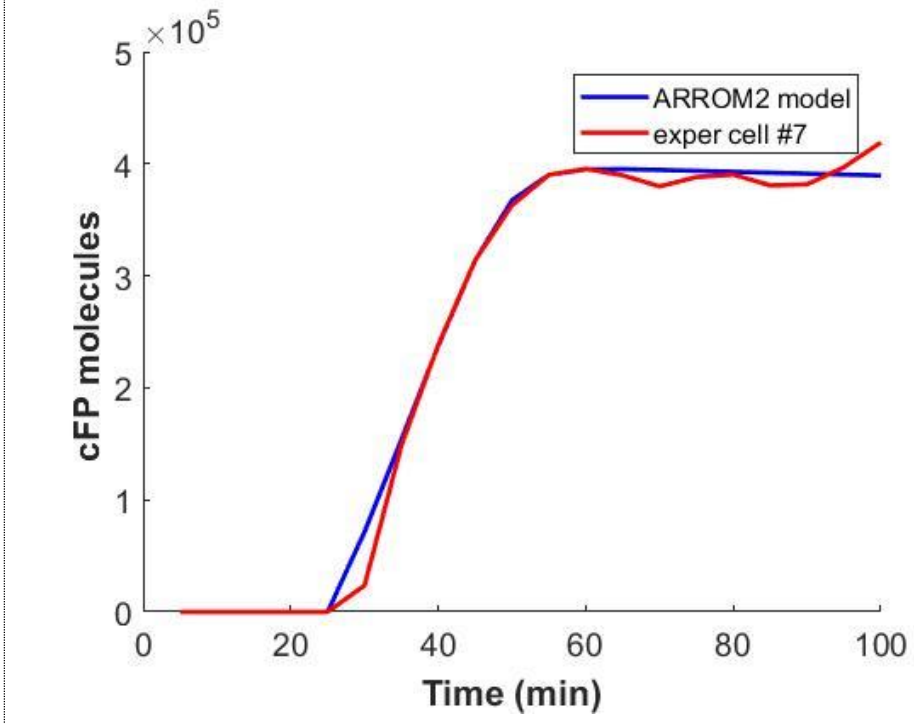

Figure 20. Fitting ARROM2 to single cells requires protein number variability and small parameter variation to reproduce the cell population trajectories.
The three fits assemble the possible type of curves faced by the algorithm when fitting the data set. The general quality of the fit of the model is optimal for curves in any of the three represented geometries. Cell#5 is described for a time frame of 600 minutes and is thus a resistant cell. Cell#6 and Cell#7 have shorter time lengths, corresponding to sensitive cells. Both cell#6, with a parabolic shape trajectory, and cell #5 and cell#7, with a sigmoidal trajectory, are well fitted by ARROM2 model. The fitting was performed with *fminsearchbnd* and the set of initial conditions in table A3.1 was allowed to vary one order of magnitude around the *initial_guess_values*. The parameter vector varied in an interval of 2-fold around the values in table A3.2.

In **(15)** and **(16)** , where α and β are real numbers, a simplified representation of a positive and negative feedback interactions are given, respectively, from C8 to X2. These assumptions can validate if a direct or an indirect relationship between C8, a major pro-apoptotic protein, and X2, a suggested new element, could exist in the simulated system. To confirm or reject this hypothesis the X2 protein was replaced by both expressions in ARROM2 equations and, in each case, different alpha and beta values were simulated together with the list of parameters and initial conditions in table A3.1 and A3.2. To verify the interactions **(15)** and **(16)** at the population level, the generated curve was simulated with varying initial conditions in a range of 30%, similar to the previous test in figure 18. For any values of α and β , X2 had no relevant contribution on the simulated heterogeneity of the cFP signal. Interactions of the form **(15)** and **(16)** were then discarded for X2.

With the test failing for X2 we then evaluated the impact of the same interactions on protein X1. Considering a positive feedback input from C8 to X1, of the same form as in **(15)**, an unexpected result was obtained. The dispersion of the simulated curve, with 30% variation on protein initial condition values, generated a window of heterogeneity on the cFP signal that

recovered the broad landscape of the experimental trajectories. This result can be confirmed in figure 22, for $\alpha = 1000$ and $\beta = 0.05 * maximum\ (C8[t])$. The value of α refers to the initial amount of X1 set to 1000, as in table A3.1. On the other hand β is a fraction of the maximum $C8[t]$ value, computed from the original model ARROM2 without feedback, to reflect the dependency of the feedback strength on the absolute C8 values. In light of these results, a connection was then supposed to exist between the two mentioned proteins. A positive feedback of the form HP (C8) implies that, in the initial stages of apoptosis, low C8 levels lead to low receptor dissociation thus favoring DISC formation. With C8 increasing in concentration in the sensitive phenotype, receptor dissociation also increases, inhibiting DISC formation. Therefore, the role of X1 may be related to a fine-tuned regulation of C8 signaling, possibly amplifying the differences between initial C8 concentrations, to be reflected in a larger range of kick-off slopes, which are a main distinguishing property between phenotypes. Searching the literature for proteins playing similar tasks to the hypothesized X1 interactions a possible candidate was found to be Caspase-10 (C10). The experiments reported in (Horn et al., 2017) indicate interesting dynamics for C10, a protein that shares some properties with C8. Among other observations the authors found that: (i) C10 impairs DISC-mediated C8 activation and (ii) in the absence of C8, neither C10 nor FLIP can bind to the DISC. Thus protein C10 seems to be under direct influence of C8. Based on these features and the model simulations with X1 = HP(C8), a reasonable hypothesis is that the unknown protein X1 may represent the contribution of C10 on the extrinsic apoptosis pathway and a proposed map of interactions is given in figure 23, where the described negative feedback loop was included into the receptor reaction network of the extrinsic apoptosis pathway.

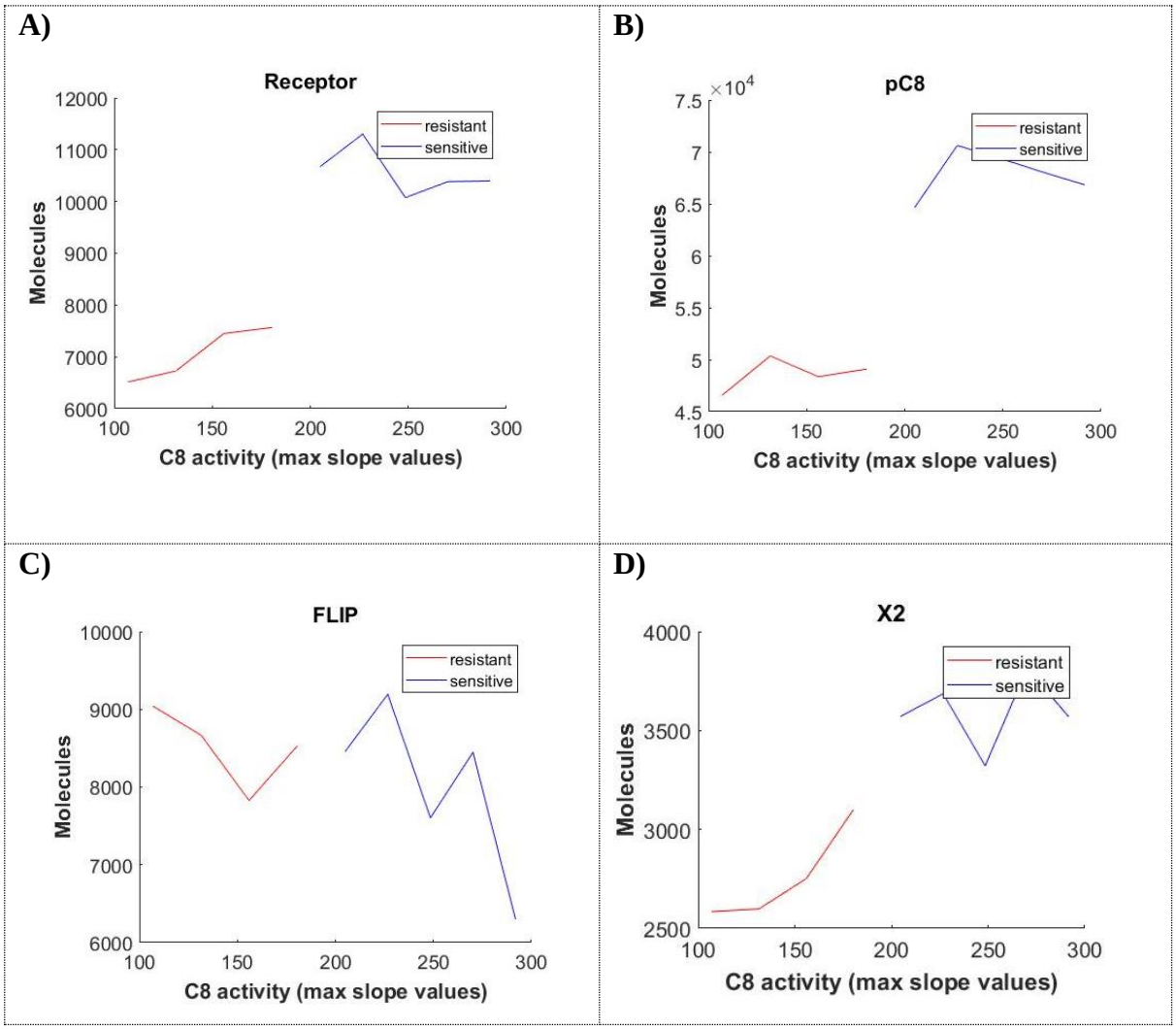

Figure 21. Moving-average reveals trends on initial conditions that correlate with increase in C8 activity. Extrinsic noise actuates in all of the proteins of the system and different combinations may lead to a different phenotypic outcome. The C8 activity in the interval [120-180] corresponds to the largest fraction of fitted maximum derivative values in resistant cells (red line). The interval of C8 activity [200-260] represents the largest fraction of fitted maximum derivative values in sensitive cells (blue line). Each point in the vertical axis refers to the mean value found for the cells having the C8 activity indicated in the horizontal axis. **A)-D)** Initial conditions with distinct landscapes for increasing C8 activity in resistant vs. sensitive cells. **A)** Receptor distribution **B)** pC8 distribution **C)** FLIP distribution **D)** X2 distribution.

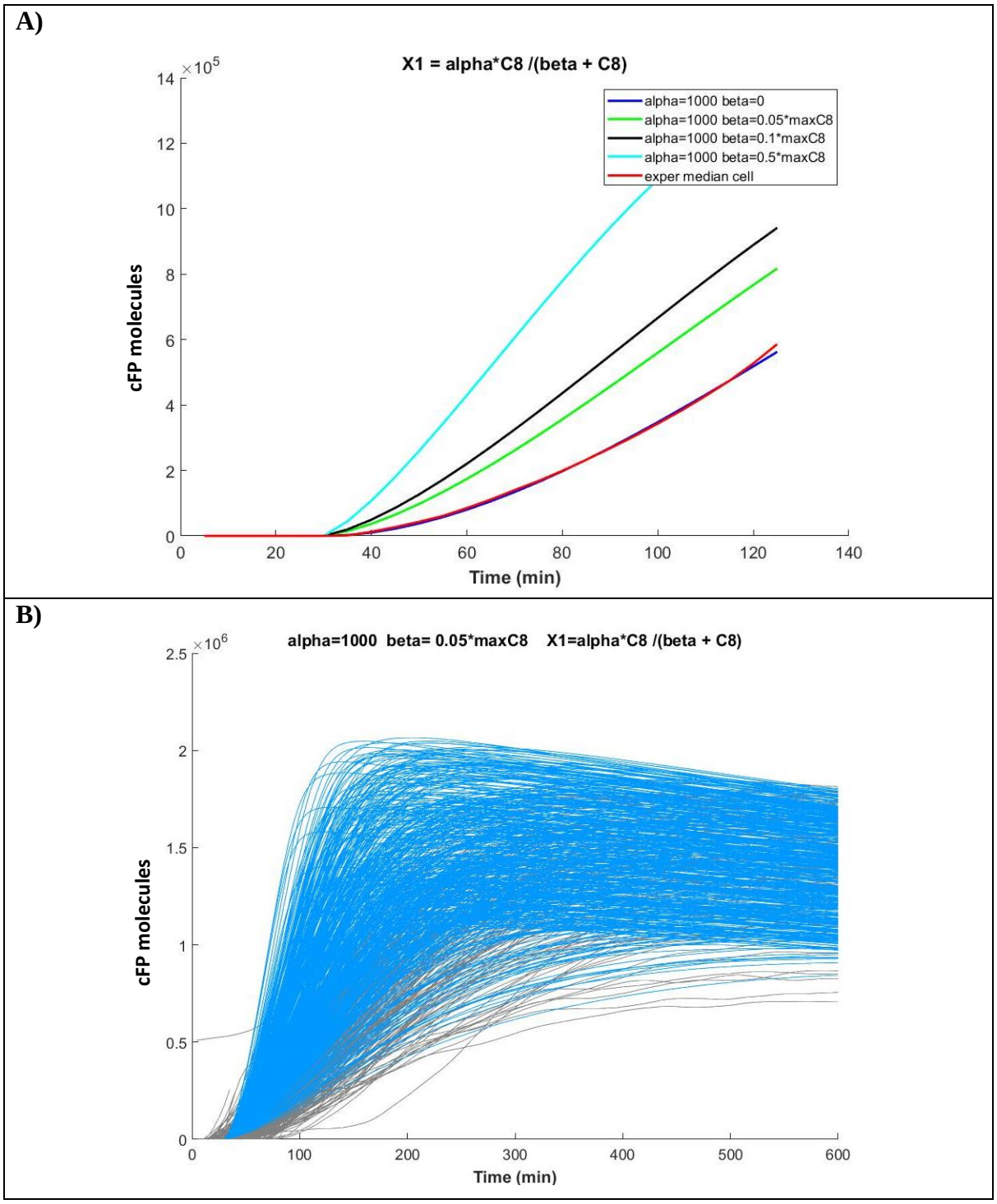

Figure 22. A possible negative feedback loop between X1 and C8.

Replacing X1 by expression (15) returns a population dynamics similar to the one obtained with ARROM2 model when simulated without any assumption for X1 (figure 18). **A)** The experimental *median_cell* trajectory is compared against cFP curves for increasing values of beta. **B)** A 30% variation on protein initial condition values recovers a very good extent of the population dynamics with the assumed positive feedback interaction.

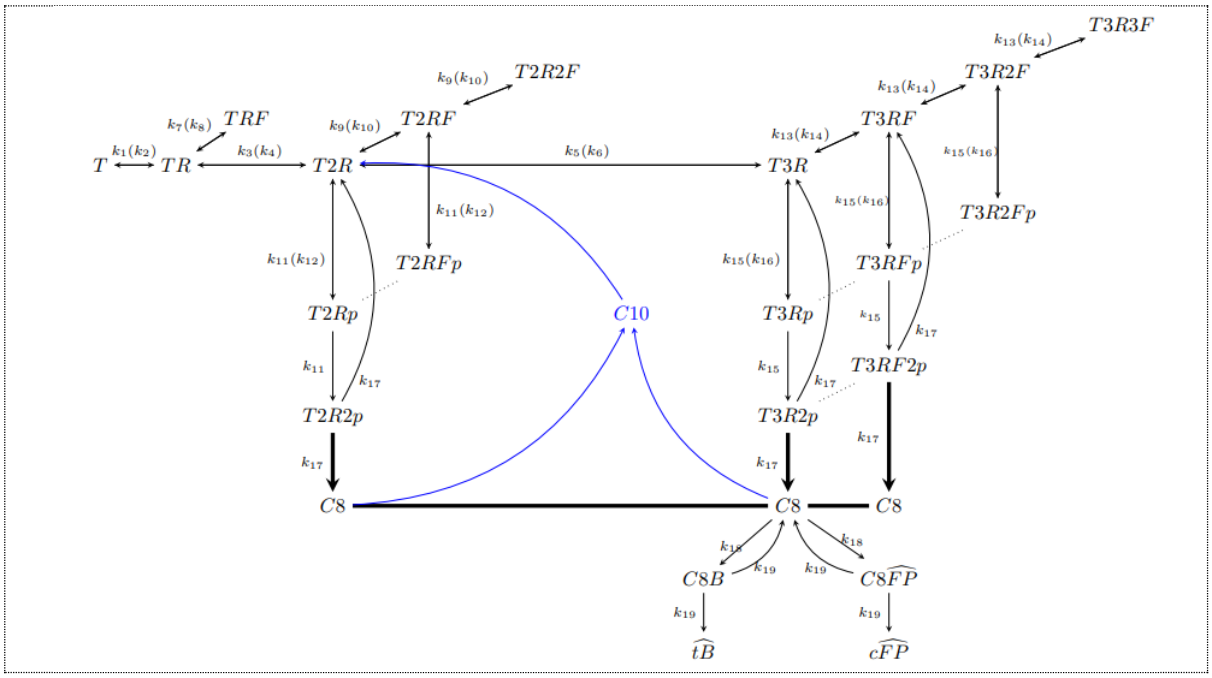

Figure 23. Inclusion of a negative feedback in the receptor reactions of the extrinsic apoptosis pathway.

Novel interactions are colored in blue. Simplified notations were used for representation purposes: T stands for TRAIL, R for death receptors, F for FLIP, p for pC8, B for Bid, tB for tBid, FP for fluorescent reporter protein and cFP for cleaved fluorescence protein. Reaction rates of the forward and reverse reactions are indicated outside and inside brackets, respectively. C8 induces the activation of the protein X1, that we here assume to represent the role of C10, and C10 extracts receptors from the DISC complexes. C10 leads a trimeric complex into a dimeric form and, although not represented, C10 can also retrieve a receptor from the T:2R conformation and convert it into a monomeric form.

Chapter 6

Discussion and perspectives

"We are what we repeatedly do. Excellence, then, is not an act, but a habit"

- Aristotle

In this thesis, a large data set of HeLa cells treated with the death-inducing ligand TRAIL was analyzed in order to study the dynamical behavior of the proteins participating in the receptor-associated reactions of the extrinsic apoptosis pathway. The population of treated cells was described by a highly heterogeneous output fluorescent signal that was quantitatively translated into levels of active C8, an important pro-apoptotic agent whose activity is known to be correlated with the strength of the apoptotic signal. Relating the timing and activity of C8 protein in each treated cell generated a previous separation criteria for resistant and sensitive cells, with sensitive cells lending into a region in space with higher C8 activity values and/or higher timing of maximal C8 activity (Roux et al., 2015). Here, the strategy was to extend this concept by augmenting the description of the resistant and the sensitive phenotypes.

To address these questions, an exhaustive inclusion of the underlying chemical reactions of the extrinsic apoptosis pathway was implemented and translated into a system of ODE's to obtain a global picture of the intervening proteins acting upstream of C8 activation. The

implemented network reflected a local layer of reactions associated to the receptor compartment of the cell and intuitively the model was named ARROM (Apoptosis receptor reactions ODE model). The model represented new features of the apoptotic pathway that were generally simplified in other models, namely the correct receptor stoichiometry with multiple ligand-complexes combinations in the DISC structure before activation of C8. This elaborated version allowed for a more detailed analysis of the receptor-layer events and a more robust study of the signal variability of the data-set. In the work of (Roux et al., 2015), that variability was assessed in terms of the rate of C8 activation ($\mathbf{k}$) and the time of maximum C8 activity ($\boldsymbol{\tau}$), which spanned tenfold and two to threefold, respectively, among individual C8 trajectories. In this thesis each cell-attained maximum C8 activity level, defined in (Roux et al., 2015) as a distinguishing feature between sensitive from resistant cells, was obtained directly from the maximum derivative of the fitted cFP(t) signal.

To extract single cell features and later correlate them to one of the two phenotypes, the ARROM model was independently fitted to every single cell creating a high-dimensional matrix of initial conditions and parameter values, a strategy that differed from the usual approach of selecting a median-cell and fitting the model exclusively to that median-cell profile. This method allowed the obtained distributions of protein numbers and parameter values to be examined and led us to the conclusion that a too-high parameter variability was a possible sign of missing components in the considered network of reactions. Since the parameter variability was especially large in two specific nodes of the network a hypothesis emerged about the existence of two unknown proteins X1 and X2. Further tests confirmed that the adjustment of the ARROM model, redefined to include X1 and X2, decreased the fitted parameter variability among single-cells to acceptable levels, providing an evidence for the existence of proteins that were not yet described in the literature. The exact dynamics of these proteins are naturally unknown but some simple tests elucidated that a positive feedback interaction from C8 to X1 could define a regulatory mechanism through which cells regulate their levels of active C8 and avoid weak apoptotic signals, triggering apoptosis in a more efficient manner. For the protein X1, we considered its dynamics to relate to those of C10, a protein that was recently identified as an anti-apoptotic agent contributing importantly for apoptosis resistance (Horn et al., 2017). Further work would be to extend ARROM2 and explicitly model the dynamics of C10 and include the cooperative binding effects between C8 and C10. These dynamics are studied in more detail in the publication that resulted from this

thesis (Gomes-Pereira et al., 2020). In any case, the most important message brought by X1 and X2 is that agreement of ARROM1 with previous reaction rates in the literature required extra elements to be inserted in the modeled cascade of reactions and its inclusion allowed novel proteomic signatures to be established for the sensitive and resistant phenotypes. For a given treated cell to cross a biological threshold on C8 activity and become sensitive, the model simulations show that the cell should present considerable amounts of R, pC8, X1 and X2 proteins and reduced amounts of FLIP, otherwise the cell resists the treatment.

Interesting insights about FLIP and the interaction schemes in receptor clusters were also deduced from the ARROM simulations. For FLIP, a strong inhibitor of apoptosis, congruence between simulations and a previous result from (Roux et al., 2015), which correlated overexpression of FLIP with a decrease in C8 activity, imposed the FLIP dissociation rates from the DISC to be extremely low, supporting the hypothesis that FLIP is a blocking agent forbidding the attachment of other molecules to the DISC structures. This result is in line with the recent view of C8 being activated from a chain of interacting molecules that can be interrupted by the addition of FLIP (Hughes et al., 2016). As for the receptor interactions in the cell membrane, an old result mentioning an increase in apoptotic signal for higher receptor structures could only be reproduced if those clusters became more and more stable as they grew in number, a new result that may help to characterize and understand the death-receptor interactions inside these clusters. Specifically, the addition of extra receptors supports a rise in C8 signal if and only if the association and dissociation rates of the new complex increases and decreases, respectively, compared to the same rates of the complex with less attached receptors, which might indicate increased stability for higher-order receptor structures.

In order to associate the heterogeneity of the data-set with biological noise sources described in the literature several tests were made. Intrinsic noise for instance, the noise related to the propensity of every chemical reaction, didn’t create sufficient variability to recover the dispersion of the signal output and was ruled out from the possible mechanisms through which cells vary their response and deviate their phenotype outcome. Alternatively, both extrinsic noise and parameter noise were capable of inducing sufficient perturbation on a random curve and recover entirely and partially, respectively, the profile of the whole data set. Simulations with extrinsic noise, often assumed as variability on protein initial quantities in distinct cells, reproduced several features including the dispersion in slope values and in final steady state levels. The parameter noise, an approach to model unknown global noise components, captured

the distribution of maximum slope values but failed to generate enough variability on steady state levels. Extrinsic noise then urged as a possible justification for cell fate decision, either to escape or enroll into apoptosis, although it is not clear if parameter noise can also participate up to some extent in this choice. As mentioned in previous studies of apoptosis, the heterogeneity of response of individual cells results from an interplay of multiple contributing factors (Gaudet et al., 2012; Spencer et al., 2009), and further ameliorations on the model could disentangle the extrinsic and parameter noise contributions and give a clearer justification of their contributing percentages on the total observed heterogeneity.

The set of ODE equations, as contemplated on the ARROM model, presents advantages and disadvantages. One limitation of the model is that cell commitment into apoptosis is measured in terms of the maximum derivative value of the cFP signal in time, which results from the receptor-associated network of reactions. Consequently, the described propensity for cell-death refers to a C8-related threshold and not to the overall global propensity for cell-death. Downstream of C8 activation, the full apoptotic pathway encompasses other restraining steps such as the MOMP threshold and those also contribute for the treatment outcome. The simplicity of adding more mass-action law rates into the ARROM2 model could compensate for this limitation and upgrade the model to more solid versions. The NF-kB survival pathway, which is known to be also induced by TRAIL was not included in the discussed ARROM versions. These survival pathways may modulate the C8 activity and its dynamics may be important to add in the future in order to provide a more complete representation of the underlying biology. Another known feature is the "memory" effect observed for cells after a first TRAIL treatment, in which a lag-period is later-on required for the cell population to respond equally to a second TRAIL treatment (Flusberg et al., 2013). In a future study these mechanisms could be studied and adequately included into ARROM2 in order to extract associated molecular factors and enrich our view of these events. Nonetheless, ARROM2 can be used as a robust tool to analyze potentially interesting experimental scenarios, such as co-drugging treatments, and check for consequent impacts in C8 activity in terms of the dynamics of the already considered proteins. Also, in line with the results of (Roux et al., 2015), the conclusions presented in this text can be extended into other cell lines other than HeLa-cells, such as H1993, ACHN, H2170 and H1703 which show similar C8-dynamics in time after TRAIL exposure.

The continued usage of quantitative approaches has already highlighted several features of the apoptosis network in the past and is an undeniable tool to keep deepening our understanding of how cells flee from the dead phenotype. A more robust comprehension of these processes could solidify existing clinical strategies and maybe recover the once-promising anti-cancer therapy using TRAIL agonists.

Chapter 7

Appendix

7.1 Appendix 1: ARROM1 model inputs

TABLE A1.1. LIST OF AVERAGED NON-ZERO INITIAL CONDITION VALUES FOR ARROM1 AND ARROM2 MODEL SIMULATIONS.

The values attributed to R, FLIP, pC8 and Bid were experimentally determined from western blots extracts. TRAIL quantity was extracted from the work of (Albeck et al., 2008). The fluorescent-reporter protein FP is known to be produced in excessive amounts compared to its homologous protein Bid and was assumed to exist in a double amount.

List of variables with non-zero initial values	Number of Molecules
TRAIL	1500 $(50ng/ml)$
R	32000
FLIP	10000
pC8	150000
Bid	2000000
FP	4000000

TABLE A1.2. LIST OF ARROM1 MODEL REACTIONS AND CORRESPONDING PARAMETER VALUES. Some parameters were extracted from known references in the field of Apoptosis modeling. The unit "Mol" refers to molecules.

Reactions	Parameter values	Units	Reference
Core Reactions			
TRAIL + R → TRAIL:R	k1=5e-7	$mol^{-1}.s^{-1}$	(Szegezdi et al., 2012)
TRAIL:R → TRAIL + R	k2=3.81e-3	s^{-1}	(Szegezdi et al., 2012)
TRAIL:R + R → TRAIL:2R	k3=1.92e-5*	$mol^{-1}.s^{-1}$	(Szegezdi et al., 2012)
TRAIL:2R → TRAIL:R + R	k4=k2	s^{-1}	(Szegezdi et al., 2012)
TRAIL:2R + R → TRAIL:3R	k5=k3	$mol^{-1}.s^{-1}$	(Szegezdi et al., 2012)
TRAIL:3R → TRAIL:2R + R	k6=k4	s^{-1}	(Szegezdi et al., 2012)
TRAIL:R + FLIP → TRAIL:R:FLIP	k7=1e-6	$mol^{-1}.s^{-1}$	(Albeck et al., 2008)
TRAIL:R:FLIP → TRAIL:R + FLIP	k8=1e-3	s^{-1}	(Albeck et al., 2008)

TRAIL:2R: nFLIP: mpC8 + FLIP→ TRAIL:2R:(n+1)FLIP:mpC8
n=0,1;
m=0,1;
n+1+m=1,2;
	k9=k7	$mol^{-1}.s^{-1}$	

TRAIL:2R: nFLIP: mpC8 → TRAIL:2R:(n-1)FLIP:mpC8 + FLIP
n=1,2;
m=0,1;
n+m-1=0,1;
	k10=k8	s^{-1}	

TRAIL:2R:npC8:mFLIP + pC8→ TRAIL:2R:(n+1)pC8:mFLIP
n=0,1;
m=0,1;
n+1+m=1,2;
	k11=k7	$mol^{-1}.s^{-1}$	

TRAIL:2R:npC8:mFLIP →
TRAIL:2R:(n-1)pC8:mFLIP + pC8
n=1;
m=0,1;
n+m=1,2;
	k12=k8	s^{-1}	

TRAIL:3R:nFLIP:mpC8 + FLIP →
TRAIL:3R:(n+1)FLIP:mpC8
n=0,1,2;
m=0,1,2;
n+1+m=1,2,3;
	k13=k7	$mol^{-1}.s^{-1}$	

TRAIL:3R:nFLIP:mpC8 →
TRAIL:3R:(n-1)FLIP:mpC8 + FLIP
n=0,1,2;
m=0,1,2;
n+m=1,2,3;
	k14=k8	s^{-1}	

TRAIL:3R:npC8:mFLIP + pC8 →
TRAIL:3R:(n+1)pC8:mFLIP
n=0,1,2;
m=0,1,2;
n+1+m=1,2,3;
	k15=k7	$mol^{-1}.s^{-1}$	

TRAIL:3R:npC8:mFLIP →
TRAIL:3R:(n-1)pC8:mFLIP + pC8
n=1;
m=0,1,2;
n+m=1,2,3;
	k16=k8	s^{-1}	

Activation of Caspase-8			
TRAIL:2R:2pC8 → TRAIL:2R + C8 TRAIL:3R:2pC8 → TRAIL:3R + C8 TRAIL:3R:FLIP:2pC8 → TRAIL:3R:FLIP + C8	k17=1	s^{-1}	(Albeck et al., 2008)

Caspase-8 reactions			
C8 + Bid → C8:Bid C8 + FP → C8:FP	k18=1e-7	$mol^{-1}.s^{-1}$	(Albeck et al., 2008)

Caspase-8 substrate cleavage			
C8:Bid → C8 + tBid C8:FP → C8 + cFP	k19=1	s^{-1}	(Albeck et al., 2008)

Protein synthesis			
→ TRAIL	0	$mol.s^{-1}$	
→ R	k20=1e-4	$mol.s^{-1}$	
→ pC8	k21=1e-4	$mol.s^{-1}$	
→ FLIP **	k22=1e-2	$mol.s^{-1}$	
→ Bid **	k23=1e-2	$mol.s^{-1}$	
→ FP **	k32=1e-2	$mol.s^{-1}$	

Protein degradation			
TRAIL →	k24=1e-7	s^{-1}	
R →	k25=7.13e-6	s^{-1}	(Bertaux et al., 2014)
FLIP →	k26=3.9e-4	s^{-1}	(Bertaux et al., 2014)
pC8 →	k27=7.13e-6	s^{-1}	(Bertaux et al., 2014)
C8 →	k28=7.13e-4	s^{-1}	
Bid →	k29=7.13e-6	s^{-1}	(Bertaux et al., 2014)
tBid →	k30=7.13e-6	s^{-1}	
cFP →	k31=1e-7	s^{-1}	

* Using the reaction rates available for DR5 receptors. The original values were given in units of $M^{-1}.s^{-1}$. A conversion to mol-1.s-1 was done using the scaling factor 5.8824e11 deduced from EARM1's supplementary table s5 in (Albeck et al., 2008).

** Following the same proportions as in (Bertaux et al., 2014), FLIP and Bid synthesis rate were set to a magnitude of 100-fold the synthesis rates of R and pC8. FP has a protein structure equivalent to Bid and as so its basal synthesis rate was set to an equal value.

7.2 Appendix 2: ARROM1 fit to the *median_cell*

TABLE A2.1 : FULL LIST OF RELATIVE DEVIATIONS FOR THE PARAMETER SET IN THE ARROM1 MODEL AFTER FITTING THE *MEDIAN_CELL* TRAJECTORY.

Parameters with relative deviations higher than $5 * 10^2$ are highlighted in black boxes, lower than 10^2 in white boxes and all the values in between in grey boxes.

All parameters	Initial Guess (i)	k(i) after fitting	Relative Deviation $\frac{\lvert \text{Initial guess [i]} - \text{k[i]} \rvert}{\text{Initial guess [i]}}$
k1	$5 * 10^{-7}$	$1.3 * 10^{-5}$	24.7
k2	$3.8 * 10^{-3}$	1	$2.64 * 10^2$
k3	$1.9 * 10^{-5}$	$4.3 * 10^{-4}$	21.5
k4	$3.8 * 10^{-3}$	3.7	$9.7 * 10^2$
k5	$1.9 * 10^{-5}$	$7.1 * 10^{-4}$	36.2
k6	$3.8 * 10^{-3}$	1.5	$3.9 * 10^2$
k7	10^{-6}	$1.3 * 10^{-4}$	$1.2 * 10^2$
k8	10^{-3}	0.2	$2.3 * 10^2$
k9	10^{-6}	$9 * 10^{-5}$	87.6
k10	10^{-3}	$3.4 * 10^{-2}$	32.7
k11	10^{-6}	$8.4 * 10^{-5}$	82.5
k12	10^{-3}	$5.1 * 10^{-3}$	4.1
k13	10^{-6}	$2.3 * 10^{-4}$	$2.3 * 10^2$
k14	10^{-3}	$1.9 * 10^{-2}$	18
k15	10^{-6}	$7.5 * 10^{-6}$	6.5
k16	10^{-3}	1.4	$1.4 * 10^3$
k17	1	62	61
k18	10^{-7}	$1.2 * 10^{-5}$	$3.19 * 10^2$
k19	1	10^{-2}	1
k20	10^{-4}	$3.4 * 10^{-2}$	$3.3 * 10^2$
k21	10^{-4}	$2.1 * 10^{-2}$	$2.1 * 10^2$

k22	10^{-2}	$6.5 * 10^{-2}$	5.5
k23	10^{-2}	1.2	$1.2 * 10^{2}$
k24	10^{-7}	$8.6 * 10^{-6}$	85
k25	$7.1 * 10^{-6}$	$5.7 * 10^{-5}$	7
k26	$3.9 * 10^{-4}$	$5.2 * 10^{-4}$	$3.4 * 10^{-1}$
k27	$7.1 * 10^{-6}$	$1.5 * 10^{-4}$	20.6
k28	$7 * 10^{-4}$	5.7	$7.9 * 10^{2}$
k29	$7.1 * 10^{-6}$	$7.7 * 10^{-5}$	9.9
k30	$7.1 * 10^{-6}$	$2.9 * 10^{-4}$	40.1
k31	10^{-7}	$3.1 * 10^{-5}$	$3.2 * 10^{2}$
k32	10^{-2}	$2.1 * 10^{-1}$	20.4

7.3 Appendix 3: ARROM2 fit to the *median_cell*

TABLE A3.1 PROTEIN INITIAL CONDITION VALUES BEFORE AND AFTER FITTING THE *MEDIAN_CELL* TO THE ARROM2 MODEL.

List of variables with non-zero initial values	Number of Molecules (*initial_guess*)	Number of Molecules (*after_fitting*)
TRAIL	1500 $(50ng/ml)$	1500
R	32000	9028
FLIP	10000	11674
pC8	150000	50533
Bid	2000000	2265400
FP	4000000	844770
X1	1000	1000
X2	1000	3050

TABLE A3.2 PARAMETER LIST VECTOR BEFORE AND AFTER FITTING THE *MEDIAN_CELL* TO THE ARROM2 MODEL.

The *initial_guess* was part of the input introduced into the *fminsearchbnd* algorithm to initiate the fit.

All parameters	Initial Guess	ARROM2 fitting *median_cell*
k1	$5 * 10^{-7}$	$7.14 * 10^{-6}$
k2	$3.8 * 10^{-3}$	$4.3 * 10^{-3}$
k3	$1.9 * 10^{-5}$	$2.38 * 10^{-5}$
k4	$3.8 * 10^{-3}$	$4.5 * 10^{-3}$
k5	$1.9 * 10^{-5}$	$1.46 * 10^{-5}$
k6	$3.8 * 10^{-3}$	$9.8 * 10^{-3}$
k7	10^{-6}	$7.14 * 10^{-6}$

k8	10^{-3}	$5.12 * 10^{-4}$
k9	10^{-6}	$7.14 * 10^{-6}$
k10	10^{-3}	10^{-3}
k11	10^{-6}	$7.14 * 10^{-6}$
k12	10^{-3}	10^{-3}
k13	10^{-6}	$7.14 * 10^{-6}$
k14	10^{-3}	$1.2 * 10^{-3}$
k15	10^{-6}	$7.14 * 10^{-6}$
k16	10^{-3}	$2 * 10^{-3}$
k17	1	0.68
k18	10^{-7}	$7.14 * 10^{-6}$
k19	1	0.92
k20	10^{-4}	$1.24 * 10^{-4}$
k21	10^{-4}	$1.12 * 10^{-4}$
k22	10^{-2}	$9.5 * 10^{-3}$
k23	10^{-2}	$1.48 * 10^{-2}$
k24	10^{-7}	$7.14 * 10^{-6}$
k25	$7.1 * 10^{-6}$	$7.14 * 10^{-6}$
k26	$3.9 * 10^{-4}$	$1.95 * 10^{-4}$
k27	$7.1 * 10^{-6}$	$7.14 * 10^{-6}$
k28	$7 * 10^{-4}$	$1.7 * 10^{-3}$
k29	$7.1 * 10^{-6}$	$7.14 * 10^{-6}$
k30	$7.1 * 10^{-6}$	$7.18 * 10^{-6}$
k31	10^{-7}	$7.14 * 10^{-6}$
k32	10^{-2}	$1.17 * 10^{-2}$

7.4 Appendix 4 : ARROM1 model equations

All equations were written using mass-action rate laws. The models were implemented and simulated in *Matlab (2017)*, using the built-in solver of ordinary differential equations *ode15s*. Parameter estimation was performed using the command *fminsearchbnd*.

$$\frac{d\,TRAIL(t)}{dt} = -k_1 * TRAIL(t) * R(t) + k_2 * TRAIL{:}R(t) - k_{24} * TRAIL(t) \quad \textbf{(13)}$$

$$\begin{aligned}\frac{d\,R(t)}{dt} = {} & k_{20} + k_1 * TRAIL(t) * R(t) - k_4 * TRAIL{:}2R(t) - k_5 * R(t) * TRAIL{:}2R(t) \\ & + k_6 * TRAIL{:}3R(t) + k_2 * TRAIL{:}R(t) - k_3 * R(t) * TRAIL{:}R(t) \\ & - k_{25} * R(t)\end{aligned} \quad \textbf{(14)}$$

$$\begin{aligned}\frac{d\,TRAIL{:}R(t)}{dt} = {} & k_1 * TRAIL(t) * R(t) + k_4 * TRAIL{:}2R(t) - k_2 * TRAIL{:}R(t) \\ & - k_3 * TRAIL{:}R(t) * R(t) - k_7 * TRAIL{:}R(t) * FLIP(t) \\ & + k_8 * TRAIL{:}R{:}FLIP(t)\end{aligned} \quad \textbf{(15)}$$

$$\begin{aligned}\frac{d\,TRAIL{:}2R(t)}{dt} = {} & -k_4 * TRAIL{:}2R(t) - k_5 * TRAIL{:}2R(t) * R(t) \\ & - k_9 * FLIP(t) * TRAIL{:}2R(t) - k_{11} * pC8(t) * TRAIL{:}2R(t) \\ & + k_{17} * TRAIL{:}2R{:}2pC8(t) + k_{10} * TRAIL{:}2R{:}FLIP(t) \\ & + k_{12} * TRAIL{:}2R{:}pC8(t) + k_6 * TRAIL{:}3R(t) \\ & + k_3 * R(t) * TRAIL{:}R(t)\end{aligned} \quad \textbf{(16)}$$

$$\frac{d\,TRAIL{:}3R(t)}{dt} = -k_5 * R(t) * TRAIL{:}2R(t) - k_6 * TRAIL{:}3R(t)$$
$$-k_{13} * FLIP(t) * TRAIL{:}3R(t) - k_{15} * pC8(t) * TRAIL{:}3R(t)$$
$$-k_{17} * TRAIL{:}3R{:}2pC8(t) + k_{14} * TRAIL{:}3R{:}FLIP(t)$$
$$-k_{16} * TRAIL{:}3R{:}pC8(t) \quad \textbf{(17)}$$

$$\frac{d\,FLIP(t)}{dt} = k_{22} - k_9 * FLIP(t) * TRAIL{:}2R(t) + k_{10} * TRAIL{:}2R{:}2FLIP(t)$$
$$+k_{10} * TRAIL{:}2R{:}FLIP(t) - k_9 * FLIP(t) * TRAIL{:}2R{:}FLIP(t)$$
$$-k_{13} * FLIP(t) * TRAIL{:}3R(t) + k_{14} * TRAIL{:}3R{:}2FLIP(t)$$
$$-k_{13} * FLIP(t) * TRAIL{:}3R{:}2FLIP(t) + k_{14} * TRAIL{:}3R{:}3FLIP(t)$$
$$+k_{14} * TRAIL{:}3R{:}FLIP - k_{13} * FLIP(t) * TRAIL{:}3R{:}FLIP(t)$$
$$-k_7 * FLIP(t) * TRAIL{:}R(t) + k_8 * TRAIL{:}R{:}FLIP(t) - k_{26} * FLIP(t)$$
$$+k_{10} * TRAIL{:}2R{:}FLIP{:}pC8(t) + k_{14} * TRAIL{:}3R{:}2FLIP{:}pC8(t) \quad \textbf{(18)}$$

$$\frac{d\,TRAIL{:}R{:}FLIP(t)}{dt} = k_7 * FLIP(t) * TRAIL{:}R(t) - k_8 * TRAIL{:}R{:}FLIP(t) \quad \textbf{(19)}$$

$$\frac{d\,TRAIL{:}2R{:}FLIP(t)}{dt} = k_9 * FLIP(t) * TRAIL{:}2R(t) + k_{10} * TRAIL{:}2R{:}2FLIP(t)$$
$$-k_{10} * FLIP(t) * TRAIL{:}2R{:}FLIP(t)$$
$$-k_{11} * pC8(t) * TRAIL{:}2R{:}FLIP(t)$$
$$+k_{12} * TRAIL{:}2R{:}FLIP{:}pC8(t) \quad \textbf{(20)}$$

$$\frac{d\,TRAIL{:}2R{:}2FLIP(t)}{dt} = -k_{10} * TRAIL{:}2R{:}2FLIP(t)$$
$$+k_9 * FLIP(t) * TRAIL{:}2R{:}FLIP(t) \quad \textbf{(21)}$$

$$\frac{d\ pC8(t)}{dt} = k_{21} - k_{11} * pC8(t) * TRAIL{:}\,2R(t) - k_{11} * pC8(t) * TRAIL{:}\,2R{:}\,FLIP(t)$$
$$+k_{12} * TRAIL{:}\,2R{:}\,FLIP{:}\,pC8(t) + k_{12} * TRAIL{:}\,2R{:}\,pC8(t)$$
$$-k_{11} * TRAIL{:}\,2R{:}\,pC8(t) * pC8(t) - k_{15} * pC8(t) * TRAIL{:}\,3R(t)$$
$$-k_{15} * pC8(t) * TRAIL{:}\,3R{:}\,2FLIP(t) + k_{16} * TRAIL{:}\,3R{:}\,2FLIP{:}\,pC8(t)$$
$$-k_{15} * pC8(t) * TRAIL{:}\,3R{:}\,FLIP(t) + k_{16} * TRAIL{:}\,3R{:}\,FLIP{:}\,pC8(t)$$
$$-k_{15} * pC8(t) * TRAIL{:}\,3R{:}\,FLIP{:}\,pC8(t) + k_{16} * TRAIL{:}\,3R{:}\,pC8(t)$$
$$-k_{15} * pC8(t) * TRAIL{:}\,3R{:}\,pC8(t) - k_{27} * pC8(t) \quad \textbf{(22)}$$

$$\frac{d\ TRAIL{:}2R{:}FLIP{:}pC8(t)}{dt} = k_{11} * pC8(t) * TRAIL{:}\,2R{:}\,FLIP(t)$$
$$-k_{12} * TRAIL{:}\,2R{:}\,FLIP{:}\,pC8(t)$$
$$-k_{10} * TRAIL{:}\,2R{:}\,FLIP{:}\,pC8(t) \quad \textbf{(23)}$$

$$\frac{d\ TRAIL{:}3R{:}FLIP(t)}{dt} = k_{13} * FLIP(t) * TRAIL{:}\,3R(t) + k_{14} * TRAIL{:}\,3R{:}\,2FLIP(t)$$
$$-k_{14} TRAIL{:}\,3R{:}\,FLIP(t)$$
$$-k_{13} * FLIP(t) * TRAIL{:}\,3R{:}\,FLIP(t)$$
$$-k_{15} * pC8(t) * TRAIL{:}\,3R{:}\,FLIP(t)$$
$$+k_{17} * TRAIL{:}\,3R{:}\,FLIP{:}\,2pC8(t)$$
$$+k_{16} * pC8(t) * TRAIL{:}\,3R{:}\,FLIP{:}\,pC8(t) \quad \textbf{(24)}$$

$$\frac{d\ TRAIL{:}3R{:}2FLIP(t)}{dt} = -k_{14} * TRAIL{:}\ 3R{:}\ 2FLIP(t)$$
$$-k_{13} * FLIP(t) * TRAIL{:}\ 3R{:}\ 2FLIP(t)$$
$$-k_{15} * pC8(t) * TRAIL{:}\ 3R{:}\ 2FLIP(t)$$
$$+k_{16} * FLIP(t) * TRAIL{:}\ 3R{:}\ 2FLIP{:}\ pC8(t)$$
$$+k_{14} * TRAIL{:}\ 3R{:}\ 3FLIP(t)$$
$$+k_{13} * FLIP(t) * TRAIL{:}\ 3R{:}\ FLIP(t) \quad \textbf{(25)}$$

$$\frac{d\ TRAIL{:}3R{:}3FLIP(t)}{dt} = k_{13} * FLIP(t) * TRAIL{:}\ 3R{:}\ 2FLIP(t)$$
$$-k_{14} * TRAIL{:}\ 3R{:}\ 3FLIP(t) \quad \textbf{(26)}$$

$$\frac{d\ TRAIL{:}3R{:}2FLIP{:}pC8(t)}{dt} = k_{15} * pC8(t) * TRAIL{:}\ 3R{:}\ 2FLIP(t)$$
$$-k_{16} * pC8(t) * TRAIL{:}\ 3R{:}\ 2FLIP{:}\ pC8(t)$$
$$-k_{14} * pC8(t) * TRAIL{:}\ 3R{:}\ 2FLIP{:}\ pC8(t) \quad \textbf{(27)}$$

$$\frac{d\ TRAIL{:}2R{:}pC8(t)}{dt} = -k_{17} * TRAIL{:}\ 2R{:}\ 2pC8(t) + k_{11} * pC8(t) * TRAIL{:}\ 2R{:}\ pC8(t) \quad \textbf{(28)}$$

$$\frac{d\ TRAIL{:}2R{:}2pC8}{dt} = -k_{17} * TRAIL{:}\ 2\text{R}{:}2pC8(t) + k_{11} * TRAIL{:}\ 2R{:}\ pC8(t) * pC8(t) \quad \textbf{(29)}$$

$$\frac{d\ TRAIL{:}3R{:}pC8(t)}{dt} = k_{15} * pC8(t) * TRAIL{:}\ 3R(t) - k_{16} * TRAIL{:}\ 3R{:}\ pC8(t)$$
$$-k_{15} * pC8(t) * TRAIL{:}\ 3R{:}\ pC8(t)$$
$$-k_{13} * FLIP(t) * TRAIL{:}\ 3R{:}\ pC8(t) \quad \textbf{(30)}$$

$$\frac{d\ TRAIL{:}3R{:}2pC8(t)}{dt} = -k_{17} * TRAIL{:}\ 3R{:}\ 2pC8(t)$$

$$+k_{15} * pC8(t) * TRAIL{:}\ 3R{:}\ pC8(t) \quad \textbf{(31)}$$

$$\frac{d\ TRAIL{:}3R{:}FLIP{:}pC8(t)}{dt} = k_{15} * pC8(t) * TRAIL{:}\ 3R{:}\ FLIP(t)$$

$$-k_{16} * TRAIL{:}\ 3R{:}\ FLIP{:}\ pC8(t)$$

$$-k_{15} * pC8(t) * TRAIL{:}\ 3R{:}\ FLIP{:}\ pC8(t)$$

$$+k_{14} * TRAIL{:}\ 3R{:}\ 2FLIP{:}\ pC8(t)$$

$$+k_{13} * FLIP(t) * TRAIL{:}\ 3R{:}\ pC8(t) \quad \textbf{(32)}$$

$$\frac{d\ TRAIL{:}3R{:}FLIP{:}2pC8(t)}{dt} = -k_{17} * TRAIL{:}\ 3R{:}\ FLIP{:}\ 2pC8(t)$$

$$+k_{15} * pC8(t) * TRAIL{:}\ 3R{:}\ FLIP{:}\ pC8(t)$$

$$+k_{13} * TRAIL{:}\ 3R{:}\ 2pC8(t) \quad \textbf{(33)}$$

$$\frac{d\ C8(t)}{dt} = -k_{18} * C8(t) * Bid(t) + k_{19} * C8{:}\ Bid(t) - k_{18} * C8(t) * FP(t)$$

$$+k_{19} * C8(t) * FP(t) + k_{19} * C8{:}\ Bid(t) + k_{17} * TRAIL{:}\ 2R{:}\ 2pC8(t)$$

$$+k_{17} * TRAIL{:}\ 3R{:}\ 2pC8(t) + k_{17} * TRAIL{:}\ 3R{:}\ FLIP{:}\ 2pC8(t)$$

$$-k_{28} * C8(t) \quad \textbf{(34)}$$

$$\frac{d\ Bid(t)}{dt} = k_{23} - k_{18} * C8(t) * Bid(t) - k_{29} * Bid(t) \quad \textbf{(35)}$$

$$\frac{d\ C8{:}Bid(t)}{dt} = k_{18} * C8(t) * Bid(t) - k_{19} * C8{:}\ Bid(t) \quad \textbf{(36)}$$

$$\frac{d\ tBid(t)}{dt} = k_{19} * C8{:}\ Bid(t) - k_{30} * tBid(t) \quad \textbf{(37)}$$

$$\frac{d\ FP(t)}{dt} = k_{32} - k_{18} * C8(t) * FP(t) \quad \textbf{(38)}$$

$$\frac{d\ C8{:}FP(t)}{dt} = k_{18} * C8(t) * FP(t) - k_{19} * C8{:}\ FP(t) \quad \textbf{(39)}$$

$$\frac{d\ cFP(t)}{dt} = k_{19} * C8{:}\ FP(t) - k_{31} * cFP(t) \quad \textbf{(40)}$$

7.5 Appendix 5: A new method to quantify parameter variability among different parameter populations

One of the problems studied in this thesis is that of using a mathematical model of the apoptosis pathway to distinguish between two groups of cells, resistant and sensitive. In the case of single-cell data, several approaches may be considered to model parameter estimation. In a direct approach, each single cell trace is first separately fitted to the model, to obtain one parameter set for each cell; in a second step, the distribution of parameters can then be studied. To take into account both population and individual effects, (Llamosi et al., 2016) proposed a new mixed-effect population-based parameter estimation, where all cell traces are fitted to obtain the parameters of a single lognormal distribution; the individual cell parameters are then characterized by this distribution. However, here the entire cell sample is divided into subpopulations exhibiting distinct physiological responses, and a slightly different question is considered: that of finding the global aspects distinguishing between two separate subpopulations within the same population. To address this question, first, the direct approach will be used to fit each single trace and obtain one set of parameters for each cell. Second, the parameter distributions for each subpopulation will be compared to extract distinguishing features. In this method, two distributions are said to be "different", in a generic view, in three standard scenarios.

- Different *mean_values* and different *standard_deviations* **(A7.1)**
- Different *mean_values* and same *standard_deviations* **(A7.2)**
- Same *mean_values* and different *standard_deviations* **(A7.3)**

In these three scenarios one can seek for parameter differences, independently of the form of the corresponding distributions. The first step is to calculate the mean and standard deviation (std) of the parameters in each of the fitted populations. Afterwards, these mean and std quantities have to be normalized so that the set of parameters can be compared, regardless of their differences in magnitudes and unit dimensions. The normalization step is achieved simply by dividing the mean and std of every parameter by the corresponding norm. This procedure is done according to expressions **(41)** and **(42),** with each parameter vector entry designated by " *par_i* " .

$$k_{mean\_norm\_population\_1} = \frac{k_{mean\_par\_i,population\_1}}{\sqrt{\sum_{j=1}^{n}\left(k_{mean\_par\_i,population\_j}\right)^2}} \quad \textbf{(41)}$$

$$k_{std\_norm\_population\_1} = \frac{k_{std\_par\_i,population\_1}}{\sqrt{\sum_{j=1}^{n}\left(k_{std\_par\_i,population\_j}\right)^2}} \quad \textbf{(42)}$$

The index " j ", in both expressions is an integer number representing a given sampled subpopulation and " n " is the total number of fitted subpopulations. The denominator in those expressions is thus the Euclidian norm of the vector of *means* or *std_values* among the subpopulations. Both **(41)** and **(42)** are then repeated for all subpopulations j such that a normalized mean and std value exists for every fitted subpopulation.

Once the first-order moments (mean and std) are normalized, a reference point is established. Supposing that the parameters have exactly the same fitted values across all the sampled subpopulations, expressions **(41)** and **(42)** equal $\frac{1}{\sqrt{n}}$, and the reference point becomes $\left(\frac{1}{\sqrt{n}}, \dots, \frac{1}{\sqrt{n}}\right)$ in R^n space, with n the number of subpopulations. Treating separately the mean and the std normalized space, the distance d between the reference point and each normalized value is determined by the usual Euclidian distance.

$$d_{mean\_norm} = \left\| \left(\frac{1}{\sqrt{n}}, \dots, \frac{1}{\sqrt{n}}\right) - \left(k_{mean\_norm\_population\_1}, \dots, k_{mean\_norm\_population\_n}\right) \right\| \quad \textbf{(43)}$$

$$d_{std\_norm} = \left\| \left(\frac{1}{\sqrt{n}}, \dots, \frac{1}{\sqrt{n}}\right) - \left(k_{std\_norm\_population\_1}, \dots, k_{std\_norm\_population\_n}\right) \right\| \quad \textbf{(44)}$$

Both expressions **(43)** and **(44)** are then to be applied to all the parameter vector entries so that a list of distances can be obtained for the whole vector. In this situation an ordered list can be produced, from the furthest to the closest parameter distances relative to the reference point. For $n = 2$ or $n = 3$, the normalized first-order moments can be represented on the positive quadrant of an orthogonal axis of dimension n, through circles centered on the reference point

and with a radius of d_{mean_norm} or d_{std_norm} in the normalized mean and the std space, respectively [see figure A.1) and A.2)].

The final step is to use the already ordered distance d_{mean_norm} and d_{std_norm} to define the groups A7.1 , A7.2 and A7.3. The first group A7.1, contains the parameters with the highest distances in both d_{mean_norm} and d_{std_norm}. The second group A7.2, contains the parameters with the highest d_{mean_norm} and lowest d_{std_norm}. Finally, the group A7.3, contains the parameters which appear in the lowest d_{mean_norm} and highest d_{std_norm} entries. Defining the *low_value_list* and the *high_value_list* is not trivial. Once the d_{mean_norm} and d_{std_norm} lists are organized, in increasing or decreasing fashion, both lists have a length equal to the total number of parameters. Choosing the first and the last ceil[*0.3*number_of_parameters*] (*high_30%_candidates* and *low_30%_candidates*) entries of those lists seems to return a correct prediction for this algorithm, for models with *number_of_parameters* >10, as in all the model versions in this thesis.

Example:

Application of the methodology for identification of distinguishing parameters, among the populations of sensitive and resistant cells, fitted by the ARROM1 model in section 2.5

1) Population = [sensitive cells ; resistant cells] $\rightarrow n = 2$

2) $$k_{mean\_norm\_population\_1} = \frac{k_{mean\_par\_i,population\_1}}{\sqrt{\sum_{j=1}^{2}\left(k_{mean\_par\_i,population\_j}\right)^2}}$$

$$k_{mean\_norm\_population\_2} = \frac{k_{mean\_par\_i,population\_2}}{\sqrt{\sum_{j=1}^{2}\left(k_{mean\_par\_i,population\_j}\right)^2}}$$

$$k_{std\_norm\_population\_1} = \frac{k_{std\_par\_i,population\_1}}{\sqrt{\sum_{j=1}^{2}\left(k_{std\_par\_i,population\_j}\right)^2}}$$

$$k_{std\_norm\_population\_2} = \frac{k_{std\_par\_i,population\_2}}{\sqrt{\sum_{j=1}^{2}\left(k_{std\_par\_i,population\_j}\right)^2}}$$

3) *Number_of_parameters*= 32

Reference point = $\left(\frac{1}{\sqrt{2}}, \frac{1}{\sqrt{2}}\right)$

4) Obtain d_{mean_norm} and d_{std_norm} for every par={1,…,32}:

$$d_{mean\_norm} = \left\| \left(\frac{1}{\sqrt{2}}, \frac{1}{\sqrt{2}}\right) - \left(k_{mean\_norm\_population\_1}, k_{mean\_norm\_population\_2}\right) \right\|$$

$$d_{std\_norm} = \left\| \left(\frac{1}{\sqrt{2}}, \frac{1}{\sqrt{2}}\right) - \left(k_{std\_norm\_population\_1}, k_{std\_norm\_population\_2}\right) \right\|$$

5) Organize d_{mean_norm} and d_{std_norm} in ascending order, from the lowest valued distances to the highest valued distances.

6) Define *low_30%_value_list* and *high_30%_value_list* as the first and the last 10 entries of each sorted d_{mean_norm} and d_{std_norm} lists, in ascending order (10 entries = ceil [0.3 * 32]).

7) Represent the normalized *mean_parameter_space* and the normalized *std_parameter_space* as proposed in the text [figure A.1) and A.2)]

8) With the *low_30%_value_list* and *high_30%_value_list* construct the groups A7.1, A7.2 and A7.3.

A7.1 = {*high_30%_value_list_mean*} ∩ {*high_30%_value_list_std*}

= {18, 11, 28, 31, 14, 24, 5, 32, 21, 7} ∩ {27, 18, 4, 6, 32, 21, 13, 26, 24, 2}

= {18 , 21, 24 , 32}

A7.2 = {*high_30%_value_list_mean*} ∩ {*low_30%_value_list_std*}

= {18, 11, 28, 31, 14, 24, 5, 32, 21, 7} ∩ {23, 1, 22, 14, 19, 25, 17, 8, 10, 11}

= {11, 14}

A7.3 = {*low_30%_value_list_mean*} ∩ {*high_30%_value_list_std*}

= {3, 8, 15, 16, 2, 9, 20, 12, 26, 13} ∩ {27, 18, 4, 6, 32, 21, 13, 26, 24, 2}

= {2 , 13, 26}

9) The list of most deviating parameters is then $p = \bigcup_{i=1}^{3}\{A7.i\}$

= {2, 11, 13, 14, 18, 21, 24, 26, 32}

Among the candidates, the list *p* contains k2 as one of the most deviating parameters. This parameter was identified in section 2.5 was one of the nodes of the network where the parameter discrepancy after the fit was most pronounced, showing that this algorithm also allows the detection of some of the critical nodes. Nonetheless, it is important to highlight that the analysis in section 2.5 resulted from a single fit of the ARROM1 model to the *median_cell* and in this algorithm all the curves, on both sensitive and resistant subpopulations, had to be fitted and their parameters compared. The most deviating parameters across an entire data-set are not expected to be exactly equal as the ones that deviate the most in one single fit.

This methodology is at the basis of an ongoing complementary study of the ARROM2 model, focusing on the output list *p* and on the role of these parameters and how they shape the apoptosis pathway dynamics.

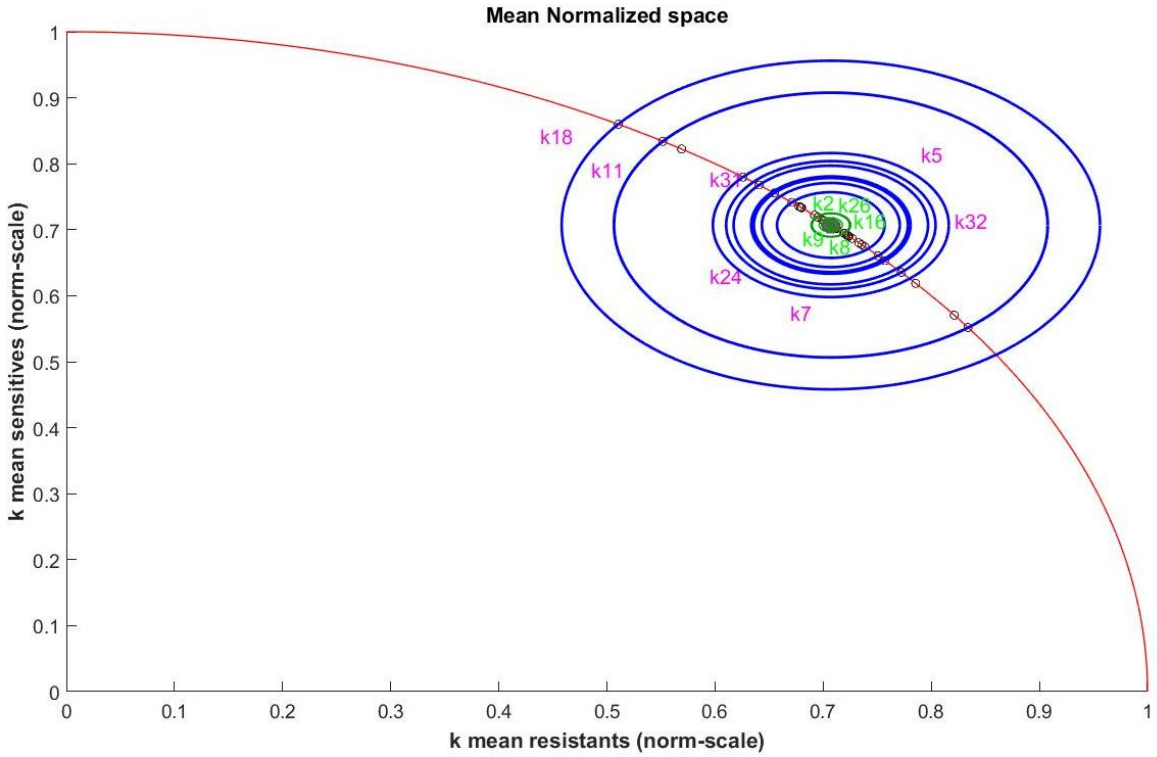

Figure A.1) Representation of the parameter set of the ARROM2 model in the normalized mean space after fitting the sensitive and the resistant cell populations

Fitting the entire collection of resistant and sensitive cells in the data-set returned a matrix of fitted parameter vectors that best matched every single-cell trajectory. Following the algorithm proposed in this section led to the identification of the parameters [2, 8, 9, 16, 26] as a subset of those that deviated the least in terms of their means and their circular orbits are thus in the vicinity of the reference point $=\left(\frac{1}{\sqrt{2}},\frac{1}{\sqrt{2}}\right)$ [green orbits with parameters represented in green]. Oppositely, the parameters [5, 7, 11, 18, 24, 31, 32] are a subset of those with the largest differences in means among the population of sensitive and resistant cells and their orbits are the furthest away from the reference point (blue orbits with parameters represented in pink). For illustration purposes, only a subset of the least and most deviating parameters is represented. The algorithm returned a total of 10 least-deviating parameters and 10 most-deviating parameters in total.

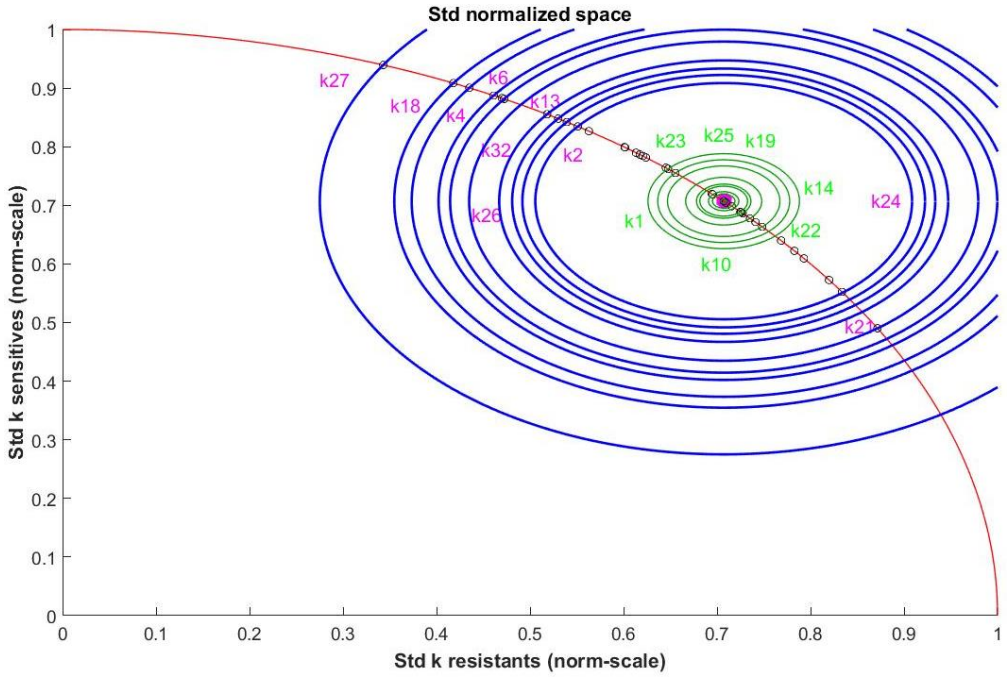

Figure A.2) Representation of the parameter set of the ARROM2 model in the normalized standard deviation space after fitting the sensitive and the resistant cell populations

Fitting the entire collection of resistant and sensitive cells in the data-set returned a matrix of fitted parameter vectors that best matched every single-cell trajectory. Following the algorithm proposed in this section led to the identification of the parameters [1, 10, 14, 19, 23, 25] as a subset of those that deviated the least in terms of their standard deviations and their circular orbits are thus in the vicinity of the reference point $=\left(\frac{1}{\sqrt{2}},\frac{1}{\sqrt{2}}\right)$ [green orbits, with parameters represented in green]. Oppositely, the parameters [2, 4, 6, 13, 18, 21, 24, 26, 27, 32] are the parameters with the largest differences in standard deviations among the population of sensitive and resistant cells and their orbits are the furthest away from the reference point (blue orbits with parameters represented in pink). For illustration purposes, only a subset of the least deviating parameters is represented. The algorithm returned a total of 10 least-deviating parameters.

The End

Bibliography

Albeck, J.G., Burke, J.M., Spencer, S.L., Lauffenburger, D.A., Sorger, P.K., 2008. Modeling a Snap-Action, Variable-Delay Switch Controlling Extrinsic Cell Death. PLoS Biol. 6, e299. https://doi.org/10.1371/journal.pbio.0060299

Aldridge, B.B., Gaudet, S., Lauffenburger, D.A., Sorger, P.K., 2011. Lyapunov exponents and phase diagrams reveal multi-factorial control over TRAIL-induced apoptosis. Mol. Syst. Biol. 7, 553. https://doi.org/10.1038/msb.2011.85

Almendro, V., Marusyk, A., Polyak, K., 2013. Cellular Heterogeneity and Molecular Evolution in Cancer. Annu. Rev. Pathol. Mech. Dis. 8, 277–302. https://doi.org/10.1146/annurev-pathol-020712-163923

Ashkenazi, A., Pai, R.C., Fong, S., Leung, S., Lawrence, D.A., Marsters, S.A., Blackie, C., Chang, L., McMurtrey, A.E., Hebert, A., DeForge, L., Koumenis, I.L., Lewis, D., Harris, L., Bussiere, J., Koeppen, H., Shahrokh, Z., Schwall, R.H., 1999. Safety and antitumor activity of recombinant soluble Apo2 ligand. J. Clin. Invest. 104, 155–162. https://doi.org/10.1172/JCI6926

Azijli, K., Yuvaraj, S., Peppelenbosch, M.P., Wurdinger, T., Dekker, H., Joore, J., van Dijk, E., Quax, W.J., Peters, G.J., de Jong, S., Kruyt, F.A.E., 2012. Kinome profiling of non-canonical TRAIL signaling reveals RIP1-Src-STAT3-dependent invasion in resistant non-small cell lung cancer cells. J. Cell Sci. 125, 4651–4661. https://doi.org/10.1242/jcs.109587

Bagci, E.Z., Vodovotz, Y., Billiar, T.R., Ermentrout, G.B., Bahar, I., 2006. Bistability in Apoptosis: Roles of Bax, Bcl-2, and Mitochondrial Permeability Transition Pores. Biophys. J. 90, 1546–1559. https://doi.org/10.1529/biophysj.105.068122

Balázsi, G., van Oudenaarden, A., Collins, J.J., 2011. Cellular Decision Making and Biological Noise: From Microbes to Mammals. Cell 144, 910–925. https://doi.org/10.1016/j.cell.2011.01.030

Ballweg, R., Paek, A.L., Zhang, T., 2017. A dynamical framework for complex fractional killing. Sci. Rep. 7, 8002. https://doi.org/10.1038/s41598-017-07422-2

Becker, A., Crombag, L., Heideman, D.A.M., Thunnissen, F.B., van Wijk, A.W., Postmus, P.E., Smit, E.F., 2011. Retreatment with erlotinib: Regain of TKI sensitivity following a drug holiday for patients with NSCLC who initially responded to EGFR-

TKI treatment. Eur. J. Cancer 47, 2603–2606. https://doi.org/10.1016/j.ejca.2011.06.046

Bentele, M., Lavrik, I., Ulrich, M., Stößer, S., Heermann, D.W., Kalthoff, H., Krammer, P.H., Eils, R., 2004. Mathematical modeling reveals threshold mechanism in CD95-induced apoptosis. J. Cell Biol. 166, 839–851. https://doi.org/10.1083/jcb.200404158

Bertaux, F., Stoma, S., Drasdo, D., Batt, G., 2014. Modeling Dynamics of Cell-to-Cell Variability in TRAIL-Induced Apoptosis Explains Fractional Killing and Predicts Reversible Resistance. PLoS Comput. Biol. 10, e1003893. https://doi.org/10.1371/journal.pcbi.1003893

Bhola, P.D., Letai, A., 2016. Mitochondria—Judges and Executioners of Cell Death Sentences. Mol. Cell 61, 695–704. https://doi.org/10.1016/j.molcel.2016.02.019

Bhola, P.D., Simon, S.M., 2009. Determinism and divergence of apoptosis susceptibility in mammalian cells. J. Cell Sci. 122, 4296–4302. https://doi.org/10.1242/jcs.055590

Birtwistle, M.R., von Kriegsheim, A., Kida, K., Schwarz, J.P., Anderson, K.I., Kolch, W., 2011. Linear Approaches to Intramolecular Förster Resonance Energy Transfer Probe Measurements for Quantitative Modeling. PLoS ONE 6, e27823. https://doi.org/10.1371/journal.pone.0027823

Blake, W.J., Balázsi, G., Kohanski, M.A., Isaacs, F.J., Murphy, K.F., Kuang, Y., Cantor, C.R., Walt, D.R., Collins, J.J., 2006. Phenotypic Consequences of Promoter-Mediated Transcriptional Noise. Mol. Cell 24, 853–865. https://doi.org/10.1016/j.molcel.2006.11.003

Blake, W.J., KÆrn, M., Cantor, C.R., Collins, J.J., 2003. Noise in eukaryotic gene expression. Nature 422, 633–637. https://doi.org/10.1038/nature01546

Bódi, Z., Farkas, Z., Nevozhay, D., Kalapis, D., Lázár, V., Csörgő, B., Nyerges, Á., Szamecz, B., Fekete, G., Papp, B., Araújo, H., Oliveira, J.L., Moura, G., Santos, M.A.S., Székely Jr, T., Balázsi, G., Pál, C., 2017. Phenotypic heterogeneity promotes adaptive evolution. PLOS Biol. 15, e2000644. https://doi.org/10.1371/journal.pbio.2000644

Bouhaddou, M., Barrette, A.M., Stern, A.D., Koch, R.J., DiStefano, M.S., Riesel, E.A., Santos, L.C., Tan, A.L., Mertz, A.E., Birtwistle, M.R., 2018. A mechanistic pan-cancer pathway model informed by multi-omics data interprets stochastic cell fate responses to drugs and mitogens. PLOS Comput. Biol. 14, e1005985. https://doi.org/10.1371/journal.pcbi.1005985

Brenner, D., Mak, T.W., 2009. Mitochondrial cell death effectors. Curr. Opin. Cell Biol. 21, 871–877. https://doi.org/10.1016/j.ceb.2009.09.004

Brock, A., Chang, H., Huang, S., 2009. Non-genetic heterogeneity — a mutation-independent driving force for the somatic evolution of tumours. Nat. Rev. Genet. 10, 336–342. https://doi.org/10.1038/nrg2556

Brown, J.M., Attardi, L.D., 2005. The role of apoptosis in cancer development and treatment response. Nat. Rev. Cancer 5, 231–237. https://doi.org/10.1038/nrc1560

Brune, W., Andoniou, C., 2017. Die Another Day: Inhibition of Cell Death Pathways by Cytomegalovirus. Viruses 9, 249. https://doi.org/10.3390/v9090249

Buchbinder, J.H., Pischel, D., Sundmacher, K., Flassig, R.J., Lavrik, I.N., 2018. Quantitative single cell analysis uncovers the life/death decision in CD95 network. PLOS Comput. Biol. 14, e1006368. https://doi.org/10.1371/journal.pcbi.1006368

Calzone, L., Tournier, L., Fourquet, S., Thieffry, D., Zhivotovsky, B., Barillot, E., Zinovyev, A., 2010. Mathematical Modelling of Cell-Fate Decision in Response to Death Receptor Engagement. PLoS Comput. Biol. 6, e1000702. https://doi.org/10.1371/journal.pcbi.1000702

Casagranda, S., Touzeau, S., Ropers, D., Gouzé, J.-L., 2018. Principal process analysis of biological models. BMC Syst. Biol. 12, 68. https://doi.org/10.1186/s12918-018-0586-6

Chabot, J.R., Pedraza, J.M., Luitel, P., van Oudenaarden, A., 2007. Stochastic gene expression out-of-steady-state in the cyanobacterial circadian clock. Nature 450, 1249–1252. https://doi.org/10.1038/nature06395

Chan, F.K.-M., 2000. A Domain in TNF Receptors That Mediates Ligand-Independent Receptor Assembly and Signaling. Science 288, 2351–2354. https://doi.org/10.1126/science.288.5475.2351

Chaudhary, P.M., Eby, M., Jasmin, A., Bookwalter, A., Murray, J., Hood, L., 1997. Death Receptor 5, a New Member of the TNFR Family, and DR4 Induce FADD-Dependent Apoptosis and Activate the NF-κB Pathway. Immunity 7, 821–830. https://doi.org/10.1016/S1074-7613(00)80400-8

Chaves, M., Eissing, T., Allgöwer, F., 2009. Regulation of Apoptosis via the NFκB Pathway: Modeling and Analysis, in: Ganguly, N., Deutsch, A., Mukherjee, A. (Eds.), Dynamics On and Of Complex Networks. Birkhäuser Boston, Boston, MA, pp. 19–33. https://doi.org/10.1007/978-0-8176-4751-3_2

Chen, C., Cui, J., Lu, H., Wang, R., Zhang, S., Shen, P., 2007a. Modeling of the Role of a Bax-Activation Switch in the Mitochondrial Apoptosis Decision. Biophys. J. 92, 4304–4315. https://doi.org/10.1529/biophysj.106.099606

Chen, C., Cui, J., Zhang, W., Shen, P., 2007b. Robustness analysis identifies the plausible model of the Bcl-2 apoptotic switch. FEBS Lett. 581, 5143–5150. https://doi.org/10.1016/j.febslet.2007.09.063

Chipuk, J.E., Moldoveanu, T., Llambi, F., Parsons, M.J., Green, D.R., 2010. The BCL-2 Family Reunion. Mol. Cell 37, 299–310. https://doi.org/10.1016/j.molcel.2010.01.025

Chong, K.H., Samarasinghe, S., Kulasiri, D., Zheng, J., 2019. Mathematical modelling of core regulatory mechanism in p53 protein that activates apoptotic switch. J. Theor. Biol. 462, 134–147. https://doi.org/10.1016/j.jtbi.2018.11.008

Clancy, L., Mruk, K., Archer, K., Woelfel, M., Mongkolsapaya, J., Screaton, G., Lenardo, M.J., Chan, F.K.-M., 2005. Preligand assembly domain-mediated ligand-independent association between TRAIL receptor 4 (TR4) and TR2 regulates TRAIL-induced apoptosis. Proc. Natl. Acad. Sci. 102, 18099–18104. https://doi.org/10.1073/pnas.0507329102

Cohen, A.A., Geva-Zatorsky, N., Eden, E., Frenkel-Morgenstern, M., Issaeva, I., Sigal, A., Milo, R., Cohen-Saidon, C., Liron, Y., Kam, Z., Cohen, L., Danon, T., Perzov, N., Alon, U., 2008. Dynamic Proteomics of Individual Cancer Cells in Response to a Drug. Science 322, 1511–1516. https://doi.org/10.1126/science.1160165

Cowling, V., Downward, J., 2002. Caspase-6 is the direct activator of caspase-8 in the cytochrome c-induced apoptosis pathway: absolute requirement for removal of caspase-6 prodomain. Cell Death Differ. 9, 1046–1056. https://doi.org/10.1038/sj.cdd.4401065

Cui, J., Chen, C., Lu, H., Sun, T., Shen, P., 2008a. Two Independent Positive Feedbacks and Bistability in the Bcl-2 Apoptotic Switch. PLoS ONE 3, e1469. https://doi.org/10.1371/journal.pone.0001469

Das Thakur, M., Salangsang, F., Landman, A.S., Sellers, W.R., Pryer, N.K., Levesque, M.P., Dummer, R., McMahon, M., Stuart, D.D., 2013. Modelling vemurafenib resistance in melanoma reveals a strategy to forestall drug resistance. Nature 494, 251–255. https://doi.org/10.1038/nature11814

De Miguel, D., Lemke, J., Anel, A., Walczak, H., Martinez-Lostao, L., 2016. Onto better TRAILs for cancer treatment. Cell Death Differ. 23, 733–747. https://doi.org/10.1038/cdd.2015.174

Degli-Esposti, M.A., Dougall, W.C., Smolak, P.J., Waugh, J.Y., Smith, C.A., Goodwin, R.G., 1997. The Novel Receptor TRAIL-R4 Induces NF-κB and Protects against TRAIL-Mediated Apoptosis, yet Retains an Incomplete Death Domain. Immunity 7, 813–820. https://doi.org/10.1016/S1074-7613(00)80399-4

Deng, Y., 2002. TRAIL-induced apoptosis requires Bax-dependent mitochondrial release of Smac/DIABLO. Genes Dev. 16, 33–45. https://doi.org/10.1101/gad.949602

Dewson, G., Kluck, R.M., 2009. Mechanisms by which Bak and Bax permeabilise mitochondria during apoptosis. J. Cell Sci. 122, 2801–2808. https://doi.org/10.1242/jcs.038166

Dickens, L.S., Boyd, R.S., Jukes-Jones, R., Hughes, M.A., Robinson, G.L., Fairall, L., Schwabe, J.W.R., Cain, K., MacFarlane, M., 2012. A Death Effector Domain Chain DISC Model Reveals a Crucial Role for Caspase-8 Chain Assembly in Mediating

Apoptotic Cell Death. Mol. Cell 47, 291–305. https://doi.org/10.1016/j.molcel.2012.05.004

Dueck, H., Eberwine, J., Kim, J., 2016. Variation is function: Are single cell differences functionally important?: Testing the hypothesis that single cell variation is required for aggregate function. BioEssays 38, 172–180. https://doi.org/10.1002/bies.201500124

Edlich, F., Banerjee, S., Suzuki, M., Cleland, M.M., Arnoult, D., Wang, C., Neutzner, A., Tjandra, N., Youle, R.J., 2011. Bcl-xL Retrotranslocates Bax from the Mitochondria into the Cytosol. Cell 145, 104–116. https://doi.org/10.1016/j.cell.2011.02.034

Eissing, T., Conzelmann, H., Gilles, E.D., Allgöwer, F., Bullinger, E., Scheurich, P., 2004. Bistability Analyses of a Caspase Activation Model for Receptor-induced Apoptosis. J. Biol. Chem. 279, 36892–36897. https://doi.org/10.1074/jbc.M404893200

Eling, N., Morgan, M.D., Marioni, J.C., 2019. Challenges in measuring and understanding biological noise. Nat. Rev. Genet. 20, 536–548. https://doi.org/10.1038/s41576-019-0130-6

Elowitz, M.B., 2002. Stochastic Gene Expression in a Single Cell. Science 297, 1183–1186. https://doi.org/10.1126/science.1070919

Flusberg, D.A., Roux, J., Spencer, S.L., Sorger, P.K., 2013. Cells surviving fractional killing by TRAIL exhibit transient but sustainable resistance and inflammatory phenotypes. Mol. Biol. Cell 24, 2186–2200. https://doi.org/10.1091/mbc.e12-10-0737

Fulda, S., Vucic, D., 2012. Targeting IAP proteins for therapeutic intervention in cancer. Nat. Rev. Drug Discov. 11, 109–124. https://doi.org/10.1038/nrd3627

Fussenegger, M., Bailey, J.E., Varner, J., 2000. A mathematical model of caspase function in apoptosis. Nat. Biotechnol. 18, 768–774. https://doi.org/10.1038/77589

Galluzzi, L., Blomgren, K., Kroemer, G., 2009. Mitochondrial membrane permeabilization in neuronal injury. Nat. Rev. Neurosci. 10, 481–494. https://doi.org/10.1038/nrn2665

Gaudet, S., Spencer, S.L., Chen, W.W., Sorger, P.K., 2012. Exploring the Contextual Sensitivity of Factors that Determine Cell-to-Cell Variability in Receptor-Mediated Apoptosis. PLoS Comput. Biol. 8, e1002482. https://doi.org/10.1371/journal.pcbi.1002482

Ghusinga, K.R., Singh, A., 2019. Analysis of stochastic timing of intracellular events with gene switching (preprint). Systems Biology. https://doi.org/10.1101/710442

Gibellini, D., Borderi, M., De Crignis, E., Cicola, R., Vescini, F., Caudarella, R., Chiodo, F., Re, M.C., 2007. RANKL/OPG/TRAIL plasma levels and bone mass loss evaluation in antiretroviral naive HIV-1-positive men. J. Med. Virol. 79, 1446–1454. https://doi.org/10.1002/jmv.20938

Gillespie, D.T., 1977. Exact stochastic simulation of coupled chemical reactions. J. Phys. Chem. 81, 2340–2361. https://doi.org/10.1021/j100540a008

Gillespie, D.T., 1976. A general method for numerically simulating the stochastic time evolution of coupled chemical reactions. J. Comput. Phys. 22, 403–434. https://doi.org/10.1016/0021-9991(76)90041-3

Golding, I., Paulsson, J., Zawilski, S.M., Cox, E.C., 2005. Real-Time Kinetics of Gene Activity in Individual Bacteria. Cell 123, 1025–1036. https://doi.org/10.1016/j.cell.2005.09.031

Goldstein, J.C., Waterhouse, N.J., Juin, P., Evan, G.I., Green, D.R., 2000. The coordinate release of cytochrome c during apoptosis is rapid, complete and kinetically invariant. Nat. Cell Biol. 2, 156–162. https://doi.org/10.1038/35004029

Gomes-Pereira, L.C., Chaves, M., Roux, J., 2020. The role of caspase-10 in apoptosis: a positive feedback loop to explain cell response heterogeneity in a Trail-receptor model.

Gonze, D., Ouattara, A., 2014. Stochastic simulations_applications to biomolecular networks.pdf.

Green, D.R., 2004. The Pathophysiology of Mitochondrial Cell Death. Science 305, 626–629. https://doi.org/10.1126/science.1099320

Hantusch, A., Rehm, M., Brunner, T., 2018. Counting on Death – Quantitative aspects of Bcl-2 family regulation. FEBS J. 285, 4124–4138. https://doi.org/10.1111/febs.14516

Harper, C.V., Finkenstädt, B., Woodcock, D.J., Friedrichsen, S., Semprini, S., Ashall, L., Spiller, D.G., Mullins, J.J., Rand, D.A., Davis, J.R.E., White, M.R.H., 2011. Dynamic Analysis of Stochastic Transcription Cycles. PLoS Biol. 9, e1000607. https://doi.org/10.1371/journal.pbio.1000607

Herbst, R.S., Kurzrock, R., Hong, D.S., Valdivieso, M., Hsu, C.-P., Goyal, L., Juan, G., Hwang, Y.C., Wong, S., Hill, J.S., Friberg, G., LoRusso, P.M., 2010. A First-in-Human Study of Conatumumab in Adult Patients with Advanced Solid Tumors. Clin. Cancer Res. 16, 5883–5891. https://doi.org/10.1158/1078-0432.CCR-10-0631

Holohan, C., Van Schaeybroeck, S., Longley, D.B., Johnston, P.G., 2013. Cancer drug resistance: an evolving paradigm. Nat. Rev. Cancer 13, 714–726. https://doi.org/10.1038/nrc3599

Horn, S., Hughes, M.A., Schilling, R., Sticht, C., Tenev, T., Ploesser, M., Meier, P., Sprick, M.R., MacFarlane, M., Leverkus, M., 2017. Caspase-10 Negatively Regulates Caspase-8-Mediated Cell Death, Switching the Response to CD95L in Favor of NF-κB Activation and Cell Survival. Cell Rep. 19, 785–797. https://doi.org/10.1016/j.celrep.2017.04.010

Howells, C.C., Baumann, W.T., Samuels, D.C., Finkielstein, C.V., 2011. The Bcl-2-associated death promoter (BAD) lowers the threshold at which the Bcl-2-interacting

domain death agonist (BID) triggers mitochondria disintegration. J. Theor. Biol. 271, 114–123. https://doi.org/10.1016/j.jtbi.2010.11.040

Hua, F., Cornejo, M.G., Cardone, M.H., Stokes, C.L., Lauffenburger, D.A., 2005. Effects of Bcl-2 Levels on Fas Signaling-Induced Caspase-3 Activation: Molecular Genetic Tests of Computational Model Predictions. J. Immunol. 175, 985–995. https://doi.org/10.4049/jimmunol.175.2.985

Huang, K., Zhang, J., O'Neill, K.L., Gurumurthy, C.B., Quadros, R.M., Tu, Y., Luo, X., 2016. Cleavage by Caspase 8 and Mitochondrial Membrane Association Activate the BH3-only Protein Bid during TRAIL-induced Apoptosis. J. Biol. Chem. 291, 11843–11851. https://doi.org/10.1074/jbc.M115.711051

Huber, H.J., Duessmann, H., Wenus, J., Kilbride, S.M., Prehn, J.H.M., 2011. Mathematical modelling of the mitochondrial apoptosis pathway. Biochim. Biophys. Acta BBA - Mol. Cell Res. 1813, 608–615. https://doi.org/10.1016/j.bbamcr.2010.10.004

Hughes, M.A., Powley, I.R., Jukes-Jones, R., Horn, S., Feoktistova, M., Fairall, L., Schwabe, J.W.R., Leverkus, M., Cain, K., MacFarlane, M., 2016. Co-operative and Hierarchical Binding of c-FLIP and Caspase-8: A Unified Model Defines How c-FLIP Isoforms Differentially Control Cell Fate. Mol. Cell 61, 834–849. https://doi.org/10.1016/j.molcel.2016.02.023

Hymowitz, S.G., Christinger, H.W., Fuh, G., Ultsch, M., O'Connell, M., Kelley, R.F., Ashkenazi, A., de Vos, A.M., 1999. Triggering Cell Death. Mol. Cell 4, 563–571. https://doi.org/10.1016/S1097-2765(00)80207-5

Iwamoto, K., Shindo, Y., Takahashi, K., 2016. Modeling Cellular Noise Underlying Heterogeneous Cell Responses in the Epidermal Growth Factor Signaling Pathway. PLOS Comput. Biol. 12, e1005222. https://doi.org/10.1371/journal.pcbi.1005222

Jacobson, M.D., Weil, M., Raff, M.C., 1997. Programmed Cell Death in Animal Development. Cell 88, 347–354. https://doi.org/10.1016/S0092-8674(00)81873-5

Jones, E.Y., Mongkolsapaya, J., Grimes, J.M., Chen, N., Xu, X.-N., Stuart, D.I., Screaton, G.R., 1999. [No title found]. Nat. Struct. Biol. 6, 1048–1053. https://doi.org/10.1038/14935

Juin, P., Geneste, O., Gautier, F., Depil, S., Campone, M., 2013. Decoding and unlocking the BCL-2 dependency of cancer cells. Nat. Rev. Cancer 13, 455–465. https://doi.org/10.1038/nrc3538

Kallenberger, S.M., Beaudouin, J., Claus, J., Fischer, C., Sorger, P.K., Legewie, S., Eils, R., 2014. Intra- and Interdimeric Caspase-8 Self-Cleavage Controls Strength and Timing of CD95-Induced Apoptosis. Sci. Signal. 7, ra23–ra23. https://doi.org/10.1126/scisignal.2004738

Kerr, J.F.R., Wyllie, A.H., Currie, A.R., 1972. Apoptosis: A Basic Biological Phenomenon with Wideranging Implications in Tissue Kinetics. Br. J. Cancer 26, 239–257. https://doi.org/10.1038/bjc.1972.33

Kolch, W., Halasz, M., Granovskaya, M., Kholodenko, B.N., 2015. The dynamic control of signal transduction networks in cancer cells. Nat. Rev. Cancer 15, 515–527. https://doi.org/10.1038/nrc3983

Kozłowska, E., Puszynski, K., 2016. Application of bifurcation theory and siRNA-based control signal to restore the proper response of cancer cells to DNA damage. J. Theor. Biol. 408, 213–221. https://doi.org/10.1016/j.jtbi.2016.08.017

Kreso, A., O'Brien, C.A., van Galen, P., Gan, O.I., Notta, F., Brown, A.M.K., Ng, K., Ma, J., Wienholds, E., Dunant, C., Pollett, A., Gallinger, S., McPherson, J., Mullighan, C.G., Shibata, D., Dick, J.E., 2013. Variable Clonal Repopulation Dynamics Influence Chemotherapy Response in Colorectal Cancer. Science 339, 543–548. https://doi.org/10.1126/science.1227670

Kretz, A.-L., von Karstedt, S., Hillenbrand, A., Henne-Bruns, D., Knippschild, U., Trauzold, A., Lemke, J., 2018. Should We Keep Walking along the Trail for Pancreatic Cancer Treatment? Revisiting TNF-Related Apoptosis-Inducing Ligand for Anticancer Therapy. Cancers 10, 77. https://doi.org/10.3390/cancers10030077

Labavić, D., Ladjimi, M.T., Thommen, Q., Pfeuty, B., 2019. Scaling laws of cell-fate responses to transient stress. J. Theor. Biol. 478, 14–25. https://doi.org/10.1016/j.jtbi.2019.06.014

Labhsetwar, P., Cole, J.A., Roberts, E., Price, N.D., Luthey-Schulten, Z.A., 2013. Heterogeneity in protein expression induces metabolic variability in a modeled *Escherichia coli* population. Proc. Natl. Acad. Sci. 110, 14006–14011. https://doi.org/10.1073/pnas.1222569110

LeBlanc, H.N., Ashkenazi, A., 2003. Apo2L/TRAIL and its death and decoy receptors. Cell Death Differ. 10, 66–75. https://doi.org/10.1038/sj.cdd.4401187

Lederman, E.E., Hope, J.M., King, M.R., 2018. Mass Action Kinetic Model of Apoptosis by TRAIL-Functionalized Leukocytes. Front. Oncol. 8, 410. https://doi.org/10.3389/fonc.2018.00410

Lee, R.E.C., Qasaimeh, M.A., Xia, X., Juncker, D., Gaudet, S., 2016. NF-κB signalling and cell fate decisions in response to a short pulse of tumour necrosis factor. Sci. Rep. 6, 39519. https://doi.org/10.1038/srep39519

Legewie, S., Blüthgen, N., Herzel, H., 2006. Mathematical Modeling Identifies Inhibitors of Apoptosis as Mediators of Positive Feedback and Bistability. PLoS Comput. Biol. 2, e120. https://doi.org/10.1371/journal.pcbi.0020120

Lehner, B., Kaneko, K., 2011. Fluctuation and response in biology. Cell. Mol. Life Sci. 68, 1005–1010. https://doi.org/10.1007/s00018-010-0589-y

Liesche, C., Berndt, J., Fricke, F., Aschenbrenner, S., Heilemann, M., Eils, R., Beaudouin, J., 2018. CD95 receptor activation by ligand-induced trimerization is independent of its partial pre-ligand assembly (preprint). Cell Biology. https://doi.org/10.1101/293530

Lionnet, T., Singer, R.H., 2012. Transcription goes digital. EMBO Rep. 13, 313–321. https://doi.org/10.1038/embor.2012.31

Llambi, F., Moldoveanu, T., Tait, S.W.G., Bouchier-Hayes, L., Temirov, J., McCormick, L.L., Dillon, C.P., Green, D.R., 2011. A Unified Model of Mammalian BCL-2 Protein Family Interactions at the Mitochondria. Mol. Cell 44, 517–531. https://doi.org/10.1016/j.molcel.2011.10.001

Llamosi, A., Gonzalez-Vargas, A.M., Versari, C., Cinquemani, E., Ferrari-Trecate, G., Hersen, P., Batt, G., 2016. What Population Reveals about Individual Cell Identity: Single-Cell Parameter Estimation of Models of Gene Expression in Yeast. PLOS Comput. Biol. 12, e1004706. https://doi.org/10.1371/journal.pcbi.1004706

Lopes, R.B., Gangeswaran, R., McNeish, I.A., Wang, Y., Lemoine, N.R., 2007. Expression of the IAP protein family is dysregulated in pancreatic cancer cells and is important for resistance to chemotherapy. Int. J. Cancer 120, 2344–2352. https://doi.org/10.1002/ijc.22554

Mariani, S.M., Matiba, B., Armandola, E.A., Krammer, P.H., 1997. Interleukin 1 -converting Enzyme Related Proteases/Caspases Are Involved in TRAIL-induced Apoptosis of Myeloma and Leukemia Cells. J. Cell Biol. 137, 9.

Márquez-Jurado, S., Díaz-Colunga, J., das Neves, R.P., Martinez-Lorente, A., Almazán, F., Guantes, R., Iborra, F.J., 2018. Mitochondrial levels determine variability in cell death by modulating apoptotic gene expression. Nat. Commun. 9, 389. https://doi.org/10.1038/s41467-017-02787-4

Merchant, M.S., Geller, J.I., Baird, K., Chou, A.J., Galli, S., Charles, A., Amaoko, M., Rhee, E.H., Price, A., Wexler, L.H., Meyers, P.A., Widemann, B.C., Tsokos, M., Mackall, C.L., 2012. Phase I Trial and Pharmacokinetic Study of Lexatumumab in Pediatric Patients With Solid Tumors. J. Clin. Oncol. 30, 4141–4147. https://doi.org/10.1200/JCO.2012.44.1055

Miura, H., Kondo, Y., Matsuda, M., Aoki, K., 2018. Cell-to-Cell Heterogeneity in p38-Mediated Cross-Inhibition of JNK Causes Stochastic Cell Death. Cell Rep. 24, 2658–2668. https://doi.org/10.1016/j.celrep.2018.08.020

Mori, M., Hwa, T., Martin, O.C., De Martino, A., Marinari, E., 2016. Constrained Allocation Flux Balance Analysis. PLOS Comput. Biol. 12, e1004913. https://doi.org/10.1371/journal.pcbi.1004913

Muller, P.A.J., Vousden, K.H., 2013. p53 mutations in cancer. Nat. Cell Biol. 15, 2–8. https://doi.org/10.1038/ncb2641

Neumann, S., Hasenauer, J., Pollak, N., Scheurich, P., 2014. Dominant Negative Effects of Tumor Necrosis Factor (TNF)-related Apoptosis-inducing Ligand (TRAIL) Receptor 4 on TRAIL Receptor 1 Signaling by Formation of Heteromeric Complexes. J. Biol. Chem. 289, 16576–16587. https://doi.org/10.1074/jbc.M114.559468

Newman, J.R.S., Ghaemmaghami, S., Ihmels, J., Breslow, D.K., Noble, M., DeRisi, J.L., Weissman, J.S., 2006. Single-cell proteomic analysis of S. cerevisiae reveals the architecture of biological noise. Nature 441, 840–846. https://doi.org/10.1038/nature04785

Olivier, M., Hollstein, M., Hainaut, P., 2010. TP53 Mutations in Human Cancers: Origins, Consequences, and Clinical Use. Cold Spring Harb. Perspect. Biol. 2, a001008–a001008. https://doi.org/10.1101/cshperspect.a001008

Ozbudak, E.M., Thattai, M., Kurtser, I., Grossman, A.D., van Oudenaarden, A., 2002. Regulation of noise in the expression of a single gene. Nat. Genet. 31, 69–73. https://doi.org/10.1038/ng869

Paek, A.L., Liu, J.C., Loewer, A., Forrester, W.C., Lahav, G., 2016. Cell-to-Cell Variation in p53 Dynamics Leads to Fractional Killing. Cell 165, 631–642. https://doi.org/10.1016/j.cell.2016.03.025

Pennarun, B., Meijer, A., de Vries, E.G.E., Kleibeuker, J.H., Kruyt, F., de Jong, S., 2010. Playing the DISC: Turning on TRAIL death receptor-mediated apoptosis in cancer. Biochim. Biophys. Acta BBA - Rev. Cancer 1805, 123–140. https://doi.org/10.1016/j.bbcan.2009.11.004

Pujadas, E., Feinberg, A.P., 2012. Regulated Noise in the Epigenetic Landscape of Development and Disease. Cell 148, 1123–1131. https://doi.org/10.1016/j.cell.2012.02.045

Qi, H., Shuai, J., 2016. Alzheimer's disease via enhanced calcium signaling caused by the decrease of endoplasmic reticulum–mitochondrial distance. Med. Hypotheses 89, 28–31. https://doi.org/10.1016/j.mehy.2016.01.022

R Safa, A., 2013. Roles of c-FLIP in Apoptosis, Necroptosis, and Autophagy. J. Carcinog. Mutagen. https://doi.org/10.4172/2157-2518.S6-003

Raj, A., Peskin, C.S., Tranchina, D., Vargas, D.Y., Tyagi, S., 2006. Stochastic mRNA Synthesis in Mammalian Cells. PLoS Biol. 4, e309. https://doi.org/10.1371/journal.pbio.0040309

Raj, A., van Oudenaarden, A., 2008. Nature, Nurture, or Chance: Stochastic Gene Expression and Its Consequences. Cell 135, 216–226. https://doi.org/10.1016/j.cell.2008.09.050

Raser, J.M., 2004. Control of Stochasticity in Eukaryotic Gene Expression. Science 304, 1811–1814. https://doi.org/10.1126/science.1098641

Rehm, M., Düßmann, H., Jänicke, R.U., Tavaré, J.M., Kögel, D., Prehn, J.H.M., 2002. Single-cell Fluorescence Resonance Energy Transfer Analysis Demonstrates That Caspase Activation during Apoptosis Is a Rapid Process: ROLE OF CASPASE-3. J. Biol. Chem. 277, 24506–24514. https://doi.org/10.1074/jbc.M110789200

Rehm, M., Huber, H.J., Dussmann, H., Prehn, J.H.M., 2006. Systems analysis of effector caspase activation and its control by X-linked inhibitor of apoptosis protein. EMBO J. 25, 4338–4349. https://doi.org/10.1038/sj.emboj.7601295

Rehm, M., Huber, H.J., Hellwig, C.T., Anguissola, S., Dussmann, H., Prehn, J.H.M., 2009. Dynamics of outer mitochondrial membrane permeabilization during apoptosis. Cell Death Differ. 16, 613–623. https://doi.org/10.1038/cdd.2008.187

Renault, T.T., Chipuk, J.E., 2014. Death upon a Kiss: Mitochondrial Outer Membrane Composition and Organelle Communication Govern Sensitivity to BAK/BAX-Dependent Apoptosis. Chem. Biol. 21, 114–123. https://doi.org/10.1016/j.chembiol.2013.10.009

Riedl, S.J., Salvesen, G.S., 2007. The apoptosome: signalling platform of cell death. Nat. Rev. Mol. Cell Biol. 8, 405–413. https://doi.org/10.1038/nrm2153

Roberts, N.J., Zhou, S., Diaz, L.A., Holdhoff, M., 2011. Systemic use of tumor necrosis factor alpha as an anticancer agent. Oncotarget 2. https://doi.org/10.18632/oncotarget.344

Rocha Lima, C.M., Bayraktar, S., Flores, A.M., MacIntyre, J., Montero, A., Baranda, J.C., Wallmark, J., Portera, C., Raja, R., Stern, H., Royer-Joo, S., Amler, L.C., 2012. Phase Ib Study of Drozitumab Combined With First-Line mFOLFOX6 Plus Bevacizumab in Patients with Metastatic Colorectal Cancer. Cancer Invest. 30, 727–731. https://doi.org/10.3109/07357907.2012.732163

Roesch, A., Fukunaga-Kalabis, M., Schmidt, E.C., Zabierowski, S.E., Brafford, P.A., Vultur, A., Basu, D., Gimotty, P., Vogt, T., Herlyn, M., 2010. A Temporarily Distinct Subpopulation of Slow-Cycling Melanoma Cells Is Required for Continuous Tumor Growth. Cell 141, 583–594. https://doi.org/10.1016/j.cell.2010.04.020

Roux, J., Hafner, M., Bandara, S., Sims, J.J., Hudson, H., Chai, D., Sorger, P.K., 2015. Fractional killing arises from cell-to-cell variability in overcoming a caspase activity threshold. Mol. Syst. Biol. 11, 803. https://doi.org/10.15252/msb.20145584

Sarosiek, K.A., Ni Chonghaile, T., Letai, A., 2013. Mitochondria: gatekeepers of response to chemotherapy. Trends Cell Biol. 23, 612–619. https://doi.org/10.1016/j.tcb.2013.08.003

Schellenberg, B., Wang, P., Keeble, J.A., Rodriguez-Enriquez, R., Walker, S., Owens, T.W., Foster, F., Tanianis-Hughes, J., Brennan, K., Streuli, C.H., Gilmore, A.P., 2013. Bax Exists in a Dynamic Equilibrium between the Cytosol and Mitochondria to Control Apoptotic Priming. Mol. Cell 49, 959–971. https://doi.org/10.1016/j.molcel.2012.12.022

Schlatter, R., Schmich, K., Avalos Vizcarra, I., Scheurich, P., Sauter, T., Borner, C., Ederer, M., Merfort, I., Sawodny, O., 2009. ON/OFF and Beyond - A Boolean Model of Apoptosis. PLoS Comput. Biol. 5, e1000595. https://doi.org/10.1371/journal.pcbi.1000595

Schleich, K., Buchbinder, J.H., Pietkiewicz, S., Kähne, T., Warnken, U., Öztürk, S., Schnölzer, M., Naumann, M., Krammer, P.H., Lavrik, I.N., 2016. Molecular architecture of the DED chains at the DISC: regulation of procaspase-8 activation by short DED proteins c-FLIP and procaspase-8 prodomain. Cell Death Differ. 23, 681–694. https://doi.org/10.1038/cdd.2015.137

Schneider, P., Thome, M., Burns, K., Bodmer, J.-L., Hofmann, K., Kataoka, T., Holler, N., Tschopp, J., 1997. TRAIL Receptors 1 (DR4) and 2 (DR5) Signal FADD-Dependent Apoptosis and Activate NF-κB. Immunity 7, 831–836. https://doi.org/10.1016/S1074-7613(00)80401-X

Scott, N.E., Rogers, L.D., Prudova, A., Brown, N.F., Fortelny, N., Overall, C.M., Foster, L.J., 2017. Interactome disassembly during apoptosis occurs independent of caspase cleavage. Mol. Syst. Biol. 13, 906. https://doi.org/10.15252/msb.20167067

Sharma, S., de Vries, E.G., Infante, J.R., Oldenhuis, C.N., Gietema, J.A., Yang, L., Bilic, S., Parker, K., Goldbrunner, M., Scott, J.W., Burris, H.A., 2014. Safety, pharmacokinetics, and pharmacodynamics of the DR5 antibody LBY135 alone and in combination with capecitabine in patients with advanced solid tumors. Invest. New Drugs 32, 135–144. https://doi.org/10.1007/s10637-013-9952-9

Sharma, S.V., Lee, D.Y., Li, B., Quinlan, M.P., Takahashi, F., Maheswaran, S., McDermott, U., Azizian, N., Zou, L., Fischbach, M.A., Wong, K.-K., Brandstetter, K., Wittner, B., Ramaswamy, S., Classon, M., Settleman, J., 2010. A Chromatin-Mediated Reversible Drug-Tolerant State in Cancer Cell Subpopulations. Cell 141, 69–80. https://doi.org/10.1016/j.cell.2010.02.027

Sherman, M.S., Lorenz, K., Lanier, M.H., Cohen, B.A., 2015. Cell-to-Cell Variability in the Propensity to Transcribe Explains Correlated Fluctuations in Gene Expression. Cell Syst. 1, 315–325. https://doi.org/10.1016/j.cels.2015.10.011

Shlyakhtina, Y., Pavet, V., Gronemeyer, H., 2017. Dual role of DR5 in death and survival signaling leads to TRAIL resistance in cancer cells. Cell Death Dis. 8, e3025–e3025. https://doi.org/10.1038/cddis.2017.423

Sigal, A., Milo, R., Cohen, A., Geva-Zatorsky, N., Klein, Y., Liron, Y., Rosenfeld, N., Danon, T., Perzov, N., Alon, U., 2006. Variability and memory of protein levels in human cells. Nature 444, 643–646. https://doi.org/10.1038/nature05316

Sohn, D., Schulze-Osthoff, K., Jänicke, R.U., 2005. Caspase-8 Can Be Activated by Interchain Proteolysis without Receptor-triggered Dimerization during Drug-induced Apoptosis. J. Biol. Chem. 280, 5267–5273. https://doi.org/10.1074/jbc.M408585200

Spencer, S.L., Gaudet, S., Albeck, J.G., Burke, J.M., Sorger, P.K., 2009. Non-genetic origins of cell-to-cell variability in TRAIL-induced apoptosis. Nature 459, 428–432. https://doi.org/10.1038/nature08012

Stewart-Ornstein, J., Weissman, J.S., El-Samad, H., 2012. Cellular Noise Regulons Underlie Fluctuations in Saccharomyces cerevisiae. Mol. Cell 45, 483–493. https://doi.org/10.1016/j.molcel.2011.11.035

Stoma, S., Donzé, A., Bertaux, F., Maler, O., Batt, G., 2013. STL-based Analysis of TRAIL-induced Apoptosis Challenges the Notion of Type I/Type II Cell Line Classification. PLoS Comput. Biol. 9, e1003056. https://doi.org/10.1371/journal.pcbi.1003056

Stucki, J.W., Simon, H.-U., 2005. Mathematical modeling of the regulation of caspase-3 activation and degradation. J. Theor. Biol. 234, 123–131. https://doi.org/10.1016/j.jtbi.2004.11.011

Suter, D.M., Molina, N., Gatfield, D., Schneider, K., Schibler, U., Naef, F., 2011. Mammalian Genes Are Transcribed with Widely Different Bursting Kinetics. Science 332, 472–474. https://doi.org/10.1126/science.1198817

Suzuki, Y., Nakabayashi, Y., Takahashi, R., 2001. Ubiquitin-protein ligase activity of X-linked inhibitor of apoptosis protein promotes proteasomal degradation of caspase-3 and enhances its anti-apoptotic effect in Fas-induced cell death. Proc. Natl. Acad. Sci. 98, 8662–8667. https://doi.org/10.1073/pnas.161506698

Swers, J.S., Grinberg, L., Wang, L., Feng, H., Lekstrom, K., Carrasco, R., Xiao, Z., Inigo, I., Leow, C.C., Wu, H., Tice, D.A., Baca, M., 2013. Multivalent Scaffold Proteins as Superagonists of TRAIL Receptor 2-Induced Apoptosis. Mol. Cancer Ther. 12, 1235–1244. https://doi.org/10.1158/1535-7163.MCT-12-1107

Szegezdi, E., van der Sloot, A.M., Mahalingam, D., O'Leary, L., Cool, R.H., Muñoz, I.G., Montoya, G., Quax, W.J., de Jong, S., Samali, A., Serrano, L., 2012. Kinetics in Signal Transduction Pathways Involving Promiscuous Oligomerizing Receptors Can Be Determined by Receptor Specificity: Apoptosis Induction by TRAIL. Mol. Cell. Proteomics 11, M111.013730. https://doi.org/10.1074/mcp.M111.013730

Tait, S.W.G., Green, D.R., 2010. Mitochondria and cell death: outer membrane permeabilization and beyond. Nat. Rev. Mol. Cell Biol. 11, 621–632. https://doi.org/10.1038/nrm2952

Tan, C., Dlugosz, P.J., Peng, J., Zhang, Z., Lapolla, S.M., Plafker, S.M., Andrews, D.W., Lin, J., 2006. Auto-activation of the Apoptosis Protein Bax Increases Mitochondrial Membrane Permeability and Is Inhibited by Bcl-2. J. Biol. Chem. 281, 14764–14775. https://doi.org/10.1074/jbc.M602374200

Thome, M., Schneider, P., Hofmann, K., Fickenscher, H., Meinl, E., Neipel, F., Mattmann, C., Burns, K., Bodmer, J.-L., Schröter, M., Scaffidi, C., Krammer, P.H., Peter, M.E., Tschopp, J., 1997. Viral FLICE-inhibitory proteins (FLIPs) prevent apoptosis induced by death receptors. Nature 386, 517–521. https://doi.org/10.1038/386517a0

Todt, F., Cakir, Z., Reichenbach, F., Emschermann, F., Lauterwasser, J., Kaiser, A., Ichim, G., Tait, S.W., Frank, S., Langer, H.F., Edlich, F., 2015. Differential

retrotranslocation of mitochondrial Bax and Bak. EMBO J. 34, 67–80. https://doi.org/10.15252/embj.201488806

Tran, S.E.F., Holmström, T.H., Ahonen, M., Kähäri, V.-M., Eriksson, J.E., 2001. MAPK/ERK Overrides the Apoptotic Signaling from Fas, TNF, and TRAIL Receptors. J. Biol. Chem. 276, 16484–16490. https://doi.org/10.1074/jbc.M010384200

Trauzold, A., Wermann, H., Arlt, A., Schütze, S., Schäfer, H., Oestern, S., Röder, C., Ungefroren, H., Lampe, E., Heinrich, M., Walczak, H., Kalthoff, H., 2001. CD95 and TRAIL receptor-mediated activation of protein kinase C and NF-κB contributes to apoptosis resistance in ductal pancreatic adenocarcinoma cells. Oncogene 20, 4258–4269. https://doi.org/10.1038/sj.onc.1204559

Wajant, 2019. Molecular Mode of Action of TRAIL Receptor Agonists—Common Principles and Their Translational Exploitation. Cancers 11, 954. https://doi.org/10.3390/cancers11070954

Wakamoto, Y., Dhar, N., Chait, R., Schneider, K., Signorino-Gelo, F., Leibler, S., McKinney, J.D., 2013. Dynamic Persistence of Antibiotic-Stressed Mycobacteria. Science 339, 91–95. https://doi.org/10.1126/science.1229858

Walczak, H., Miller, R.E., Ariail, K., Gliniak, B., Griffith, T.S., Kubin, M., Chin, W., Jones, J., Woodward, A., Le, T., Smith, C., Smolak, P., Goodwin, R.G., Rauch, C.T., Schuh, J.C.L., Lynch, D.H., 1999. Tumoricidal activity of tumor necrosis factor–related apoptosis–inducing ligand in vivo. Nat. Med. 5, 157–163. https://doi.org/10.1038/5517

Willis, S.N., 2005. Proapoptotic Bak is sequestered by Mcl-1 and Bcl-xL, but not Bcl-2, until displaced by BH3-only proteins. Genes Dev. 19, 1294–1305. https://doi.org/10.1101/gad.1304105

Würstle, M.L., Zink, E., Prehn, J.H.M., Rehm, M., 2014. From computational modelling of the intrinsic apoptosis pathway to a systems-based analysis of chemotherapy resistance: achievements, perspectives and challenges in systems medicine. Cell Death Dis. 5, e1258–e1258. https://doi.org/10.1038/cddis.2014.36

Xu, J., Zhou, J.-Y., Wei, W.-Z., Wu, G.S., 2010. Activation of the Akt Survival Pathway Contributes to TRAIL Resistance in Cancer Cells. PLoS ONE 5, e10226. https://doi.org/10.1371/journal.pone.0010226

Yin, Z., Qi, H., Liu, L., Jin, Z., 2017. The optimal regulation mode of Bcl-2 apoptotic switch revealed by bistability analysis. Biosystems 162, 44–52. https://doi.org/10.1016/j.biosystems.2017.09.011

Younes, A., Vose, J.M., Zelenetz, A.D., Smith, M.R., Burris, H.A., Ansell, S.M., Klein, J., Halpern, W., Miceli, R., Kumm, E., Fox, N.L., Czuczman, M.S., 2010. A Phase 1b/2 trial of mapatumumab in patients with relapsed/refractory non-Hodgkin's lymphoma. Br. J. Cancer 103, 1783–1787. https://doi.org/10.1038/sj.bjc.6605987

Zhang, T., Brazhnik, P., Tyson, J.J., 2009. Computational Analysis of Dynamical Responses to the Intrinsic Pathway of Programmed Cell Death. Biophys. J. 97, 415–434. https://doi.org/10.1016/j.bpj.2009.04.053

Zhang, X.D., Franco, A.V., Nguyen, T., Gray, C.P., Hersey, P., 2000. Differential Localization and Regulation of Death and Decoy Receptors for TNF-Related Apoptosis-Inducing Ligand (TRAIL) in Human Melanoma Cells. J. Immunol. 164, 3961–3970. https://doi.org/10.4049/jimmunol.164.8.3961

Воропаева, О.Ф., Voropaeva, O.F., 2017. Deregulation of p53-dependent microRNAs: the results of mathematical modeling. Математическая Биология И Биоинформатика 12, 151–175. https://doi.org/10.17537/2017.12.151